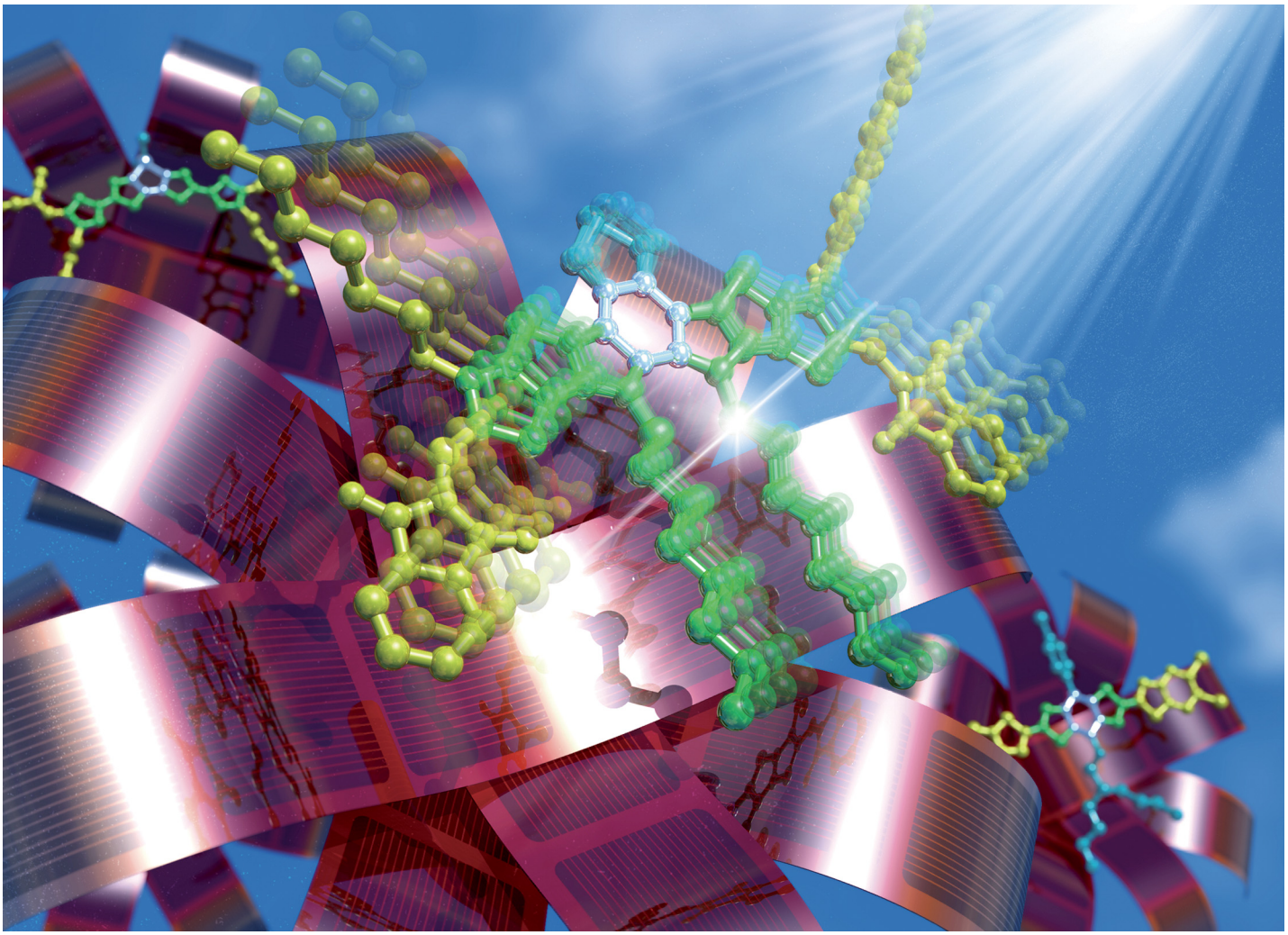

Showcasing work from the group of Osaka University and Nara Institute of Science and Technology (NAIST), Japan.

Impact of substituents on the performance of small-molecule semiconductors in organic photovoltaic devices *via* regulating morphology

A review on substituent engineering of small-molecule organic semiconductors for photovoltaic applications. The relationship between the structure of electronically inert peripheral substituents and the resultant photovoltaic efficiency is highlighted.

As featured in:

See Mitsuharu Suzuki, Hiroko Yamada *et al.*, *J. Mater. Chem. C*, 2022, **10**, 1162.

ROYAL SOCIETY OF CHEMISTRY

rsc.li/materials-c

Registered charity number: 207890

Journal of Materials Chemistry C

ROYAL SOCIETY OF CHEMISTRY

REVIEW

View Article Online
View Journal | View Issue

Cite this: J. Mater. Chem. C, 2022, 10, 1162

Impact of substituents on the performance of small-molecule semiconductors in organic photovoltaic devices *via* regulating morphology

Mitsuharu Suzuki, *[a] Kanta Suzuki,[a] Taehyun Won[b] and Hiroko Yamada *[c]

Received 7th September 2021,
Accepted 6th December 2021

DOI: 10.1039/d1tc04237h

rsc.li/materials-c

Recent years have witnessed a rapid development of organic photovoltaic devices (OPVs). The significant improvement in power conversion efficiency is due to not only the discovery of new π-conjugated frameworks, but also careful substituent engineering to achieve optimal morphology in bulk-heterojunction active layers. Indeed, all aspects of the light-to-electricity conversion in OPVs, such as light absorption, exciton diffusion, and charge-carrier transport, are influenced by the morphological characteristics of active layers. The importance of active-layer morphology on the performance of OPVs has made substituent engineering an increasingly important part of OPV semiconductor design. Herein, we overview recent prominent examples of substituent engineering, focusing on flexible substituents that regulate morphology, rather than the molecular electronic structure, of small-molecule organic semiconductors.

1. Introduction

Organic photovoltaic technologies have experienced a marked development in recent years,[1] achieving an excellent power conversion efficiency (PCE) of 19% in a single-junction cell.[2] This progress was largely enabled by the creation of new organic semiconductors (SCs) comprising a meticulously designed π-conjugated backbone, as typified by recent non-fullerene n-type (or acceptor) SCs bearing a highly ring-fused core unit flanked by strongly electron-withdrawing end

[a] Department of Applied Chemistry, Graduate School of Engineering, Osaka University, 2-1 Yamadaoka, Suita, Osaka 565-0871, Japan. E-mail: msuzuki@chem.eng.osaka-u.ac.jp
[b] Division of Applied Science, School of Engineering, Osaka University, 2-1 Yamadaoka, Suita, Osaka 565-0871, Japan
[c] Division of Materials Science, Graduate School of Science and Technology, Nara Institute of Science and Technology, 8916-5 Takayama-cho, Ikoma, Nara 630-0192, Japan. E-mail: hyamada@ms.naist.jp

Mitsuharu Suzuki

Mitsuharu Suzuki received his Bachelor's (2000) and Master's (2002) degrees from Kyoto University (Japan). After working in Mitsubishi Gas Chemical Company, he moved to the United States and received his PhD in chemistry from University of California, Los Angeles in 2011. He then worked as a postdoctoral fellow at University of California, Los Angeles then Lawrence Berkeley National Laboratory, before joining Nara Institute of Science and Technology (Japan) as an assistant professor in 2013. Since 2018, he has been an associate professor at Osaka University. His current research focuses on the design, synthesis, and controlled assembly of organic compounds for optoelectronic applications.

Kanta Suzuki

Kanta Suzuki received his bachelor's degree in Science from University of Hyogo in 2020. Since 2020, he has been working as a graduate student with Profs. Ken-ichi Nakayama and Mitsuharu Suzuki at Osaka University. His research work focuses on the design and synthesis of organic semiconductors for photovoltaic applications.

groups.[3–8] In general, active layers of organic photovoltaic devices (OPVs) are composed of p-type (or donor) and n-type SCs to form the p/n interface (*i.e.*, the heterojunction). The photovoltaic process in OPVs starts with light absorption by either the p- or n-type material to form excitons, which then diffuse into the p/n interface and form a charge transfer (CT) state. The CT state is generated by the electron or hole transfer process between the p- and n-type materials, and in an ideal sequence these CT states dissociate into free electrons and holes to be transported towards and extracted at the respective electrodes. Thus, strong light absorption over a wide range of wavelengths and efficient generation of CT states at the p/n interface, which can both be achieved by tuning the molecular orbital (MO) energy level, are the main concerns in designing SCs for OPVs. This MO tuning is mainly linked to the structure of π-backbones.

Another critical concern is related to the morphology of active layers.[9–13] Herein, the term 'morphology' is defined as a wide range of structural factors of active layers including molecular orientation and intermolecular arrangement, domain size, crystallinity, and surface topology. The current state-of-the-art OPVs are primarily designed to possess a solution-processed active layer of the bulk-heterojunction (BHJ) type, which is prepared from a blend solution of p- and n-type compounds to form microscale phase separation with a large heterojunction area.[13–15] The morphology of BHJ active layers affects essentially all aspects of the photovoltaic process from light absorption to charge-carrier extraction. For example, the phase-separation characteristics (*e.g.*, size, connectivity, and purity of domains) determine the behavior of excitons and charge carriers. Therefore, optimization of the BHJ morphology is a prerequisite for achieving the highest possible PCE. In relation to this, not only the resultant morphology, but also its evolution is a critical target of study, making the *in situ* morphology analysis during deposition of BHJ layers increasingly common in the development of OPVs.[16–18]

The intrinsic morphological properties of SCs can be tuned through modification of substituents on π-conjugated backbones; accordingly, substituent engineering has become a routine in the development of new OPV SCs. Note that actual morphological outcomes are also affected by extrinsic factors such as deposition conditions, annealing conditions, and the nature of the combined material(s) in target BHJ films. Additionally, substituents are, in most cases, also responsible for solution processability of SCs, and the need for solubilization is highly dependent on the structure of π-backbones. Hence, substituents must be optimized on a case-by-case basis, which makes the substituent engineering of OPV SCs quite complex and hard to generalize.

With this background in mind, this Review aims to provide a broad picture of substituent impact by overviewing recent prominent studies. We focus on the studies that directly compared the photovoltaic performance of small-molecule (SM) SCs with different substituents. Readers interested in the substituent impact among polymer SCs are referred to previous reviews and several recent papers on that topic.[19–27] Also note that the substituents compared in this Review are limited to those intended mainly for the modulation of morphological behavior of SMSCs rather than the modulation of their electronic characteristics at the molecular level. As such, studies on the 'halogen impact' are not covered in this Review, although it affects the BHJ morphology to a certain degree.[28–33] The following sections overview substituent impact on different types of SMSMs in the order of (1) phthalocyanines, (2) porphyrins, (3) perylene diimide derivatives,

Taehyun Won

Taehyun Won is an undergraduate student in the Chemistry-Biology Combined Major Program (CBCMP) at Osaka University. His research interests involve organic semiconductors, including new-generation OLEDs and device fabrication methods.

Hiroko Yamada

Hiroko Yamada received her PhD degree in 1992 from Kyoto University, under the guidance of Prof. Kazuhiro Maruyama and Prof. Atsuhiro Osuka. In 1993, she did her research under Prof. Michael R. Wasielewski in Argonne National Laboratory, USA as a JSPS Research Fellow. After working in Ciba–Geigy Ltd. and Ciba Specialty Chemicals Inc., she was a post-doctoral researcher in Osaka University. Since 2003, she was an associate professor in the group of Prof. Noboru Ono in Ehime University, and moved to an associate professor of Nara Institute of Science and Technology in 2011. She was promoted to a full professor at NAIST in 2012. In 2006–2010, she was a researcher of PRESTO, JST. She received the Japanese Photochemistry Association Award in 2012 and Chemical Society of Japan Award for Creative Work in 2018. Her current research interests include design, synthesis, morphology control of organic functional materials.

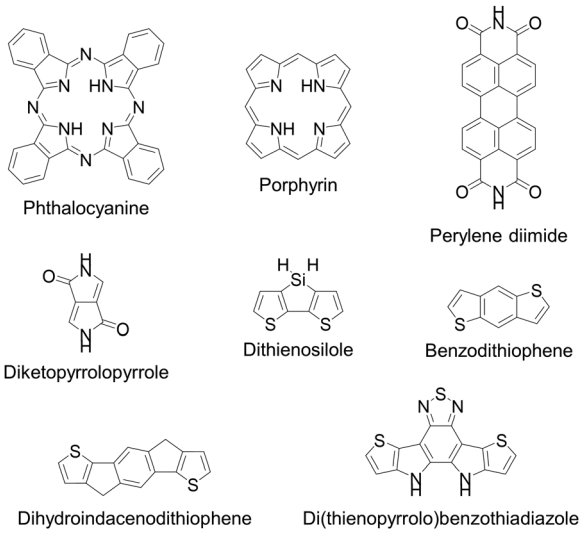

Fig. 1 Structures of the π-conjugated core units discussed in this review.

(4) diketopyrrolopyrrole derivatives, (5) dithienosilole, (6) benzodithiophene-based systems, (7) indacenodithiophene-based systems (8) di(thienopyrrolo)benzothiadiazole-based core, and (9) other systems (Fig. 1). Finally, we conclude with prospects regarding the substituent design of SMSCs for OPV applications.

2. Substituents of phthalocyanines

Phthalocyanine (H_2Pc) is a prototypical organic dye having a two-dimensionally extended π-conjugated framework associated with excellent stability and high light absorptivity. These characteristics naturally prompted the use of this dye in optoelectronic applications; indeed, pristine H_2Pc and a Cu(II) complex (CuPc) were used as p-type SMSCs in the earliest examples of heterojunction OPVs.[34,35] Thereafter, H_2Pc and its derivatives were used in a number of studies for elucidating the working mechanism of OPVs and improving device efficiencies.[36] This section overviews substituent impact on this class of compounds. The chemical structures of the relevant compounds and the corresponding photovoltaic data are summarized in Fig. 2 and Table 1, respectively.

Derivatives used as p-type materials

Non-substituted H_2Pc is essentially insoluble, and flexible alkyl chains are commonly appended on the benzo units to make it compatible with solution processing. In 2013, Dao and co-workers compared a series of liquid crystalline 1,4,8,11,15,18,22,25-octa(*n*-alkyl)phthalocyanines **1-1a–e** to identify the optimal length of linear alkyl substituents.[37] These compounds were evaluated as p-type materials in BHJ OPVs in combination with $PC_{71}BM$ as an n-type material. The results clearly showed the superiority of shorter alkyl chains over longer ones (entries 1-1–1-5). Specifically,

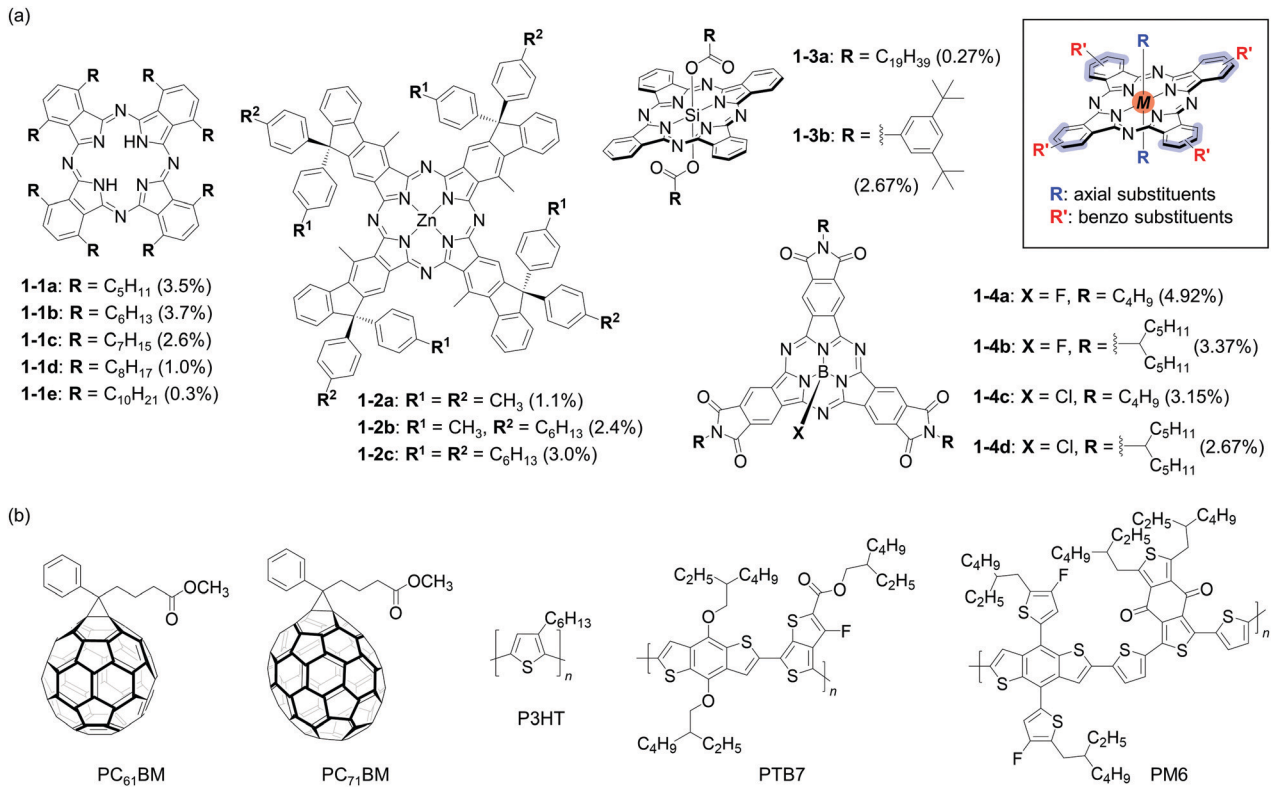

Fig. 2 Chemical structures of (a) SMSCs **1-1-1-4** and (b) the compounds employed with **1-1-1-4** in OPV active layers. The best PCEs obtained with each phthalocyanine derivative are shown in parentheses (see Table 1 for full OPV parameters). The inset shows relevant substitution positions of the phthalocyanine core.

Table 1 Photovoltaic performance of SMOCs **1-1-1-4**[a]

Entry	Active layer	Solvent	Additional conditions	V_{OC}[b] (V)	J_{SC}[b] (mA cm^{-2})	FF[b] (%)	PCE[b] (%)	Ref.
1-1	**1-1a** : $PC_{71}BM$ (3 : 2)	CF	0.2 vol% DIO	0.77	9.5	48	3.5	37
1-2	**1-1b** : $PC_{71}BM$ (3 : 2)	CF	0.2 vol% DIO	0.73	9.6	53	3.7	37
1-3	**1-1c** : $PC_{71}BM$ (3 : 2)	CF	0.2 vol% DIO	0.69	7.8	42	2.6	37
1-4	**1-1d** : $PC_{71}BM$ (3 : 2)	CF	0.2 vol% DIO	0.67	4.1	35	1.0	37
1-5	**1-1e** : $PC_{71}BM$ (3 : 2)	CF	0.2 vol% DIO	0.65	1.4	28	0.3	37
1-6	P3HT : $PC_{61}BM$: **1-2a** (1 : 1 : 0.11)	CB	145 °C, 10 min	0.49	7.9	28	1.1	39
1-7	P3HT : $PC_{61}BM$: **1-2b** (1 : 1 : 0.11)	CB	145 °C, 10 min	0.58	10.5	39	2.4	39
1-8	P3HT : $PC_{61}BM$: **1-2c** (1 : 1 : 0.11)	CB	145 °C, 10 min	0.60	10.7	46	3.0	39
1-9	PTB7 : **1-3a** (1 : 1.5)	CF	100 °C, 10 min	1.00	0.60	45	0.27	40
1-10	PTB7 : **1-3b** (1 : 1.5)	CF	100 °C, 10 min	1.03	6.18	42	2.67	40
1-11	PM6 : **1-4a** (1 : 1)	CB	0.5% DIO; 100 °C, 10 min	0.84	9.69	60	4.92	41
1-12	PM6 : **1-4b** (1 : 1)	CB	0.5% DIO; 100 °C, 10 min	0.96	7.44	47	3.37	41
1-13	PM6 : **1-4c** (1 : 1)	CB	0.5% DIO; 100 °C, 10 min	0.82	7.19	53	3.15	41
1-14	PM6 : **1-4d** (1 : 1)	CB	0.5% DIO; 100 °C, 10 min	0.89	6.4	46	2.67	41

[a] Structures of active-layer compounds are shown in Fig. 2. CF: chloroform, CB: chlorobenzene, DIO: 1,8-diiodooctane. [b] Data of the best-performing devices.

the pentyl and hexyl derivatives **1-1a** and **1-1b** yielded PCEs of 3.5% and 3.7%, respectively, while the decyl derivative **1-1e** gave a PCE of 0.3%. The PCEs obtained with the heptyl and octyl derivatives **1-1c** and **1-1d** were 2.6% and 1.0%. Based on X-ray diffraction (XRD) data, the authors suggested that columnar stacks of **1-1a** and **1-1b** adopted a pseudo-hexagonal packing, while those of **1-1c–e** formed 2D rectangular structures. This alkyl-length dependent variation in the packing motif may be the reason for the considerable difference in hole mobility (μ_h = 0.15 and 0.81 cm^2 V^{-1} s^{-1} for **1-1a** and **1-1b**; 0.03 and 0.02 m^2 V^{-1} s^{-1} for **1-1d** and **1-1e** by the time-of-flight method), and thus in J_{SC} and FF (Table 1).

In the following year, the same group reported an extension of this work to a ternary system in which a mixture of **1-1a** and **1-1b** was used as the p-type material in BHJ OPVs with phenyl-C_{61}-butylic acid methyl ester ($PC_{61}BM$) as the n-type material (data not shown in Table 1).[38] It turned out that the 25 : 75 mol% mixture of **1-1a** and **1-1b** afforded a PCE of 3.8%, working better than pure **1-1a** (PCE = 1.4%) or **1-1b** (3.1%). The improved performance of the mixture was attributed to the decreased crystallite size and balanced mobilities between holes and electrons in the BHJ active layer.

Derivatives used as co-sensitizers

The impact of linear alkyl chains was also examined with a π-extended phthalocyanine. Yamamoto and Kimura compared a series of Zn(II) fluorenocyanines **1-2a–c** as the third component in ternary BHJ OPVs (entries 1-6–1-8).[39] The frontier-orbital energy levels of **1-2a–c** were thought to allow all these compounds to work as a co-sensitizer in the BHJ system comprising poly(3-hexyl)thiophene (P3HT) and $PC_{61}BM$; however, improvement in PCE was confirmed only with the octahexyl derivative **1-2c** (3.0% and 2.6% for devices with and without **1-2c**, respectively). Indeed, PCE decreased when octamethyl derivative **1-2a** or tetrahexyltetramethyl derivative **1-2b** was doped to P3HT:$PC_{61}BM$ films (1.1% and 2.4%). The authors concluded that this observation was due to unfavourable aggregation of **1-2a** and **1-2b** in the BHJ films, based on light absorption spectra and surface topology observed using an atomic force microscope (AFM). Thus, regardless of the presence of large substituents perpendicular to the main π-framework, impact of linear alkyl chains was noticeable.

Derivatives used as n-type materials

Phthalocyanines can form complexes with various main-group or transition-metal ions, enabling the facile modulation of electronic and optoelectronic characteristics of their π-conjugated systems. Additionally, the inserted ions of these complexes provide additional sites for structural modification. The group attached to these ions generally occupies the axial position of a macrocyclic π-framework and influences intermolecular π–π interactions and photovoltaic processes. In this context, silicon phthalocyanine derivatives **1-3a** and **1-3b** reported by Zysman-Colman and co-workers showed a significantly different performance as n-type materials in BHJ OPVs.[40] When used with a p-type polymer PTB7, bis(eicosanoate) **1-3a** afforded a PCE of merely 0.27%, while bis(3,5-di-*t*-butylbenzoate) **1-3b** gave a one-order higher value of 2.67% (entries 1-9 and 1-10). This large difference in PCE could be almost fully ascribed to the difference in J_{SC} (0.60 *vs.* 6.18 mA cm^{-2}), and the authors speculated that the lower J_{SC} with **1-3a** was due to the deterioration of charge-carrier mobility caused by the insulating eicosanoate groups.

Huang *et al.* reported in 2019 a systematic evaluation of subphthalocyanine triimides with different groups on the imide nitrogen and central boron atoms.[41] They directly compared compounds **1-4a–d** as n-type materials in BHJ OPVs containing PM6 (PBDBT-2F or PBDB-TF) as the p-type material (entries 1-11–1-14). Among these four compounds, the *B*-fluoro/*N*-butyl derivative **1-4a** worked best yielding a 4.92% PCE. When its three butyl groups were all replaced with significantly larger 1-pentylhexyl groups (**1-4b**), PCE decreased to 3.37% mainly due to the large drop in J_{SC} from 9.69 to 7.44 mA cm^{-2}. The same tendency was observed also for chlorides **1-4c** and **1-4d**; namely, a higher J_{SC} and PCE were obtained with the butyl derivative (7.19 mA cm^{-2} and 3.15%) than the 2-pentylhexyl derivative (6.4 mA cm^{-2} and 2.67%). In contrast to the cases of **1-1** and **1-3** series, the alkyl-size dependency in the **1-4** series exists as an outlier because the bulkier 1-pentylhexyl group

afforded higher electron mobilities (μ_e) and better hole/electron mobility ratios (μ_e/μ_e) (μ_e = 1.39 × 10^{-5}, 5.07 × 10^{-5}, 7.76 × 10^{-6}, 4.70 × 10^{-5} cm^2 V^{-1} s^{-1} and μ_e/μ_e = 13.38, 10.10, 19.72, 9.91 for **1-4a–d**, respectively), which usually lead to higher J_{SC} and FF, thus higher PCE.

As exemplified by the **1-3** and **1-4** series, axial groups on the central atom of (sub)phthalocyanine complexes can effectively attenuate the excessive aggregation of molecules, so that relatively small substituents may suffice the need for achieving adequate solution processability and miscibility in BHJ layers. Such molecular design is unique to this class of compounds; on the other hand, covalent conjugation with other π-frameworks is scarce for phthalocyanines largely due to their unfeasibility to have *meso* substituents. The latter is in contrast quite common with porphyrins as described in the next section.

3. Substituents of porphyrin derivatives

The parent porphyrin (porphine) has a cyclic π-conjugated framework comprising four pyrrole(-like) units linked *via* methine bridges. The methine units can serve as substitution points, enabling an essentially different mode of derivatization (*i.e.*, *meso* substitution) as compared with phthalocyanines. The structure and arrangement of *meso* substituents are indeed crucial factors in tuning the solid-state packing and properties of porphyrin-based molecules.[42–44] This section overviews substituent impact on porphyrin-based SMSCs. The chemical structures of the relevant compounds and the corresponding photovoltaic data are summarized in Fig. 3, 4 and Table 2.

Derivatives used as p-type materials

Matsuo *et al.* investigated the difference between stereoisomers of 2 : 2 hetero-substituted Mg(II) porphyrins **2-1a** and **2-1b** as p-type materials in BHJ OPVs (entries 2-1–2-7).[45] The *cis*-isomer **2-1a** showed relatively low PCEs (1.5% at best), but the device performance was rather independent of the p : n-ratio between 1 : 2 and 1 : 4. In contrast, the *trans*-isomer **2-1b** gave a relatively high PCE of 2.5% at best, while the PCE is more strongly dependent on the p : n-ratio when compared with the case of **2-1a**.

So far, the most common molecular design of porphyrin-based SMSCs for OPVs is the *trans*-type fourfold *meso* substitution. The π-conjugation is extended mainly along one axis to tune the frontier-orbital energy levels and to achieve a wide light-absorption range, while the other two *meso* positions are typically substituted with bulky or flexible groups to control the molecular arrangement in active layers. According to this design, Wang and co-workers synthesized three acceptor–donor–acceptor (A–D–A) conjugates **2-2a–c** with Zn(II) porphyrin and 3-ethylrhodanine as the D and A units, respectively.[46] The three conjugates were different in the 5,15-substituents of the porphyrin core: 3,5-di(dodecyloxyl)phenyl for **2-2a**, 4-dodecyloxylphenyl for **2-2b**, and 1-hexylnonyl for **2-2c**. Among these compounds, **2-2c** performed the best as a p-type material in BHJ OPVs with the n-type $PC_{71}BM$, affording a PCE of 5.20% at best, while **2-2a** and **2-2b** gave lower PCEs of 3.21% and 5.07%, respectively, under the same conditions (entries 2-8–2-10). Note that the device with **2-2c** was further improved to show 7.70% PCE after optimizing the p:n-ratio and annealing conditions. The authors suggested that the alkyl substituents of **2-2c** are superior to the perpendicular aromatic substituents of **2-2a** and **2-2b** in terms of providing adequate miscibility with $PC_{71}BM$ and allowing effective intermolecular π–π-stacking. This suggestion was supported by the lower surface roughness and higher hole mobility for the **2-2c**:$PC_{71}BM$ blend than **2-2a**:$PC_{71}BM$ and **2-2b**:$PC_{71}BM$.

In 2018, the same group reported two modified derivatives of the A–D–A system comprising Zn(II) porphyrin and 3-ethylrhodanine (**2-3a** and **2-3b**).[47] The structural difference of these derivatives is only in the substituents on the phenylene moieties: hexylthio for **2-3a** and hexyl for **2-3b**. However, the difference in performance as p-type materials in OPVs was profound: while **2-3a** afforded an excellent PCE of 8.04%, **2-3b** gave only a 5.86% PCE (entries 2-11 and 2-12). The superiority of **2-3a** was attributed to its ability to self-assemble into J-aggregates through intermolecular S···S interactions. In contrast, compound **2-3a** without sulphur atoms did not show preferential formation of a specific self-assembly. It is worth pointing out that such relatively weak interactions can induce a drastic change in the arrangement of large π-conjugated frameworks in BHJ blended films.

Substituent impact for another type of porphyrin-based A–D–A system was reported by Ogumi *et al.* in 2017 (entries 2-13–2-17).[48] They replaced the two triisopropylsilyl (TIPS) groups of tetraethynylporphyrin **2-1b** with dithienyldiketopyrrolopyrrole (DPP) in order to enhance the light absorption capability, and introduced three different substituents (hexylphenyl, trifluoromethylphenyl, or dimethylaminophenyl) at the 4-positions of the two phenyl groups in order to modulate the morphological behaviour and frontier-orbital energies. Among the four derivatives **2-4a–d** (including one without substituents on the phenyl rings), the 4-hexylphenyl derivative **2-4b** worked best as a p-type material in BHJ OPVs with $PC_{61}BM$, affording a reasonably high PCE of 4.83%. Compound **2-4b** was found to afford a higher FF of 57% as compared to the non-substituted derivative **2-4a** (FF = 49%), probably due to a higher degree of phase separation and thus more efficient charge-carrier transport (entries 2-13 and 2-14). Indeed, this advantage allowed **2-4b** to afford an improved PCE of 5.73% in a thicker active layer deposited from a 30 mg mL^{-1} solution instead of the original 20 mg mL^{-1} solution (entry 2-15). The electron-withdrawing trifluoromethyl groups of **2-4c** and the electron-donating dimethylamino groups of **2-4d** affected the V_{OC} as expected from the corresponding changes in the energy level of the highest-occupied MOs (HOMOs); however, a positive impact on the overall photovoltaic process was not observed with these derivatives (PCEs were 1.65% and 2.33% with **2-4c** and **2-4d**, respectively, when the active layers were deposited from a 20 mg mL^{-1} solution; entries 2-16 and 2-17).

Soon after, the same group expanded the scope of structural screening of the Mg(II) porphyrin–DPP conjugate system to include asymmetrically substituted molecules **2-4e–h** (entries 2-18–2-21).[49] This study confirmed that asymmetric

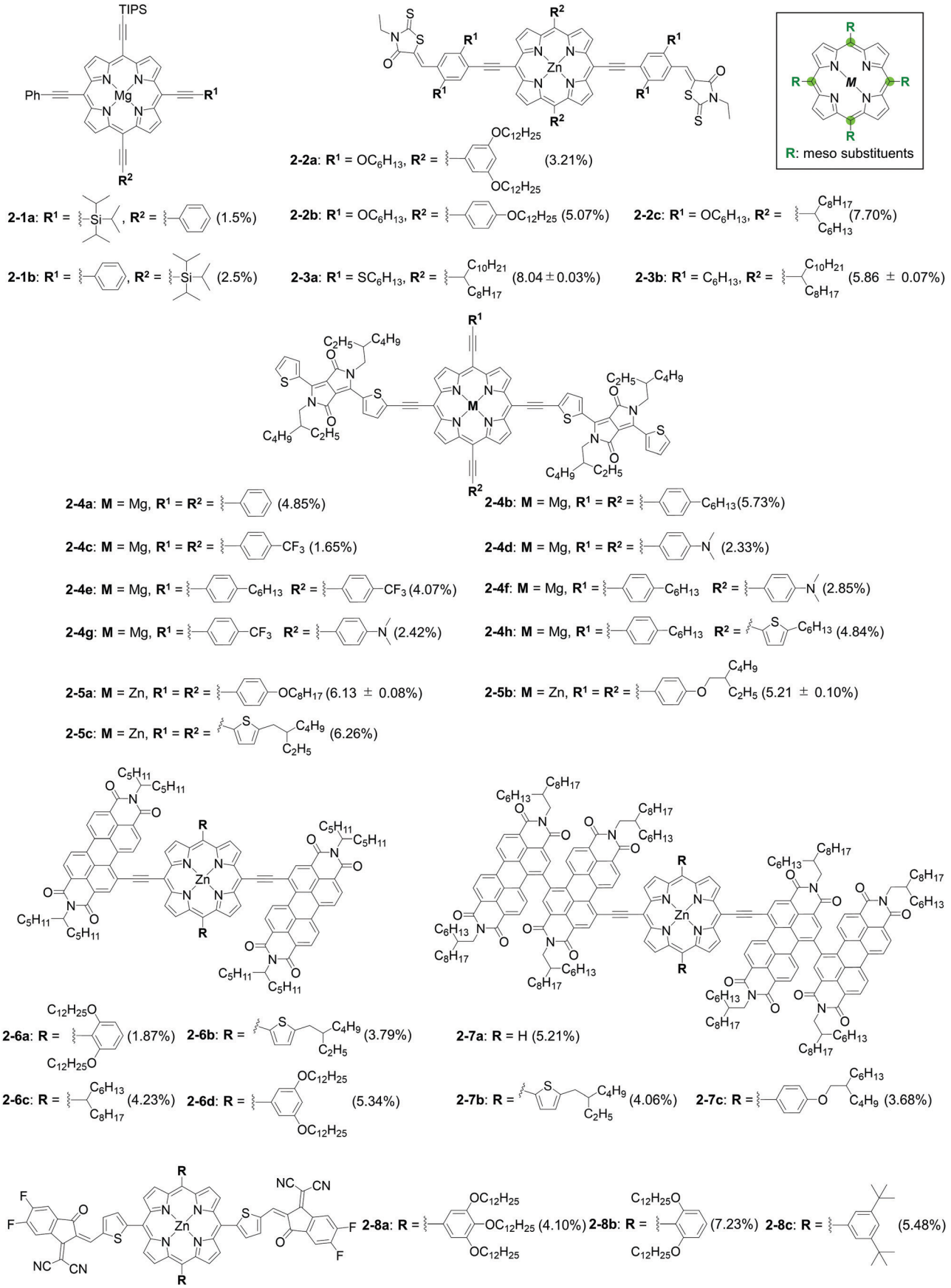

Fig. 3 Chemical structures of SMSCs **2-1-2-8**. The best PCEs obtained with each compound are shown in parentheses (see Table 2 for full OPV parameters). The inset shows relevant substitution positions of the porphyrin core.

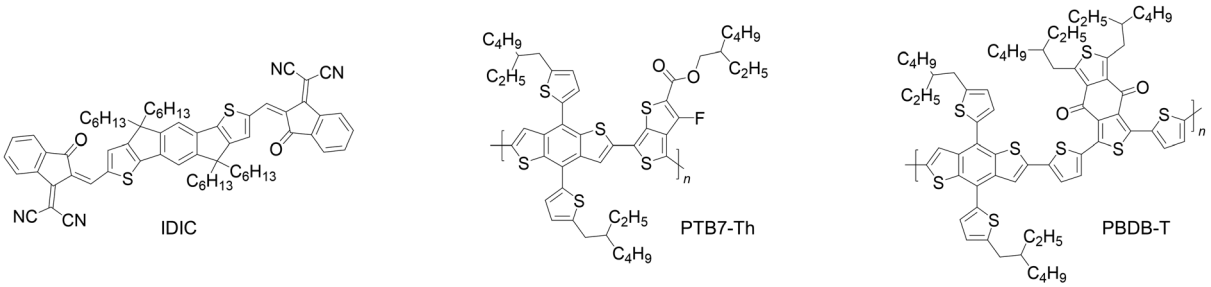

Fig. 4 Chemical structures of the compounds employed with **2-1-2-7** in OPV active layers. $PC_{61}BM$ and $PC_{71}BM$ are shown in Fig. 2.

Table 2 Photovoltaic performance of SMSCs **2-1-2-8**[a]

Entry	Active layer	Solvent	Additional conditions	V_{OC}[b] (V)	J_{SC}[b] (mA cm^{-2})	FF[b] (%)	PCE[b] (%)	Ref.
2-1	**2-1a** : $PC_{61}BM$ (1 : 2)	CB	—	0.83	4.8	36	1.4	45
2-2	**2-1a** : $PC_{61}BM$ (1 : 3)	CB	—	0.83	4.5	39	1.5	45
2-3	**2-1a** : $PC_{61}BM$ (1 : 4)	CB	—	0.85	3.9	34	1.2	45
2-4	**2-1b** : $PC_{61}BM$ (1 : 1)	CB	—	0.89	3.2	36	1.0	45
2-5	**2-1b** : $PC_{61}BM$ (1 : 3)	CB	—	0.89	4.5	42	1.7	45
2-6	**2-1b** : $PC_{61}BM$ (1 : 4)	CB	—	0.92	6.4	41	2.5	45
2-7	**2-1b** : $PC_{61}BM$ (1 : 5)	CB	—	0.91	5.8	40	2.1	45
2-8	**2-2a**/$PC_{71}BM$ (1 : 1)	CB	1% Py; 90 °C, 10 min	0.90	7.20	48.12	3.21	46
2-9	**2-2b**/$PC_{71}BM$ (1 : 1)	CB	1% Py; 90 °C, 10 min	0.90	10.14	55.60	5.07	46
2-10	**2-2c**/$PC_{71}BM$ (1 : 1)	CB	1% Py; 90 °C, 5 min	0.91	13.32	63.60	7.70	46
2-11	**2-3a** : $PC_{71}BM$ (1 : 1.2)	CB	2 vol% Py; 100 °C, 5 min; THF vapour 20 s	0.91 ± 0.01	13.19 ± 0.04	66.70 ± 0.01	8.04 ± 0.03	47
2-12	**2-3b** : $PC_{71}BM$ (1 : 1.2)	CB	2 vol% Py; 100 °C, 5 min; THF vapour 20 s	0.87 ± 0.01	11.53 ± 0.07	58.50 ± 0.03	5.86 ± 0.07	47
2-13	**2-4a** : $PC_{61}BM$ (1 : 1.5)	CB	1% Py, 20 mg mL^{-1}	0.74	13.27	49	4.85	48
2-14	**2-4b** : $PC_{61}BM$ (1 : 1.5)	CB	1% Py, 20 mg mL^{-1}	0.70	12.04	57	4.83	48
2-15	**2-4b** : $PC_{61}BM$ (1 : 1.5)	CB	1% Py, 30 mg mL^{-1}	0.69	14.80	56	5.73	48
2-16	**2-4c** : $PC_{61}BM$ (1 : 1.5)	CB	1% Py, 20 mg mL^{-1}	0.79	4.61	45	1.65	48
2-17	**2-4d** : $PC_{61}BM$ (1 : 1.5)	CB	1% Py, 20 mg mL^{-1}	0.52	9.19	48	2.33	48
2-18	**2-4e** : $PC_{61}BM$ (1 : 1.5)	CB	1% Py; THF vapour 20 s	0.73	12.01	47	4.07	49
2-19	**2-4f** : $PC_{61}BM$ (1 : 1.5)	CB	—	0.60	12.26	39	2.85	49
2-20	**2-4g** : $PC_{61}BM$ (1 : 1.5)	CB	100 °C, 10 min	0.63	10.02	38	2.42	49
2-21	**2-4h** : $PC_{61}BM$ (1 : 1.5)	CB	80 °C, 10 min	0.69	14.86	47	4.84	49
2-22	**2-5a** : IDIC (1 : 1.2)	CF	0.8 vol% DIO, 0.5 vol% Py	0.71 ± 0.01	15.46 ± 0.19	56 ± 0	6.13 ± 0.08	50
2-23	**2-5b** : IDIC (1 : 1.2)	CF	0.8 vol% DIO, 0.5 vol% Py	0.71 ± 0.01	14.03 ± 0.34	53 ± 2	5.21 ± 0.10	50
2-24	**2-5c** : IDIC (1 : 1.2)	CF	0.8 vol% DIO, 0.5 vol% Py	0.70 ± 0.01	11.46 ± 0.01	51 ± 1	4.08 ± 0.02	50
2-25	**2-5a** : $PC_{71}BM$ (1 : 1.2)	CF	0.8 vol% DIO, 0.5 vol% Py	0.72	10.56	53	4.05	50
2-26	**2-5b** : $PC_{71}BM$ (1 : 1.2)	CF	0.8 vol% DIO, 0.5 vol% Py	0.70	8.64	50	2.98	50
2-27	**2-5c** : $PC_{71}BM$ (1 : 1.2)	CF	0.8 vol% DIO, 0.5 vol% Py	0.69	14.54	62	6.26	50
2-28	PBDB-T : **2-6a** (1 : 1)	CB	10 vol% Py	0.88 ± 0.01	4.10 ± 0.01	49 ± 1	1.87 (Av. 1.78)	51
2-29	PBDB-T : **2-6b** (1 : 1)	CB	10 vol% Py	0.79 ± 0.00	9.56 ± 0.12	50 ± 2	3.79 (Av. 3.75)	51
2-30	PBDB-T : **2-6c** (1 : 1)	CB	10 vol% Py	0.80 ± 0.01	9.48 ± 0.06	53 ± 2	4.23 (Av. 3.99)	51
2-31	PBDB-T : **2-6d** (1 : 1)	CB	10 vol% Py	0.81 ± 0.01	11.02 ± 0.64	58 ± 1	5.34 (Av. 5.07)	51
2-32	PTB7-TH : **2-7a** (1 : 1.5)	CB	0.5% Py	0.66	13.54	58.29	5.21	52
2-33	PTB7-TH : **2-7b** (1 : 1.5)	CB	0.5% Py	0.67	10.55	57.15	4.06	52
2-34	PTB7-TH : **2-7c** (1 : 1.5)	CB	0.5% Py	0.68	9.61	56.20	3.68	52
2-35	PTB7-Th : **2-8a** (1 : 1)	CB	0.4 vol% Py; CF vapour, 5 min	0.78	9.88	53.2	4.10	53
2-36	PTB7-Th : **2-8b** (1 : 1)	CB	0.4 vol% Py; CF vapour, 5 min	0.80	13.94	64.8	7.23	53
2-37	PTB7-Th : **2-8c** (1 : 1)	CB	0.4 vol% Py; CF vapour, 5 min	0.77	12.55	56.7	5.48	53

[a] Structures of the active-layer compounds are shown in Fig. 3 and 4. CB: chlorobenzene, CF: chloroform, Py: pyridine, THF: tetrahydrofuran, DIO: 1,8-diiodooctane. [b] Data of the best-performing devices when available; otherwise, average of multiple devices.

substitution was beneficial not only for fine-tuning of the molecular electronic structure, but also for improving solubility. The latter aspect is rather important because large π-conjugated frameworks are intrinsically low in solubility and thus require extensive decollation with large, flexible, and insulating solubilizing substituents to be compatible with solution processes. However, such solubilizing groups tend to pose negative effects in terms of forming intermolecular contacts necessary for efficient carrier transport. Therefore, asymmetric substitution is an attractive approach to improve solubility without relying too much on an insulating solubilizing substituent. Among the four asymmetric derivatives, the 4-hexylphenyl/4-hexylthienyl substituted **2-4h** afforded the highest PCE of 4.84%. Indeed, this compound was found to be the most soluble in the **2-4** family, enabling the deposition of a thick active layer of 215 nm which afforded a 4.06% PCE.

Hadmojo *et al.* explored the substituent impact for an A–D–A system comprising Zn(II) porphyrin, instead of Mg(II) porphyrin of the **2-4** series mentioned above, and DPP moieties.[50] The 5,15-carbons of the central Zn(II) porphyrin were substituted with 4-octyloxyphenyl, 4-(2-ethylhexyloxy)phenyl, or 5-(2-ethylhexyloxy)-2-thienyl, and the resultant compounds **2-5a–c** were evaluated as p-type materials in BHJ OPVs with a non-fullerene acceptor IDIC. Compounds **2-5a–c** are very similar in frontier-orbital energy levels to afford essentially the same V_{OC}s of around 0.70 V (entries 2-22–2-24). On the other hand, the J_{SC} and FF largely depend on substituents: both parameters decreased in the order of **2-5a** > **2-5b** > **2-5c**. Accordingly, PCEs also decreased in the order of **2-5a** (6.13%) > **2-5b** (5.21%) > **2-5c** (4.08%). Based on the XRD data, the authors reasoned that the higher performance of **2-5a** could be attributed to the higher tendency of molecules to adopt a face-on orientation in the **2-5a**:IDIC layer. Interestingly, when $PC_{71}BM$ was employed as the n-type material, a better PCE was obtained with compound **2-5c** (6.26%) than **2-5a** (4.05%) and **2-5b** (2.98%) (entries 2-25–2-27). This result clearly demonstrates that the molecular design of organic semiconductors for BHJ layers must consider the structure of the partner compound as well.

Derivatives used as n-type materials

Another series of Zn(II) porphyrin-based A–D–A conjugates were reported by Guo *et al.* in 2018.[51] The authors used a perylene diimide (PDI) derivative as acceptor (A) units and introduced 2,6-di(dodecyloxy)phenyl, (2-ethylhexyl)thiophen-2-yl, pentadecan-7-yl, or 3,5-di(dodecyloxy)phenyl onto the central porphyrin core to obtain compounds **2-6a–d**. Note that these compounds were designed as n-type materials for OPVs, although porphyrin-based SMSCs have been commonly used as p-type materials. In BHJ OPVs with PBDB-T as the p-type material, compound **2-6a** gave a considerably low PCE of 1.87%, while the other three compounds afforded relatively similar PCEs of 3.79% (**2-6b**), 4.23% (**2-6c**), and 5.34% (**2-6d**) (entries 2-28–2-31). The authors suggested that the low PCE of **2-6a** was due to its tendency to form large crystalline domains in the BHJ layer, in addition to the negligible LUMO–LUMO offset against PBDB-T (LUMO: the lowest unoccupied MO). It is worth pointing out that the LUMO energy levels (E_{LUMO}s) of **2-6a–d** were found to be largely dependent on the substituents of the porphyrin unit, even though the LUMO was predicted by DFT to be localized on the PDI moieties (E_{LUMO} = −3.53, −3.68, −3.63, and −3.74 eV for **2-6a–d**, respectively). Pan *et al.* recently reported similar A–D–A conjugates based on Zn(II) porphyrin, but with a PDI dimer as the acceptor unit (**2-7a–c**).[52] In this case, non-substituted porphyrin in **2-7a** gave better PCEs than substituted ones in **2-7b** and **2-7c** (entries 2-32–2-34).

In addition, Tsai *et al.* reported three Zn(II) porphyrin-based A–D–A conjugates having 2-(5,6-difluoro-3-oxo-2,3-dihydro-1*H*-inden-1-ylidene)-malononitrile as the electron-accepting end group.[53] Similar to the above examples, the three conjugates **2-8a–c** are different from each other only in the structure of *meso* substituents of the central porphyrin unit; namely, 3,4,5-tridodecyloxyphenyl for **2-8a**, 2,6-didodecyloxyphenyl for **2-8b**, and 3,5-di-*tert*-butylphenyl for **2-8c**. These compounds were evaluated as n-type materials in BHJ OPVs with a p-type polymer PTB7-Th. Derivative **2-8b** was determined to be the best n-type material among the three, affording a PCE of 7.23%, while the corresponding values were 4.10% and 5.48% with **2-8a** and **2-8c**, respectively (entries 2-35–2-37). Superiority in the performance of the device with **2-8b** originated from its higher J_{SC} and FF than those of the other two derivatives, and the authors ascribed this to a slightly shorter π–π stacking distance (4.06 Å) as compared to those of the other systems (4.10 and 4.15 Å for PTB7-Th:**2-8a** and PTB7-Th:**2-8c**) as determined by the out-of-plane profiles of two-dimensional grazing-incident wide-angle X-ray scattering (2D-GIWAXS) data.

It is notable that all the porphyrin derivatives mentioned in this section were constructed by taking full advantage of *meso* substitution of the porphyrin core. These *meso* substituents were introduced either through or not through an acetylene linker depending on the need for coplanarity between the porphyrin framework and substituents. This aspect largely affects the molecular packing of the resultant compounds, and accordingly the optimal structure of peripheral substituents.

4. Substituents of perylene diimide derivatives

Perylene diimide (PDI) is characterized by its highly stable and strongly electron deficient π-conjugated framework. It is one of the most traditional SMSCs, and indeed its derivatives were employed as n-type materials in the earliest examples of heterojunction OPVs along with phthalocyanines.[34,35] Although they somewhat lost the popularity in the OPV community after the emergence of fullerene-based n-type materials, recent development of non-fullerene acceptors is built upon the consistent research efforts on the design and evaluation of new derivatives of PDI and other members in the rylene diimide family.[54–61] This section overviews substituent impact on PDI-based SMSCs. The chemical structures of the relevant compounds and the corresponding photovoltaic data are summarized in Fig. 5, 6 and Table 3, respectively.

PDI monomers

The study by Guide *et al.* in 2013 reports on the systematic evaluation of substituent impact on the photovoltaic performance of PDI derivatives.[62] The authors compared four differently substituted PDIs **3-1a–d** in solution processed planar heterojunction (PHJ) OPVs comprising tetrabenzoporphyrin (BP) as the p-type material (entries 3-1–3-4). The PHJ structure was constructed by depositing the insoluble BP *via* an indirect solution process called 'precursor approach' (see description of **4-7** in Section 5 for details), and then spin-coating one of the PDI derivatives on top of the BP layer. The highest PCE of 2.0% was obtained with the non-bay-substituted derivative **3-1a**, associated with a J_{SC} of 5.3 mA cm^{-2} and an FF of 61%. Derivative **3-1d** with relatively slim substituents (4-methylphenyethynyl) at the 1,7-positions of the perylene core gave a similar PCE of 1.7% with a J_{SC} of 4.7 mA cm^{-2} and an FF of 58%. In contrast, derivatives **3-1b** and **3-1c** with bulky substituents (4-*tert*-octylphenoxy) at the bay

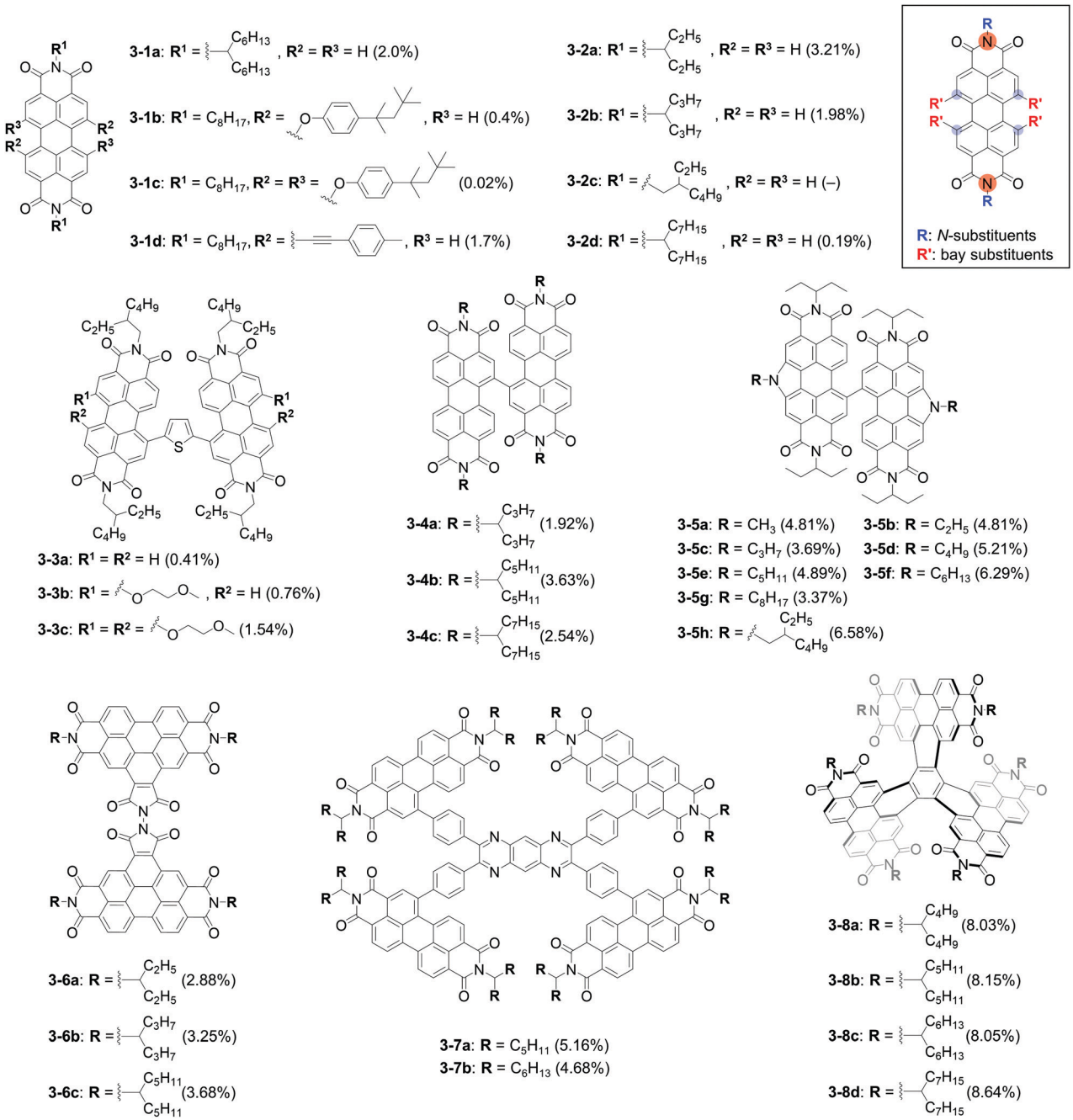

Fig. 5 Chemical structures of SMSCs **3-1**-**3-8**. The best PCEs obtained with each compound are shown in parentheses (see Table 3 for full OPV parameters). The inset shows relevant substitution positions of the PDI unit.

positions of the perylene framework afforded considerably low PCEs of 0.4% and 0.02% due to large decreases in J_{SC} and FF. This report clearly demonstrated the significance of the bay-substituent steric effects on charge transport in PDI derivatives, which is important not only in PHJ, but also in BHJ OPVs.

Sun *et al.* reported the photovoltaic performance of PDI derivatives **3-2a–d** which were different from each other in the structure of alkyl substituents on the imide nitrogens.[63] In the comparative evaluation of these PDIs, the *N*,*N*′-di(3-pentyl) derivative **3-2a** yielded the highest PCE of 3.21% when used as the n-type material in BHJ OPVs with a p-type SMSC F-DTS. Derivatives **3-2b** and **3-2d**, with 4-heptyl and 8-pentadecyl groups, respectively, afforded considerably lower PCEs of 1.98% and 0.19%, while the 2-ethylhexyl substituted derivative **3-2c** gave only negligible PCEs (entries 3-5–3-8). Thus, substitution with more compact alkyl groups resulted in higher performance in BHJ OPVs. This observation is consistent with the above-mentioned case of PHJ OPVs with **3-1a–d**.

Non-fused PDI oligomers

A common issue associated with PDI derivatives is their stronger tendency to (1) crystalize/aggregate and (2) induce excessive phase separation in blended films, which leads to low J_{SC}s and

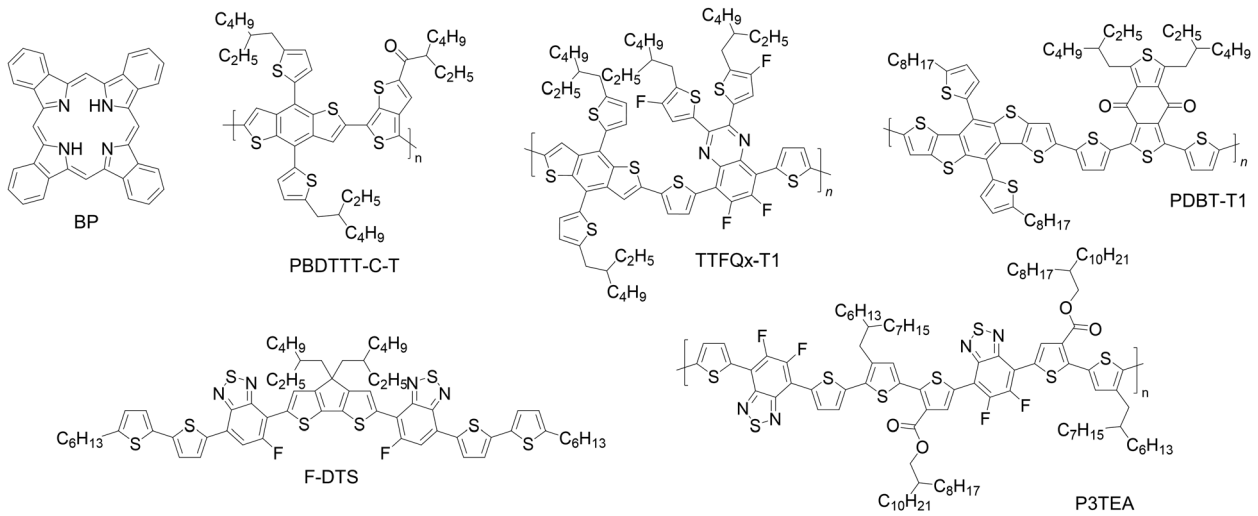

Fig. 6 Chemical structures of the compounds employed with **3-1-3-8** in OPV active layers. P3HT and PTB-7Th are shown in Fig. 2 and 4, respectively.

Table 3 Photovoltaic performance of SMSCs **3-1-3-9**[a]

Entry	Active layer	Solvent	Additional conditions	V_{OC}[b] (V)	J_{SC}[b] (mA cm^{-2})	FF[b] (%)	PCE[b] (%)	Ref.
3-1	BP/**3-1a** (50 nm/20 nm)	CF : CB = 1 : 2	180 °C, 20 min	0.62	5.3	61	2.0	62
3-2	BP/**3-1b** (50 nm/20 nm)	CF : CB = 1 : 2	180 °C, 20 min	0.74	2.2	21	0.4	62
3-3	BP/**3-1c** (50 nm/20 nm)	CF : CB = 1 : 2	180 °C, 20 min	0.64	0.2	16	0.02	62
3-4	BP/**3-1d** (50 nm/20 nm)	CF : CB = 1 : 2	180 °C, 20 min	0.64	4.7	58	1.7	62
3-5	F-DTS : **3-2a** (1 : 1)	CB	0.4 vol% DIO	0.75	8.09	53	3.21	63
3-6	F-DTS : **3-2b** (1 : 1)	CB	0.4 vol% DIO	0.75	5.88	45	1.98	63
3-7	F-DTS : **3-2c** (1 : 1)	CB	0.4 vol% DIO	0.00	0.42	—	—	63
3-8	F-DTS : **3-2d** (1 : 1)	CB	0.4 vol% DIO	0.32	1.52	38	0.19	63
3-9	P3HT : **3-3a** (1 : 1)	*o*-DCB	3 wt% CN	0.43	2.01	47.2	0.41	65
3-10	P3HT : **3-3b** (1 : 1)	*o*-DCB	8 wt% CN	0.59	2.89	44.8	0.76	65
3-11	P3HT : **3-3c** (1 : 1)	*o*-DCB	1.75 wt% CN	0.67	3.83	60.0	1.54	65
3-12	PBDTTT-C-T : **3-4a** (1 : 1)	*o*-DCB	3 vol% DIO	0.67	6.68	42.94	1.92	66
3-13	PBDTTT-C-T : **3-4b** (1 : 1)	*o*-DCB	3 vol% DIO	0.72	10.36	42.08	3.11	66
3-14	PBDTTT-C-T : **3-4c** (1 : 1)	*o*-DCB	3 vol% DIO	0.72	8.86	39.75	2.54	66
3-15	PBDTTT-C-T : **3-4b** (1 : 1)	*o*-DCB	1.5 vol% CN + 1.5 vol% DIO	0.73	10.58	46.80	3.63	66
3-16	PTB7-Th : **3-5a** (3 : 7)	2Me-THF	—	0.911 ± 0.003	11.10 ± 0.20	42 ± 3	4.81 (4.27 ± 0.28)	67
3-17	PTB7-Th : **3-5b** (3 : 7)	2Me-THF	—	0.949 ± 0.003	11.41 ± 0.65	43 ± 2	4.81 (4.64 ± 0.10)	67
3-18	PTB7-Th : **3-5c** (3 : 7)	2Me-THF	—	0.949 ± 0.008	8.99 ± 0.57	35 ± 1	3.69 (2.99 ± 0.23)	67
3-19	PTB7-Th : **3-5d** (3 : 7)	2Me-THF	—	0.939 ± 0.009	12.50 ± 0.64	41 ± 3	5.21 (4.77 ± 0.24)	67
3-20	PTB7-Th : **3-5e** (3 : 7)	2Me-THF	—	0.964 ± 0.001	11.41 ± 0.45	42 ± 3	4.89 (4.62 ± 0.13)	67
3-21	PTB7-Th : **3-5f** (3 : 7)	2Me-THF	—	0.957 ± 0.004	12.08 ± 0.86	45 ± 2	5.55 (5.16 ± 0.14)	67
3-22	PTB7-Th : **3-5g** (3 : 7)	2Me-THF	—	0.910 ± 0.005	7.46 ± 0.32	41 ± 2	3.37 (2.80 ± 0.27)	67
3-23	PTB7-Th : **3-5h** (3 : 7)	2Me-THF	—	0.956 ± 0.005	12.41 ± 0.74	45 ± 2	5.47 (5.33 ± 0.10)	67
3-24	PTB7-Th : **3-5h** (4 : 6)	2Me-THF	0.25 vol% DIO	0.955 ± 0.003	15.36 ± 0.37	43 ± 1	6.58 (6.24 ± 0.19)	67
3-25	TTFQx-T1 : **3-5f** (4 : 6)	2Me-THF	180 °C, 10 min	1.034	12.47	48.8	6.29	68
3-26	PTB7-Th : **3-6a** (1 : 1)	CB	—	0.78	8.40	45.2	2.88	69
3-27	PTB7-Th : **3-6b** (1 : 1)	CB	—	0.79	7.73	53.1	3.25	69
3-28	PTB7-Th : **3-6c** (1 : 1)	CB	—	0.80	9.94	46.4	3.68	69
3-29	P3TEA : **3-7a** (1 : 1.5)	1,2,4-TMB	2.5% DIO	1.02 ± 0.00	10.27 ± 0.37	47 ± 2	5.16 (4.92 ± 0.11)	70
3-30	P3TEA : **3-7b** (1 : 1.5)	1,2,4-TMB	2.5% DIO	1.02 ± 0.00	9.20 ± 0.14	47 ± 3	4.68 (4.40 ± 0.26)	70
3-31	PDBT-T1 : **3-8a** (1 : 1)	*o*-DCB	0.25% DIO; 100 °C, 5 min	0.963 ± 0.005	12.22 ± 0.19	67.8 ± 0.7	8.03 (7.97 ± 0.05)	74
3-32	PDBT-T1 : **3-8b** (1 : 1)	*o*-DCB	0.25% DIO; 100 °C, 5 min	0.968 ± 0.004	12.17 ± 0.25	68.1 ± 1.4	8.15 (8.02 ± 0.14)	74
3-33	PDBT-T1 : **3-8c** (1 : 1)	*o*-DCB	0.25% DIO; 100 °C, 5 min	0.976 ± 0.006	12.20 ± 0.20	66.7 ± 1.1	8.05 (7.94 ± 0.10)	74
3-34	PDBT-T1 : **3-8d** (1 : 1)	*o*-DCB	0.25% DIO; 100 °C, 5 min	0.981 ± 0.003	12.58 ± 0.19	69.2 ± 0.3	8.64 (8.54 ± 0.09)	74

[a] Structures of active-layer compounds are shown in Fig. 5 and 6. CF: chloroform, CB: chlorobenzene, *o*-DCB: *o*-dichlorobenzene, 2Me-THF: 2-methyltetrahydrofuran; 1,2,4-TMB: 1,2,4-trimethylbenzene, DIO: 1,8-diiodooctane; CN: chloronaphthalene. [b] Data of the best-performing devices when available; otherwise, average of multiple devices.

FFs of the resulting BHJ OPVs.[64] This issue can be circumvented by linking a pair of PDI cores at their bay-positions to form a twisted dimer. In 2013, Lu and co-workers reported PDI dimers with a thienylene bridge (**3-3a–c**).[65] The dihedral angles between the PDI and thienylene units were estimated to be as large as 50–65° by density-functional theory (DFT) calculations.

The authors introduced different numbers of 2-methoxyethoxy substituents on such a twisted π-framework and studied their effect on the performance of BHJ OPVs with P3HT as the p-type material. The PCE was found to improve with the number of 2-methoxyethoxy groups: 0.41% with non-substituted **3-3a**, 0.76% for di-substituted **3-3b**, and 1.54% for tetra-substituted **3-3c** (entries 3-9–3-11). The most favorable performance from **3-3c** was explained by the adequate degree of phase separation resulting from the four solvophobic 2-methoxylethoxy groups.

PDI dimers can be constructed by linking monomers directly at bay positions. This way, the twist angle between PDI units becomes much larger as compared to that of **3-3a–c** with a thienyl linker. Accordingly, crystallization or aggregation in BHJ films can be further attenuated. Jiang *et al.* studied the substituent impact on the morphological behaviour and photovoltaic performance of such a highly twisted dimeric system. Specifically, they compared three PDI dimers **3-4a–c** having different alkyl substituents on the imide nitrogens.[66] In BHJ OPVs with PBDTTT-C-T as the p-type material, the *N*,*N*′-di(6-undecyl) derivative **3-4b** afforded a higher PCE of 3.11% than the di(4-heptyl) derivative **3-4a** (PCE = 1.92%) and di(8-pentadecyl) derivative **3-4c** (2.54%) when deposited under the same conditions (entries 3-12–3-14). PCE in the PBDTTT-C-T:**3-4b** system was further improved to 3.63% by optimizing the deposition conditions (entry 3-15). These results show that despite twist-shaped dimers' low crystallinity, peripheral alkyl groups and deposition conditions are critical.

Dayneko *et al.* synthesized a series of bridge-less PDI dimers **3-5a–h** which were *N*-annulated at the bay positions of PDI units and decollated with alkyl groups at the pyrrolic *N*-atoms.[67] Their performance as n-type materials was evaluated with PTB7-Th as the p-type material (entries 3-16–3-23). The observed photovoltaic parameters did not show an apparent trend regarding the structure of alkyl groups; nonetheless, the superiority of hexyl and 2-ethylhexyl derivatives was noticeable. Indeed, the 2-ethylhexyl derivative **3-5h** afforded a 6.58% PCE after optimization of the p:n ratio and solvent additive in the cast solution (entry 3-24). In addition, the PCE with hexyl derivative **3-5f** was improved to 6.29% when a medium band-gap polymer PPTFQx-T1 was used as the p-type material (entry 3-25).[68]

Twisted PDI dimers can also be constructed in the form of *N*–*N*-linked benzo[*ghi*]perylenetriimides. Chen *et al.* investigated the substituent effect among this class of dimers by comparing three derivatives **3-6a–c** with branched alkyl chains at the imide nitrogen atoms.[69] Their performance as n-type materials in BHJ OPVs was studied using PTB7-Th as the p-type material, wherein derivative **3-6c** with the longest alkyl chains was found to give the highest PCE of 3.68% (entries 3-26–3-28). The authors attributed the better performance of **3-6c** to the formation of finer phase separation in the BHJ active layers compared to **3-6a** and **3-6b**.

Wang *et al.* compared two *N*-alkylated PDI tetramers **3-7a** and **3-7b** as n-type materials in OPVs.[70] These tetramers have pyrazino[2,3-*g*]quinoxaline (PQ) as the core unit, to which four PDI units are linked at the bay positions through phenylene linkers. The BHJ devices with P3TEA as the p-type material showed PCEs as high as 5.16% when the *N*-6-undecyl derivative **3-7a** was used as the n-type material, while the PCE was the highest at 4.68% with the *N*-7-tridecyl derivative **3-7b** (entries 3-29 and 3-30). Namely, in contrast to the cases of dimers **3-6a–c** and trimers **3-8a–d** (see below), substitution with a shorter alkyl chain resulted in higher photovoltaic performance for this PDI tetramer system. Based on 2D-GIWAXS and AFM analyses, the authors suggested that the higher crystallinity and smaller π-stack distance in the P3TEA:**3-7a** film would have contributed to the higher J_{SC}, thereby resulting in the higher PCE as compared to P3TEA:**3-7b**.

Fused PDI oligomers

Several PDI trimers have been also designed for OPVs,[71–73] and their substituent impact was investigated as an important part of structural optimization. In 2017, Fu *et al.* reported a series of propeller-shaped PDI trimers **3-8a–d** as n-type materials in OPVs.[74] The imide nitrogens of these compounds were linked to branched alkyl chains of different lengths from 5-nonyl of **3-8a** to 8-pentadecyl of **3-8d**. In BHJ OPVs with a p-type polymer PDBT-T1, the derivative with the largest alkyl substituents (**3-8d**) afforded the highest PCE of 8.64% (entry 3-32). The other three derivatives were similar to each other in terms of the resulting PCEs: 8.03% for **3-8a**, 8.15% for **3-8b**, and 8.05% for **3-8c** (entries 3-29–3-31). The authors attributed the superior photovoltaic performance of **3-8d** over other derivatives to its higher degree of face-on orientation and a smaller domain spacing as indicated by 2D-GIWAXS and resonate soft X-ray scattering (R-SoXS) measurements, respectively.

The examples in this section highlight the fact that PDI often need both twisted molecular conformation and branched alkyl substituents, reflecting their strong tendency to aggregate. Indeed, this class of chromophores generally requires longer alkyl groups to form BHJ active layers of optimal morphology as compared to the cases of phthalocyanine and porphyrin mentioned earlier.

5. Substituents of diketopyrrolopyrrole derivatives

Diketopyrrolopyrrole (DPP) has been one of the most successful dyes as a building block for organic semiconductors.[75–79] Indeed, a ternary OPV with a DPP-based SMSC was reported to show an excellent PCE of 15.6%.[80] The study of substituent impact on the electronic and semiconducting properties has contributed greatly to the successful development of DPP-based SMSCs. The chemical structures of the relevant compounds and the corresponding photovoltaic data are summarized in Fig. 7 and Table 4, respectively.

Seo pointed out in a paper published in 2009 that the structure of alkyl substituents on lactam nitrogens exerted a considerable effect on the performance of BHJ OPVs based on the comparison between two 3,6-bis(5″-hexyl[2,2′:5′,2″-terthiophen]-5-yl)diketopyrrolopyrroles **4-1a** and **4-1b** as p-type materials;[81] specifically, *N*,*N*′-di(2-ethylhexyl) derivative **4-1a** showed a 3.0% PCE,[82] while *N*,*N*′-di(2-ethylhexyl) derivative

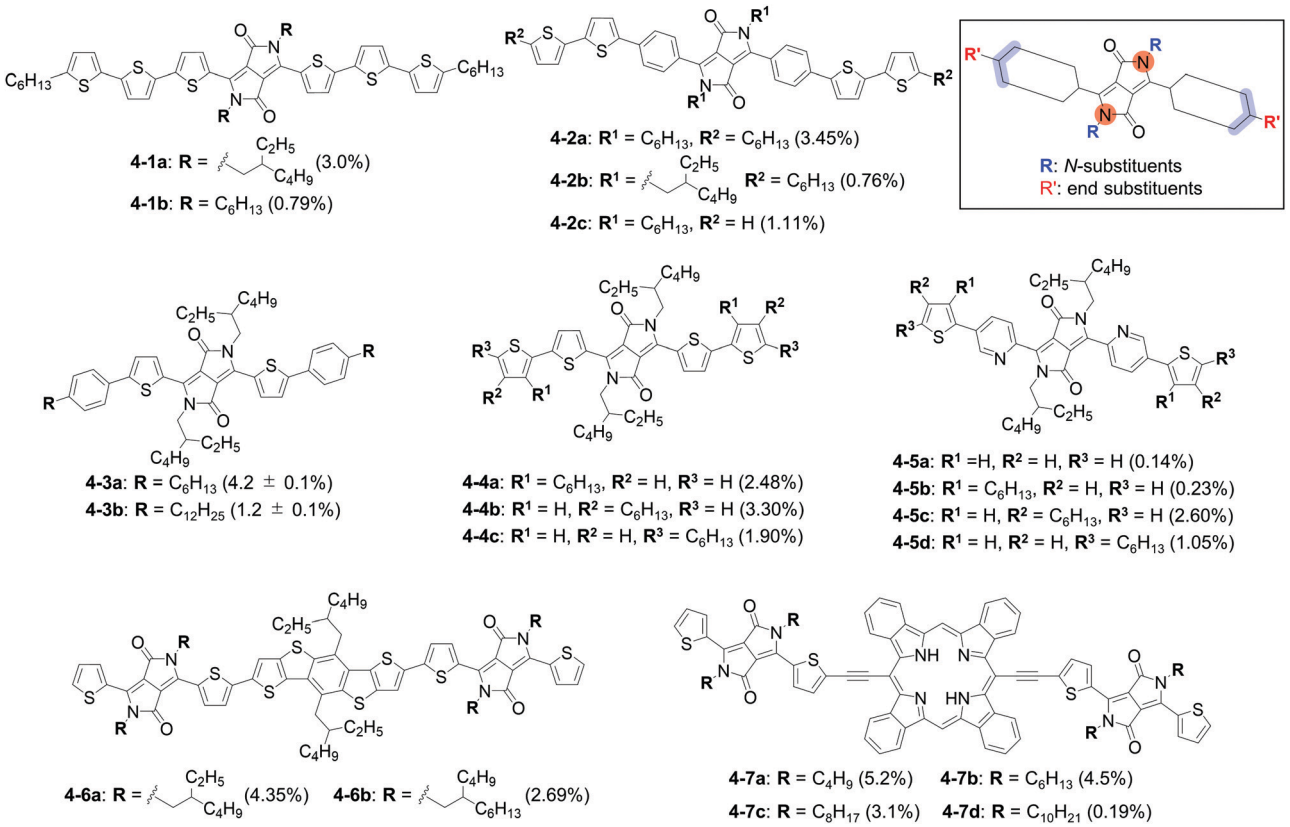

Fig. 7 Chemical structures of SMSCs **4-1**-**4-7**. The best PCEs obtained with each compound are shown in parentheses (see Table 4 for full OPV parameters). The inset shows relevant substitution positions of the DPP unit.

4-1b afforded PCEs of up to only 0.79% with $PC_{71}BM$ as the n-type material (entries 4-1 and 4-2). The V_{OC} of the **4-1b**:$PC_{71}BM$ device (0.47 V) was found to be much lower than that of the **4-1a**:$PC_{71}BM$ device (0.75 V), which could be traced back to the difference in the ionization energies in the solid state (4.92 and 4.61 eV for **4-1a** and **4-1b**, respectively). The author assumed that this dissimilarity between the two compounds was related to the disruption of molecular packing due to branched alkyl (*i.e.*, 2-ethlyhexyl) chains. In relation to the steric effect of the branched alkyl chains, Zerdan *et al.* prepared compound **4-1a** in a stereo-controlled fashion, and confirmed that the stereo-centres of the 2-ethylhexyl groups only weakly affected the overall photovoltaic process.[83]

Interestingly, 3,6-bis[4-(5′-hexyl[2,2′-bithiophen]-5-yl)phenyl] diketopyrrolopyrroles **4-2a** and **4-2b** showed an opposite dependency on the structure of *N*-alkyl groups in terms of the performance as a p-type material in BHJ OPVs. Lin *et al.* reported that **4-2a** and **4-2b** gave PCEs of 3.45% and 0.76% at best, respectively, with $PC_{71}BM$ as the n-type material (entries 4-3 and 4-4).[84] Note that the PCE obtained with **4-2b** was even lower than that with **4-2c** which did not have end-substituents (1.11%, entry 4-5). The authors reasoned that both increasing the bulkiness of the solubilizing *N*-alkyl groups and removing the linear end-alkyl groups induced micron-scale phase separations at high p : n ratios, thereby requiring large excess of the n-type material ($PC_{71}BM$) and resulting in limited photovoltaic efficiencies. The inconsistent results between **4-1** and **4-2** may be due to the steric effects of the phenylene moieties which causes deviation from coplanarity with the neighbouring DPP and thienylene units.

The importance of end-alkyl groups was also demonstrated by Shin *et al.* in 2013.[85] In this case, the authors comparatively evaluated two simple DPP derivatives **4-3a** and **4-3b**, the π-conjugated backbones of which were terminated with 4-hexylphenyl and 4-dodecylphenyl groups, respectively. While **4-3b** afforded a low PCE of 1.2%, **4-3a** performed much better as a p-type material to give a 4.2% PCE in BHJ OPVs with $PC_{71}BM$ (entries 4-6 and 4-7). The hexyl derivative **4-3a** was found to have liquid-crystalline (LC) properties, and the **4-3a**:$PC_{71}BM$ active layer showed a significant increase in J_{SC} and FF upon thermal annealing *via* the LC organization process. On the other hand, the dodecyl derivative **4-3b** did not show LC characters and the photovoltaic performance of the **4-3b**:$PC_{71}BM$ system was essentially unchanged after thermal annealing. Thus, balancing the lengths of alkyl chains and a rigid π-backbone is quite important for achieving a favourable molecular order in BHJ films and thus improving photovoltaic performance.

Gevaerts *et al.* showed that the position of end-alkyl substituents was a critical factor in OPV performance by comparing isomeric DPP derivatives **4-4a–c** having hexyl chains at different positions of the terminal thienyl groups.[86] The three compounds were found to be largely dissimilar in terms of interaction with $PC_{71}BM$, crystallization kinetics, and crystallite

Table 4 Photovoltaic performance of SMSCs **4-1-4-7**[a]

Entry	Active layer	Solvent	Additional conditions	V_{OC}[b] (V)	J_{SC}[b] (mA cm^{-2})	FF[b] (%)	PCE[b] (%)	Ref.
4-1	**4-1a** : $PC_{71}BM$ (1 : 1)	CF	—	0.75	9.2	44	3.0	81 and 82
4-2	**4-1b** : $PC_{71}BM$ (1 : 1)	CF	—	0.47	4.2	40	0.79	81
4-3	**4-2a** : $PC_{71}BM$ (3 : 2)	CF	120 °C, 10 min	0.90	7.91	49	3.45	84
4-4	**4-2b** : $PC_{71}BM$ (1 : 9)	CF	80 °C, 10 min	0.72	3.37	33	0.76	84
4-5	**4-2c** : $PC_{71}BM$ (2 : 8)	CF	80 °C, 10 min	0.87	4.33	30	1.11	84
4-6	**4-3a** : $PC_{71}BM$ (1 : 1)	CF	140 °C, 10 min	0.93	8.27 ± 0.10	54 ± 1	4.2 ± 0.1	85
4-7	**4-3b** : $PC_{71}BM$ (1 : 1)	CF	120 °C, 10 min	0.93	3.73 ± 0.17	35 ± 1	1.2 ± 0.1	85
4-8	**4-4a** : $PC_{71}BM$ (2 : 1)	CF	100 °C, 1 min	0.85	5.89	50	2.48	86
4-9	**4-4b** : $PC_{71}BM$ (2 : 1)	CF	100 °C, 1 min	0.84	7.47	53	3.30	86
4-10	**4-4c** : $PC_{71}BM$ (2 : 1)	CF	100 °C, 1 min	0.79	5.30	45	1.90	86
4-11	**4-5a** : $PC_{71}BM$ (2 : 1)	CF	CS_2 vapour, 20 s	0.85	0.74	24	0.14	87
4-12	**4-5b** : $PC_{71}BM$ (2 : 1)	CF	CS_2 vapour, 20 s	0.79	1.16	26	0.23	87
4-13	**4-5c** : $PC_{71}BM$ (2 : 1)	CF	CS_2 vapour, 20 s	1.00	5.40	48	2.60	87
4-14	**4-5d** : $PC_{71}BM$ (2 : 1)	CF	CS_2 vapour, 20 s	0.84	3.49	36	1.05	87
4-15	**4-6a** : $PC_{61}BM$ (3 : 2)	CF	—	0.95	4.0	29.0	1.10	88
4-16	**4-6b** : $PC_{61}BM$ (3 : 2)	CF	—	0.94	3.9	29.2	1.08	88
4-17	**4-6a** : $PC_{61}BM$ (3 : 2)	CF	0.6 vol% DIO; 70 °C, 10 min	0.85	9.9	51.3	4.35	88
4-18	**4-6b** : $PC_{61}BM$ (3 : 2)	CF	0.4 vol% DIO; 70 °C, 10 min	0.82	7.3	45.2	2.69	88
4-19	**4-7a** : $PC_{61}BM$ (4 : 3)	CF	10 vol% CS_2, 200 °C, 10 min	0.67	15.2	52	5.2	89
4-20	**4-7b** : $PC_{61}BM$ (2 : 1)	CF	200 °C, 10 min	0.69	13.6	49	4.5	89
4-21	**4-7c** : $PC_{61}BM$ (2 : 1)	CF	160 °C, 30 min	0.70	9.1	48	3.1	89
4-22	**4-7d** : $PC_{61}BM$ (2 : 1)	CF	180 °C, 30 min	0.66	0.88	33	0.19	89

[a] Structures of active-layer compounds are shown in Fig. 7. CF: chloroform, DIO: 1,8-diiodooctane. [b] Data of the best-performing devices when available; otherwise, average of multiple devices.

orientation. These factors were considered responsible for the observed variation in device performance, in which PCEs were 2.48%, 3.30%, and 1.90% for **4-4a**, **4-4b**, and **4-4c**, respectively (entries 4-8–4-10). Similarly, Más-Montoya and Janssen compared thienyl end-capped di(2-pyridyl)diketopyrrolopyrroles **4-5a–d**.[87] Among the four compounds, only **4-5a** had no end-alkyl chain, and the other three were substituted with hexyl groups at different positions of the thiophene units. In BHJ OPVs comprising a DPP derivative and $PC_{71}BM$, derivatives **4-5c** and **4-5d** gave relatively high PCEs of 2.60% and 1.05%, whereas **4-5a** and **4-5b** showed significantly lower PCEs of 0.14% and 0.23% (entries 4-11–4-14). Spectroscopic data clearly showed that the former two derivatives formed J-aggregates, and the latter two H-aggregates. The authors assumed that more efficient exciton diffusion in J-aggregates caused the observed faster charge generation and thus higher photovoltaic efficiency with **4-5c** and **4-5d**.

The impact of *N*-alkyl substituents was also studied regarding A–D–A-type conjugates with DPP as the acceptor unit. In 2015, Jung *et al.* reported two such compounds, **4-6a** and **4-6b**, bearing 2-ethylhexyl or 2-butyloctyl groups, respectively, on the DPP nitrogens.[88] The two compounds showed very similar photovoltaic performance as p-type materials in BHJ OPVs when deposited without a solvent additive (1,8-diiodooctane, DIO) to afford essentially the same PCEs of 1.10% and 1.08% (entries 4-15 and 4-16). In contrast, when a small amount of DIO was added to the cast solution, the PCE obtained with **4-6a** was considerably higher than that of **4-6b** (4.35% *vs.* 2.69%, entries 4-17 and 4-18). The authors concluded that compound **4-6b** with longer alkyl groups suffered from excessive phase separation that limited J_{SC} and FF, while **4-6a** with shorter alkyl groups formed bicontinuous morphology with favorable domain sizes for the photovoltaic process. In relation to this report, it is worth pointing out that most of the successful DPP-based SMSCs in BHJ OPVs are equipped with relatively short branched alkyls, typically 2-ethylhexyl, as *N*-substituents and linear alkyl groups as end substituents.

Meanwhile, Takahashi *et al.* prepared DPP-based A–D–A conjugates **4-7a–d** with tetrabenzoporphyrin (BP) as the central donor unit, and studied the effect of *N*-alkyl chains on the performance of these conjugates as p-type materials.[89] A unique aspect of this series of compounds is that they are essentially insoluble because of the large, considerably rigid π-framework and the minimal alkyl substituents. Accordingly, compounds **4-7a–d** were deposited *via* a thermal precursor approach, wherein soluble precursor compounds **4-8a–d** were deposited as a solution then transformed to the target compounds by thermally induced retro-Diels–Alder reactions in the solid state (Scheme 1). The solubilizing dimethylbicyclo[2.2.2]octadieno units of the precursors can be quantitatively converted to the benzo units to from a BP framework, and the by-produced isobutene molecules escape from the film as a gas. By employing this approach, one can design SMSCs with a minimum of bulky flexible solubilizing substituents if not at all, and thus the role of substituents becomes largely focused on the control of molecular packing and phase-separation behaviors in the solid state.[90]

Comparative evaluation of **4-7a–d** in BHJ OPVs with $PC_{61}BM$ revealed that the PCE was higher when the *N*-alkyl groups were shorter: 5.2% for **4-7a** with butyl, 4.5% for **4-7b** with hexyl, 3.1% for **4-7c** with octyl, and 0.19% for **4-7d** with decyl (entries 4-19–4-22). One of the problems associated with longer alkyl chains was that they induced excessive phase separation with the n-type material $PC_{61}BM$ during the solid-state thermal reactions for generating **4-7a–d** from precursors **4-8a–d**. Note that the blended films before thermal reactions (*i.e.*, **4-8**:$PC_{61}BM$ films) were very smooth and highly homogeneous, probably because the steric effect of the bulky solubilizing units prevented the precursor compounds from self-aggregation. Another issue with

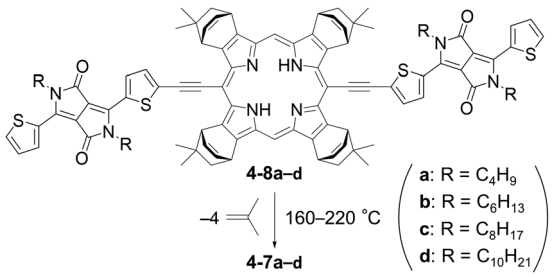

Scheme 1 Thermal conversion of precursors **4-8a–d** to **4-7a–d**. (* Mixtures of stereoisomers regarding the orientation of dimethylbicyclo[2.2.2]octadieno units.)

longer alkyl chains was that they induced edge-on arrangements of molecules during the solid-state thermal reactions, which significantly limits carrier transport in the out-of-plane direction and thus the overall photovoltaic process. The dependence of molecular arrangement on alkyl-chain lengths was clearly observed in the2D-GIWAXS patterns of neat films (Fig. 8a–d); namely, butyl and hexyl derivatives **4-7a** and **4-7b** showed clear diffractions on the q_z axis around q_z = 1.79 Å which indicated that these compounds formed π–π stacking in the out-of-plane direction with a face-on molecular orientation. The data of **4-7c** showed an arc-shaped diffraction around q = 1.75 Å, indicating a rather random orientation of π–π stacking. On the other hand, it was apparent from the strong diffraction on the q_{xy} axis around q_{xy} = 1.74 Å that **4-7d** had a high tendency to form π–π stacking in the in-plane direction with edge-on molecular orientation. The difference in molecular orientation became somewhat less distinct, but was generally preserved in BHJ films with $PC_{61}BM$ (Fig. 8e–h). These results demonstrated well the cruciality of substituent design also for those SMSCs processed *via* the thermal precursor approach.

6. Substituents of π-conjugates bearing dithienosilole as a core unit

Rigid fused-ring π-systems have been widely employed as a core unit in donor–acceptor (D–A)-linked SMSCs for BHJ OPVs. Among various synthetically accessible structures, 5–5–5-tricyclic systems such as dithienosilole (DTS) and dithienopyrrole (DTP) are the commonly employed types of electron-donating core units. A typical example of this class of compounds is a DTS-based small molecule called F-DTS or p-DTS(FBTTh$_2$)$_2$ which afforded PCEs of up to 7.0% in BHJ OPVs with $PC_{71}BM$.[91] This section overviews the substituent impact on DTS-based SMSCs. The chemical structures of the relevant compounds and the corresponding photovoltaic data are summarized in Fig. 9 and Table 5, respectively.

Several papers have reported the substituent effects on the performance of DTS-based p-type SMSCs. For example, Ye *et al.* reported three A–D–A systems **5-1a–c** bearing a DTS framework as the central D unit in 2013.[92] In BHJ OPVs with $PC_{61}BM$, compound **5-1a** performed better as a p-type material than the corresponding tetramethyl derivative **5-1b** (PCEs = 3.27% and 2.88%, entries 5-1 and 5-2). This difference was mainly attributed to the change in FF (56% *vs.* 49%), and the authors speculated that the four methyl groups on the thiophene rings in **5-1b** induced an unfavorable BHJ morphology for the photovoltaic process. Accordingly, the BHJ films of **5-1a**:$PC_{61}BM$ and **5-1b**:$PC_{61}BM$ showed opposite responses to thermal annealing; namely, the former systems gave the best device results without thermal annealing, while the latter system required thermal annealing to exhibit its optimal performance. The other compound **5-1c** afforded an even higher PCE (3.81%, entry 5-3) than **5-1a**. The authors mentioned that this improvement with **5-1c** was not only due to its wider light-absorption range caused by the replacement of the ester groups with cyano groups, but also due to a rougher morphology most likely caused by its lower solubility. Note that certain degrees of film roughening has been known to induce improvements in charge-transport efficiency.[93–95]

In addition, Min and co-workers reported substituent effects on the photovoltaic performance of a similar series of DTS-based p-type small molecules **5-2a** and **5-2b**.[96] Evaluation of these compounds in BHJ OPVs with $PC_{71}BM$ revealed much higher performance with the methyl derivative **5-2a**

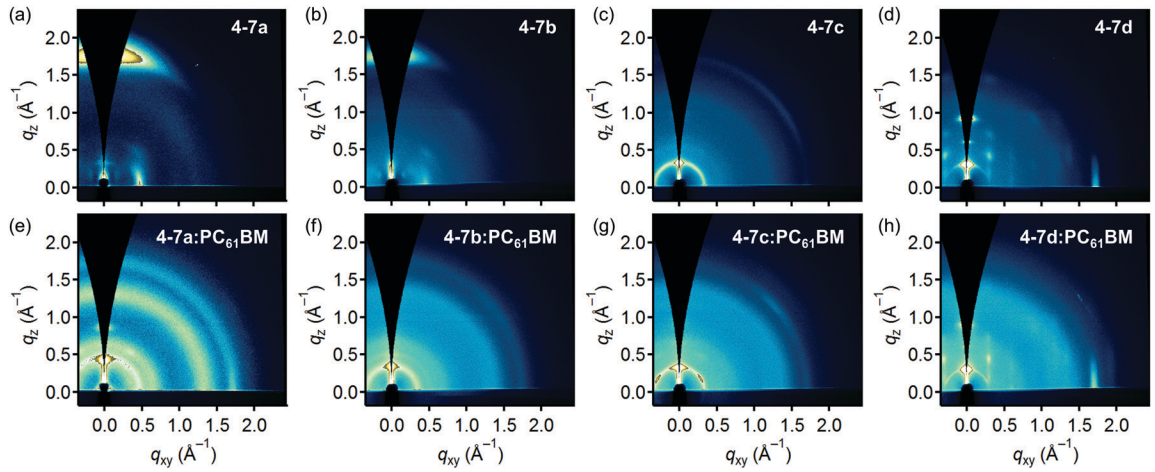

Fig. 8 2D-GIWAXS patterns of (a) **4-7a**, (b) **4-7b**, (c) **4-7c**, (d) **4-7d**, (e) **4-7a**:$PC_{61}BM$, (f) **4-7b**:$PC_{61}BM$, (g) **4-7c**:$PC_{61}BM$, and (h) **4-7d**:$PC_{61}BM$. All sample films were prepared by the thermal precursor approach. Adopted from ref. 89 with permission. Copyright 2017, Royal Society of Chemistry.

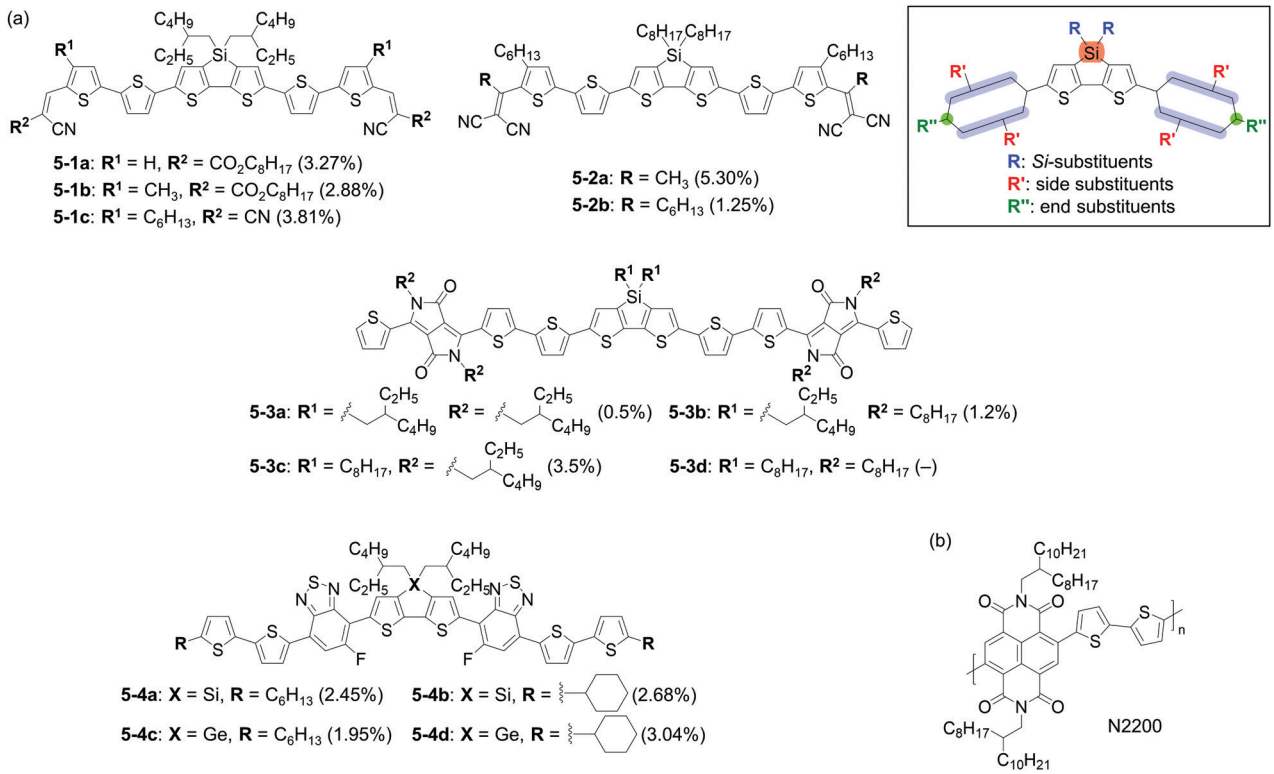

Fig. 9 Chemical structures of (a) SMSCs **6-1-6-4** and (b) n-type polymer N2200. The best PCEs obtained with each DTS derivative are shown in parentheses (see Table 5 for full OPV parameters). The inset shows relevant substitution positions of DTS-based SMSCs.

(PCE = 5.30%) than the hexyl derivative **5-2b** (1.25%) because of a higher J_{SC} and FF (entries 5-4 and 5-5). The authors showed that the terminal alkyl groups (*i.e.*, the methyl or hexyl chains) had a significant effect on the intermolecular interaction and solubility, and thus the morphological characteristics and semiconducting properties of these compounds in the BHJ active layers. In particular, the **5-2b** system showed a relatively inefficient and unbalanced charge-carrier transport which resulted in considerable non-geminated recombination. On the other hand, the **5-2a** system did not show signs of charge-mobility limitation and enhanced bimolecular recombination.

Jung *et al.* compared three A–D–A conjugates comprising the DTS and DPP frameworks (**5-3a–c**).[97] These compounds were substituted with octyl or 2-ethylhexyl, respectively, at the silicon and nitrogen atoms, and showed considerably different performances in BHJ OPVs with $PC_{61}BM$ (entries 5-6–5-8; note that the corresponding fully octyl substituted compound **5-3d** was also prepared but not evaluated in an OPV because of its insufficient solubility). In thermally annealed BHJ active layers, the *Si*-octyl/*N*-2-ethylhexyl derivative **5-3c** afforded a considerably higher PCE of 3.5% than the *Si*-2-etheylhexyl/*N*-2-ethylhexy derivative **5-3a** (0.5%) and the *Si*-octyl/*N*-2-ethylhexy derivative

Table 5 Photovoltaic performance of SMSCs **5-1-5-4**[a]

Entry	Active layer	Solvent	Additional conditions	V_{OC}[b] (V)	J_{SC}[b] (mA cm^{-2})	FF[b] (%)	PCE[b] (%)	Ref.
5-1	**5-1a** : $PC_{61}BM$ (1 : 0.8)	CF	—	0.92	6.37	56	3.27	92
5-2	**5-1b** : $PC_{61}BM$ (1 : 0.8)	CF	Thermal annealing	0.89	6.61	49	2.88	92
5-3	**5-1c** : $PC_{61}BM$ (1 : 0.8)	CF	Thermal annealing	0.92	8.73	48	3.81	92
5-4	**5-2a** : $PC_{71}BM$ (1 : 0.8)	CF	–	0.85	10.05	62.0	5.30	96
5-5	**5-2b** : $PC_{71}BM$ (1 : 0.8)	CF	–	0.91	4.37	31.5	1.25	96
5-6	**5-3a** : $PC_{61}BM$ (1 : 1)	CF	110 °C, 10 min	0.82	2.1	30	0.5	97
5-7	**5-3b** : $PC_{61}BM$ (1 : 1)	CF	110 °C, 10 min	0.70	3.7	47	1.2	97
5-8	**5-3c** : $PC_{61}BM$ (1 : 1)	CF	110 °C, 10 min	0.77	7.5	60	3.5	97
5-9	**5-4a** : N2200 (3 : 2)	CB	0.2 vol% DIO; 120 °C, 10 min	0.825	5.51	56.4	2.45	98
5-10	**5-4b** : N2200 (3 : 2)	CB	0.2 vol% DIO; 120 °C, 10 min	0.784	5.65	60.0	2.68	98
5-11	**5-4c** : N2200 (3 : 2)	CB	0.2 vol% DIO; 120 °C, 10 min	0.807	4.18	57.7	1.95	98
5-12	**5-4d** : N2200 (3 : 2)	CB	0.2 vol% DIO; 120 °C, 10 min	0.787	6.08	63.3	3.04	98

[a] Structures of active-layer compounds are shown in Fig. 9. CF: chloroform, CB: chlorobenzene, DIO: 1,8-diiodobenzene. [b] Data of the best-performing devices.

5-3b (1.2%). This superiority in the performance of **5-3c** was attributed to its isotropic arrangement of intermolecular π–π stacks in the active layer, which was more favorable for charge-carrier transport in OPVs than the edge-on-preferred orientation of **5-3a** and **5-3b**.

In 2018, Han *et al.* reported a comparison between **5-4a** (p-DTS(FBTTh$_2$)$_2$) and its cyclohexyl end-capped derivative **5-4b**.[98] The two compounds were evaluated as p-type materials in BHJ OPVs with an n-type polymer N2200 (entries 5-9 and 5-10). Analyses with 2D-GIWAXS and AFM revealed that the **5-4b**:N2200 film had a more pronounced face-on molecular orientation and a more coarse morphology than the **5-4a**:N2200 film. The authors attributed these differences in the microstructure of active layers to the higher J_{SC} and FF obtained with **5-4b**. Additionally, the same trend was observed with the corresponding dithienogermoles **5-4c** and **5-4d** in terms of both photovoltaic performance (entries 5-11 and 5-12) and film microstructure. As observed also for other DTS derivatives and similar linearly extended p-systems in the following sections, it seems generally advantageous to keep the end substituents relatively compact in order to obtain high PCEs.

7. Substituents of π-conjugates bearing benzodithiophene as the core unit

The benzo[1,2-*b*:4,5-*b*′]dithiophene (BDT) unit has been a popular building unit of organic semiconductors for OPV applications because of the rigid π-conjugated framework with a suitable electron-donating nature.[99–101] For example, BDT was used as the donor unit in PTB7 which has been one of the most studied high-performance p-type polymers for OPVs since its first report in 2010.[102] This section reviews recent prominent papers reporting the substituent impact on the performance of BDT-based SMSCs in OPVs. The compounds are separately discussed depending on the position of the substituents of interest, namely, core, end, or side substituents (Fig. 10). The chemical structures of the relevant compounds are summarized in Fig. 10 and 11, while their photovoltaic performance is listed in Table 6. The examples below demonstrate that 5-(thio)alkyl-2-thienyl is the preferred choice as core substituents, while linear alkyls are common among high-performance BDT-based conjugates.

Core substituents

Wang *et al.* evaluated a series of BDT–DPP conjugates for their performance as p-type materials in BHJ OPVs.[103] A pair of differently core substituted derivatives **6-1a** and **6-1b** were a part of the series, and the di(2-ethylhexyl) derivative **6-1a** was found to afford a higher PCE than the tetrahexyl derivative **6-1b** (4.4% *vs.* 0.6%) in thermally annealed BHJ films with PC$_{61}$BM (entries 6-1 and 6-2). The considerably lower performance of **6-1b** was attributed to its high crystallinity which induced excessive phase separation with PC$_{61}$BM upon thermal annealing as confirmed by TEM analysis of the BHJ films. Without thermal annealing, **6-1a** and **6-1b** gave PCEs of 2.4% and 1.1%, respectively; thus, the difference between the two BHJ systems was much smaller (entries 6-3 and 6-4).

Similarly, Zhang *et al.* highlighted the correlation between core substituents, molecular crystallinity, and photovoltaic performance in a comparative evaluation of BDT–DPP conjugates **6-2a** and **6-2b** (in addition to another derivative which is not mentioned here because its π-conjugated backbone is different from those of **6-2a** and **6-2b**).[104] In BHJ OPVs with PC$_{61}$BM, the dithienyl-BDT derivative **6-2a** afforded a PCE of 5.15%, while the bis(bithienyl) derivative **6-2b** gave a PCE of 6.04% at best (entries 6-5 and 6-6). The authors showed that compound **6-2b** had a lower crystallinity and finer phase separation than **6-2a** in the BHJ films, which could lead to a more effective exciton diffusion and charge-carrier transport, thus higher J_{SC} and FF. The crystallinity and phase separation in the **6-2a**:PC$_{61}$BM film were considered excessive for smooth photovoltaic process.

Meanwhile, the 2-ethylhexyloxy-substituted derivative **6-3a** showed a lower performance than the corresponding 5-(2-ethylhexyl)thienyl substituted derivative **6-3b**.[105] The substitution with relatively small 2-ethylhexyloxy groups led to a higher degree of crystallization of **6-3a** in BHJ films, but the film morphology was fixed such that the annealing effect was rather limited. In contrast, the morphology of the **6-3b**:PC$_{61}$BM film was significantly improved upon the use of a molecular additive (DIO) and thermal annealing to form well-developed phase separation. Accordingly, the best PCEs were 4.19% and 7.12% with **6-3a** and **6-3b**, respectively (entries 6-7 and 6-8). The 7.12% PCE was the highest at that time among those obtained with small-molecule DBT–DPP conjugates. Similar comparisons were performed between BDT–DTP conjugates **6-4a** and **6-4b**,[106] as well as between BDT–difluorobenzotriazole conjugates **6-5a** and **6-5b** (entries 6-9–6-12).[107] In these cases again, the 5-(2-ethylhexyl)thienyl substituted derivatives **6-4a** and **6-5a** performed better (PCE = 5.90% and 9.73%) than the corresponding 2-ethylhexyloxy substituted derivatives **6-4b** and **6-5b** (5.12% and 5.51%) in BHJ OPVs.

The same trend was further observed in a comparative evaluation of BDT–rhodanine conjugates by Yin and co-workers, wherein the dodecyloxy derivative **6-6a** and 5-dodecylthienyl derivative **6-6b** afforded PCEs of 4.25% and 6.99%, respectively, in BHJ OPVs with PC$_{71}$BM (entries 6-13 and 6-14).[108] Denser molecular packing and higher hole mobility of the alkylthienyl derivative were highlighted in this study similar to the cases of **6-3**–**6-5**; thus, the superiority of alkylthienyl over alkyloxy as core substituents of the BDT unit seems broad in scope.

Yin *et al.* also evaluated the corresponding alkylthiothienyl derivative **6-6c** in the same paper, which afforded a slightly lower PCE (6.78%) than the alkylthienyl derivative **6-6b** (entry 6-15). This result contrasted with the study by Min and co-workers in 2016 which reported that the 5-(2-ethylhexyl)thiothienyl derivative **6-7b** afforded a PCE of 9.20%, while the 5-(2-ethylhexyl)thienyl derivative **6-7a** gave only 7.44% at best in BHJ OPVs with PC$_{71}$BM (entries 6-16 and 6-17).[109] These opposite trends between **6-6** and **6-7** should be related to the structure of alkyl groups (*i.e.*, dodecyl *vs.* 2-ethylhexyl), demonstrating the subtle nature of substituent impact. Note here that the advantage of 5-(2-ethylhexylthio)thienyl

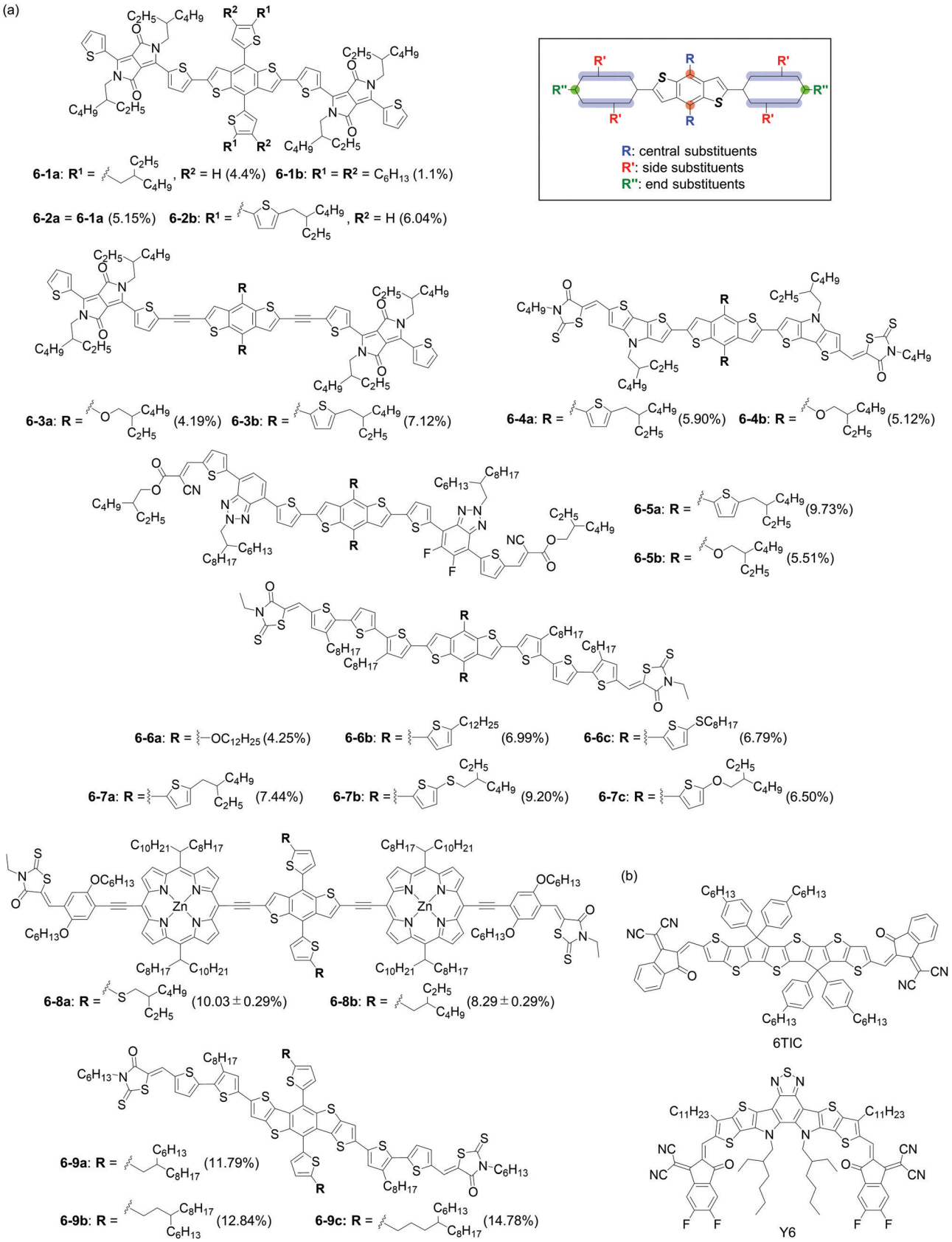

Fig. 10 Chemical structures of (a) SMSCs **6-1-6-9** and (b) the compounds employed with **6-1-6-9** in OPV active layers. PC61BM and PC71BM are shown in Fig. 2, and IDIC is shown in Fig. 4. The best PCEs obtained with each BDT derivative are shown in parentheses (see Table 6 for full OPV parameters). The inset shows relevant substitution positions of BDT-based SMSCs.

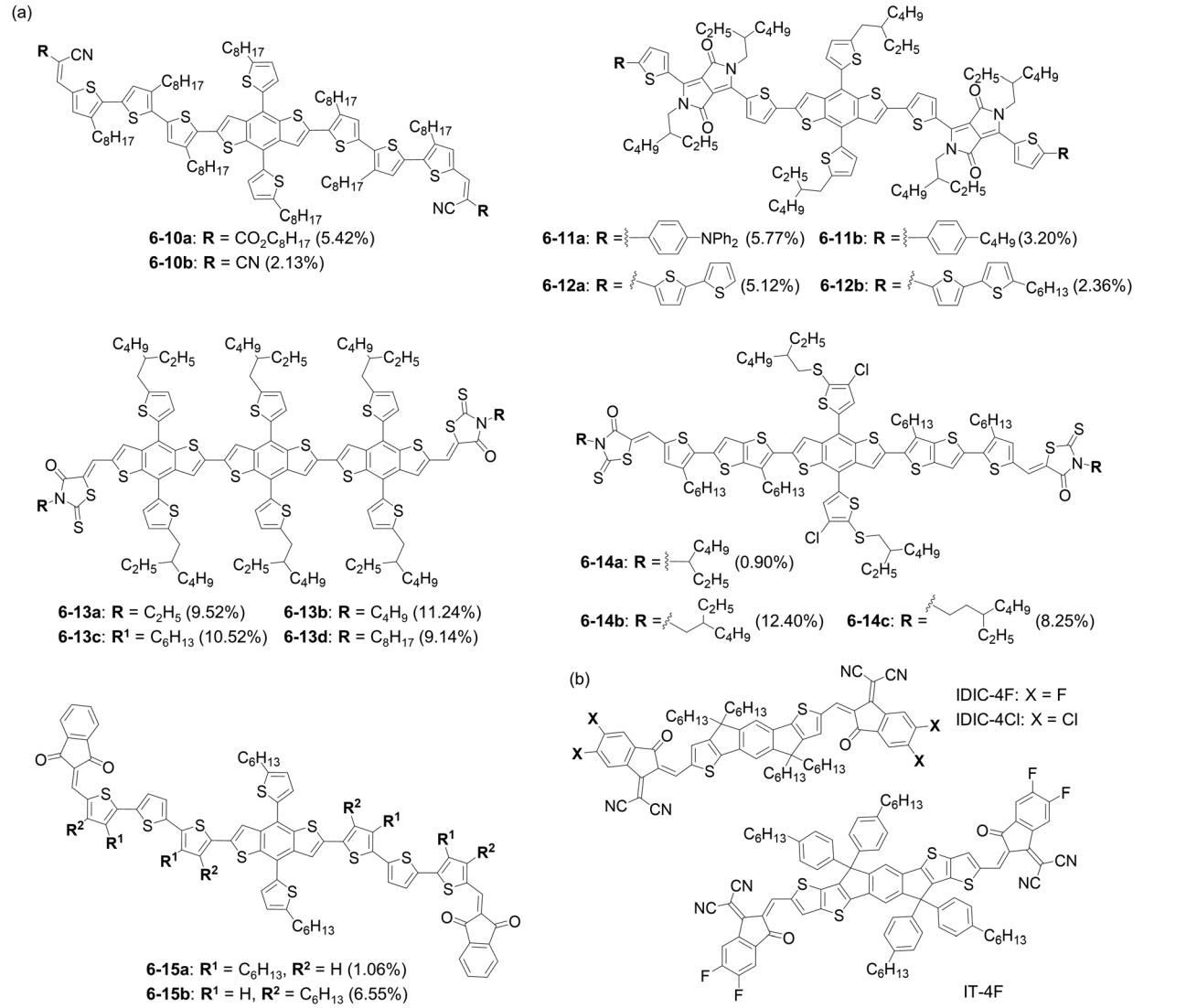

Fig. 11 Chemical structures of (a) SMSCs **6-10-6-13** and (b) the compounds employed with **6-10-6-13** in OPV active layers. $PC_{61}BM$ and $PC_{71}BM$ are shown in Fig. 2. The best PCEs obtained with each BDT derivative are shown in parentheses (see Table 6 for full OPV parameters).

over 5-(2-ethylhexyl)thienyl was also observed between dimeric porphyrin compounds **6-8a** (PCE = 10.03%) and **6-8b** (8.29%) as reported by Piradi *et al.* in 2020 (entries 6-19 and 6-20).[110]

Additionally, Min *et al.* also reported that the corresponding 5-(2-ethylhexyloxyl)thienyl derivative **6-7c** gave a good 6.50% PCE (entry 6-18). Although this PCE was somewhat lower than those of **6-7a** and **6-7b**, a significant decrease in J_{SC} as in the case of **6-6a** was not observed. Therefore, the general effectiveness of thienyl substitution, rather than direct alkyloxy substitution, on BDT was also supported in this case.

Concerning branched alkyl substituents such as 2-ethylhexyl, Zhou *et al.* studied the effect of the branching point by comparing dithienobenzodithiophene (DTBDT)-based SMSCs **6-9a–c**.[111] Their evaluation revealed that, by moving the branching point away from the DTBDT core, the crystallinity and intermolecular π–π stacking were enhanced in BHJ films with a non-fullerene n-type compound IDIC-4F or Y6. This change in molecular arrangement resulted in the improvement of J_{SC} and FF. Accordingly, PCEs of the corresponding BHJ OPVs showed monotonic increase for **6-9a–c** from 11.79% to 12.84% and to 14.78% with IDIC-4F, or from 9.27% to 9.91% and to 10.35% with Y6 (entries 6-21–26).

End substituents

Patra *et al.* compared cyanoacetate and dicyanovinyl units as electron-accepting end substituents of BDT-based A–D–A p-type molecules **6-10a** and **6-10b**.[112] In their evaluation, it was found that the *n*-octyl cyanoacetate derivative **6-10a** (PCE = 5.42%) performed better than the dicyanovinyl derivative **6-10b** (2.13%) as a p-type material in BHJ OPVs with $PC_{61}BM$ (entries 6-27 and 6-28). While the **6-10a**:$PC_{61}BM$ and **6-10b**:$PC_{61}BM$ systems were essentially the same in terms of V_{OC}, J_{SC} and FF were found to

Table 6 Photovoltaic performance of SMSCs **6-1-6-14**[a]

Entry	Active layer	Solvent	Additional conditions	V_{OC}[b] (V)	J_{SC}[b] (mA cm^{-2})	FF[b] (%)	PCE[b] (%)	Ref.
6-1	**6-1a** : $PC_{61}BM$ (1 : 1)	CF	0.2% CN; 110 °C, 10 min	0.83	9.36	56	4.4	103
6-2	**6-1b** : $PC_{61}BM$ (1 : 1)	CF	0.2% CN; 110 °C, 10 min	0.86	2.43	29	0.6	103
6-3	**6-1a** : $PC_{61}BM$ (1 : 1)	CF	0.2% CN	0.92	6.76	39	2.4	103
6-4	**6-1b** : $PC_{61}BM$ (1 : 1)	CF	0.2% CN	0.97	3.59	30	1.1	103
6-5	**6-2a** : $PC_{61}BM$ (1 : 1)	CF	110 °C, 10 min	0.837	11.00	55.8	5.15	104
6-6	**6-2b** : $PC_{61}BM$ (1 : 1)	CF	0.75% CN; 110 °C, 10 min	0.799	12.17	62.1	6.04	104
6-7	**6-3a** : $PC_{71}BM$ (1 : 1)	CB	0.4 vol% DIO; 100 °C, 10 min	0.88	7.87	60.4	4.19	105
6-8	**6-3b** : $PC_{71}BM$ (1 : 1)	CB	0.4 vol% DIO; 100 °C, 10 min	0.89	10.9	73.6	7.12	105
6-9	**6-4a** : $PC_{71}BM$ (1 : 2)	CF	TSA	0.92	10.68	60	5.90	106
6-10	**6-4b** : $PC_{71}BM$ (1 : 2)	CF	TSA	0.87	10.15	58	5.12	106
6-11	**6-5a** : IDIC (1 : 1)	CF	120 °C, 10 min	0.977	15.21	65.46	9.73	107
6-12	**6-5b** : IDIC (1 : 1)	CF	120 °C, 10 min	0.955	10.51	54.89	5.51	107
6-13	**6-6a** : $PC_{71}BM$ (1 : 1)	CF	CF vapour, 1 min	0.88	7.38	65.39	4.25	108
6-14	**6-6b** : $PC_{71}BM$ (1 : 1)	CF	CF vapour, 1 min	0.90	11.69	66.48	6.99	108
6-15	**6-6c** : $PC_{71}BM$ (1 : 1)	CF	CF vapour, 1 min	0.94	11.70	61.61	6.78	108
6-16	**6-7a** : $PC_{71}BM$ (1 : 0.8)	CF	—	0.93	11.75	68.1	7.44	109
6-17	**6-7b** : $PC_{71}BM$ (1 : 0.8)	CF	—	0.97	13.45	70.5	9.20	109
6-18	**6-7c** : $PC_{71}BM$ (1 : 0.8)	CF	—	0.90	11.03	65.5	6.50	109
6-19	**6-8a** : 6TIC (1 : 0.6)	CF	2.0 vol% Py + 0.5 vol% DIO; 120 °C, 10 min	0.79 ± 0.01	19.36 ± 0.13	65.6 ± 0.6	10.03 ± 0.29	110
6-20	**6-8b** : 6TIC (1 : 0.6)	CF	2.0 vol% Py + 0.5 vol% DIO; 120 °C, 10 min	0.75 ± 0.01	17.27 ± 0.16	64.0 ± 0.5	8.29 ± 0.25	110
6-21	**6-9a** : Y6 (1 : 0.55)	CF	120 °C, 10 min	0.848	21.35	65.12	11.79	111
6-22	**6-9b** : Y6 (1 : 0.55)	CF	120 °C, 10 min	0.852	23.03	65.43	12.84	111
6-23	**6-9c** : Y6 (1 : 0.55)	CF	120 °C, 10 min	0.854	24.69	70.06	14.78	111
6-24	**6-9a** : IDIC-4F (1 : 0.6)	CF	120 °C, 10 min	0.796	18.15	64.16	9.27	111
6-25	**6-9b** : IDIC-4F (1 : 0.6)	CF	120 °C, 10 min	0.783	18.27	69.29	9.91	111
6-26	**6-9c** : IDIC-4F (1 : 0.6)	CF	120 °C, 10 min	0.776	18.95	70.41	10.35	111
6-27	**6-10a** : $PC_{61}BM$ (1 : 0.40)	CF	—	0.90	9.08	66	5.42	112
6-28	**6-10b** : $PC_{61}BM$ (1 : 0.60)	CF	—	0.91	5.17	46	2.13	112
6-29	**6-11a** : $PC_{71}BM$ (1 : 1.5)	CF	1.0 vol% DIO	0.62	15.64	59.4	5.77	113
6-30	**6-11b** : $PC_{71}BM$ (1 : 1.5)	CF	0.8 vol% DIO	0.67	8.35	57.0	3.20	113
6-31	**6-12a** : $PC_{71}BM$ (1 : 1)	CF	0.5% CN; 120 °C, 10 min	0.69	13.39	56	5.12	114
6-32	**6-12b** : $PC_{71}BM$ (1 : 1)	CF	0.3% CN; 120 °C, 10 min	0.65	6.08	60	2.36	114
6-33	**6-13a** : IT-4F (1 : 1)	CF	THF vapour	0.893	16.66	64	9.52	115
6-34	**6-13b** : IT-4F (1 : 1)	CF	THF vapour	0.909	18.27	68	11.24	115
6-35	**6-13c** : IT-4F (1 : 1)	CF	THF vapour	0.929	17.92	63	10.52	115
6-36	**6-13d** : IT-4F (1 : 1)	CF	THF vapour	0.928	16.15	61	9.14	115
6-37	**6-14a** : IDIC-4Cl (1.5 : 1)	—[c]	120 °C; THF vapour, 40 s	0.564	4.9	33.9	0.90	116
6-38	**6-14b** : IDIC-4Cl (1.5 : 1)	—[c]	120 °C; THF vapour, 40 s	0.865	20.1	71.3	12.40	116
6-39	**6-14c** : IDIC-4Cl (1.5 : 1)	—[c]	120 °C; THF vapour, 40 s	0.870	14.2	67.0	8.25	116
6-40	**6-15a** : $PC_{71}BM$ (1.5 : 1)	CF	80 °C, 30 min	0.75	4.0	35.3	1.06	117
6-41	**6-15b** : $PC_{71}BM$ (1.5 : 1)	CF	80 °C, 30 min	0.87	8.82	68.9	5.30	117
6-42	**6-15b** : $PC_{71}BM$ (1.25 : 1)	CF	80 °C, 30 min	0.87	10.54	71.4	6.55	117

[a] Structures of active-layer compounds are shown in Fig. 10 and 11. CF: chloroform, CN: 1-chloronaphthralene, DIO: 1,8-diiodooctane, TSA: thermal followed by solvent annealing; Py: pyridine; THF: tetrahydrofuran. [b] Data of the best-performing devices when available; otherwise, average of multiple devices. [c] Information not provided.

be considerably higher in the former system. This result could be traced back to the favorable morphological characteristics of **6-10a**, namely, its higher miscibility with $PC_{61}BM$ that led to fine nanoscale phase separation and higher crystallinity, enabling the formation of effective π–π staking in the BHJ film. Both factors should bring about more efficient transport and reduced recombination of charge carriers, and thus improvements in J_{SC} and FF.

The effects of different end substituents were also studied with BDT–DPP conjugates **6-11a** and **6-11b**.[113] The *N*,*N*-diphenylamino group of **6-11a** affected the electronic characteristics of the π-conjugated system, resulting in an enhanced light absorbance by a factor of 46% when compared to that of butyl substituted **6-11b**. However, this effect did not fully explain the large difference in J_{SC}: 15.64 *vs.* 8.35 mA cm^{-2} with **6-11a** and **6-11b**, respectively (entries 6-29 and 6-30). Further analyses revealed that the aromatic branched diphenylamino end group brought about a higher compatibility with $PC_{61}BM$ to form finer phase separation that led to more efficient photon-to-charge conversion in the BHJ film. In addition, charge recombination probability was reduced. With all these factors combined, **6-11a** afforded a significantly higher J_{SC} and thus PCE (5.77%) than **6-11b** (3.20%).

In relation to the latter work, Hoang *et al.* reported the effect of a hexyl end group on the photovoltaic performance of a similar BDT–DPP system.[114] The authors compared two derivatives **6-12a** and **6-12b** as p-type materials in BHJ OPVs with $PC_{71}BM$, and found that the non-substituted derivative **6-12a** yielded a higher PCE (5.12%) than the hexyl-substituted derivative **6-12b** (2.36%) (entries 6-31 and 6-32). Again, the difference in PCE could be traced back to the morphological behavior of the two compounds, namely, the introduction of

end-hexyl groups led to excessive phase separation in the **6-12b**:$PC_{71}BM$ blend film which significantly deteriorated charge-carrier generation and transport, and thus the J_{SC} (13.39 and 6.08 mA cm^{-2} with **6-12a** and **6-12b**, respectively).

Yang *et al.* compared rhodanine-appended BDT trimers **6-13a–d** (entries 6-33–6-36).[115] These four derivatives are different from each other in the length of *N*-alkyl chains of the rhodanine units, and the *N*-butyl derivative **6-13b** was found to perform the best as a p-type material in BHJ OPVs with IT-4F, affording a PCE of 11.24% associated with a high J_{SC} of 18.27 mA cm^{-2}. Notably, the 2D-GIWAXS analysis revealed that molecular orientation in thin films shifted from edge-on to face-on with the elongation of *N*-alkyls from ethyl (**6-13a**) to octyl (**6-13d**). The authors explained the superiority of **6-13b** to other derivatives based on the molecular orientation, crystallinity, and phase-separation behavior (*i.e.*, domain sizes), which all affected charge-carrier mobility in BHJ layers. In addition, the preferable morphology brought about high tolerance of the **6-13b**:IT-4F system to film thickness; specifically, it retained 10% PCE with an active-layer thickness of up to 300 nm.

The effect of the branching point in end alkyl groups was investigated with a series of BDT–rhodanine conjugates **6-14a–c**.[116] Indeed, the difference in PCE was drastic in BHJ OPVs with IDIC-4Cl, that is, merely 0.90% with 3-heptyl substituted **6-14a**, 12.40% with 2-ethylhexyl derivative **6-14b**, and 8.25% with 3-ethylpentyl derivative **6-14c** (entries 6-37–6-39). Red-shifted absorption and enhanced crystallinity were observed as the branching point of end alkyls shifted away from the π-conjugated backbone, indicating that outer branching induced stronger intermolecular interactions among this series of compounds. An excellent PCE of 12.40% with **6-14b** could be due to its favourable degree of phase separation against the n-type material (IDIC-4Cl) to form a large heterojunction area with sufficient charge-carrier transport paths.

Side substituents

Zhang *et al.* reported a comparison between differently side-substituted BDT derivatives. They prepared two A–D–A-type π-conjugates **6-15a** and **6-15b** comprising BDT and indanedione units linked *via* terthiophene linkers, and evaluated them in BHJ OPVs with $PC_{71}BM$ as the n-type material.[117] The structural difference between the two conjugates was the alky substitution pattern at the terthiophene linkers: 3,3″-dihexyl (inward substitution) for **6-15a** and 4,4″-dihexyl (outward substitution) for **6-15b**. The outward substitution resulted in a slightly red-shifted absorption with a higher molar absorbance in solution and smoother, a more homogeneous morphology of BHJ films, which collectively contributed to the significantly higher photovoltaic performance of the **6-15b**:$PC_{71}BM$ blend (PCE = 5.30%) than that of the **6-15a**:$PC_{71}BM$ blend (1.06%) in the comparative evaluation under the same conditions (entries 6-40 and 41). Note that **6-15b**:$PC_{71}BM$ was further optimized to afford a 6.55% PCE (entry 6-42).

8. Substituents of indacenodithiophene-based π-conjugates

The five-ring-fused dihydro-*s*-indaceno[1,2-*b*:5,6-*b*′]dithiophene (ID) framework and the seven-ring-fused dihydrodithieno[2,3-*d*:2′,3′-*d*′]-*s*-indaceno[1,2-*b*:5,6-*b*′]dithiophene (IT) framework stand out as building blocks of high-performance n-type molecules. In particular, the IT and ID frameworks are the core units of ITIC and IDIC, respectively, which are both iconic non-fullerene n-type materials for OPVs (Fig. 12).[118,119] This section reviews recent studies which investigated substituent impact for n-type materials bearing an IT- or ID-based core unit. The corresponding chemical structures and photovoltaic data are shown in Fig. 13 and Table 7, respectively.

Molecules with a dithienoindacenodithiophene core

Substituents at the 6- and 12-positions of the IT units protrude from the π-plane, and thus play important roles in regulating intermolecular interactions and morphology in BHJ films. Yang *et al.* comparatively evaluated ITIC and its isomer **7-1**, which had hexyl groups on the four phenyl rings at the 6- and 12-carbons of the IT core.[120] Both compounds performed well in BHJ OPVs with a medium bandgap polymer J61[121] as the p-type material, affording PCEs of 10.57% with ITIC and 11.77% with **7-1** (entries 7-1 and 7-2). The higher performance of the *m*-hexylphenyl derivative **7-1** was attributed to its higher electron mobility (2.45×10^{-4} cm^2 V^{-1} s^{-1}) than that of the *p*-hexylphenyl derivative ITIC (1.60×10^{-4} cm^2 V^{-1} s^{-1}), which could be further traced back to higher crystallinity and stronger preference for face-on molecular orientation of **7-1** in the active layers. These factors corresponded well with the improvements in J_{SC} (17.97 → 18.31 mA cm^{-2}) and FF (65.49 → 70.55%).

On the other hand, Liu *et al.* reported that replacement of all the *p*-hexylphenyl groups of ITIC with *p*-(2-methoxyethoxy) methylphenyl to form derivative **7-2** resulted in lowering of the PCE from 10.4% to 8.5% (entries 7-3 and 7-4).[122] The polar substituents of **7-2** led to decreased crystallinity and excessive mixing with the p-type polymer PBDB-T,[123] which induced lower mobilities and enhanced recombination of charge carriers.

Liu *et al.* compared end-chlorinated ITIC derivatives **7-3a–c** which differed in their alkyl-chain length in the four *p*-alkylphenyl groups.[124] The performance of the corresponding BHJ OPVs with a p-type polymer PBDB-TF (or PM6)[125] was increased

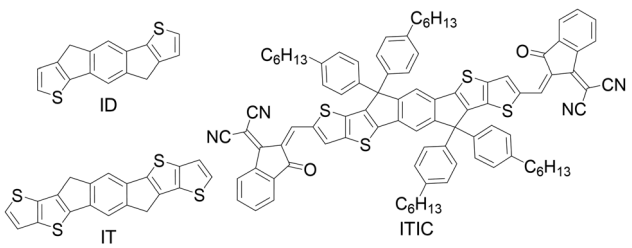

Fig. 12 Chemical structures of the ID and IT frameworks, and the non-fullerene n-type molecule ITIC. The structure of IDIC is shown in Fig. 4.

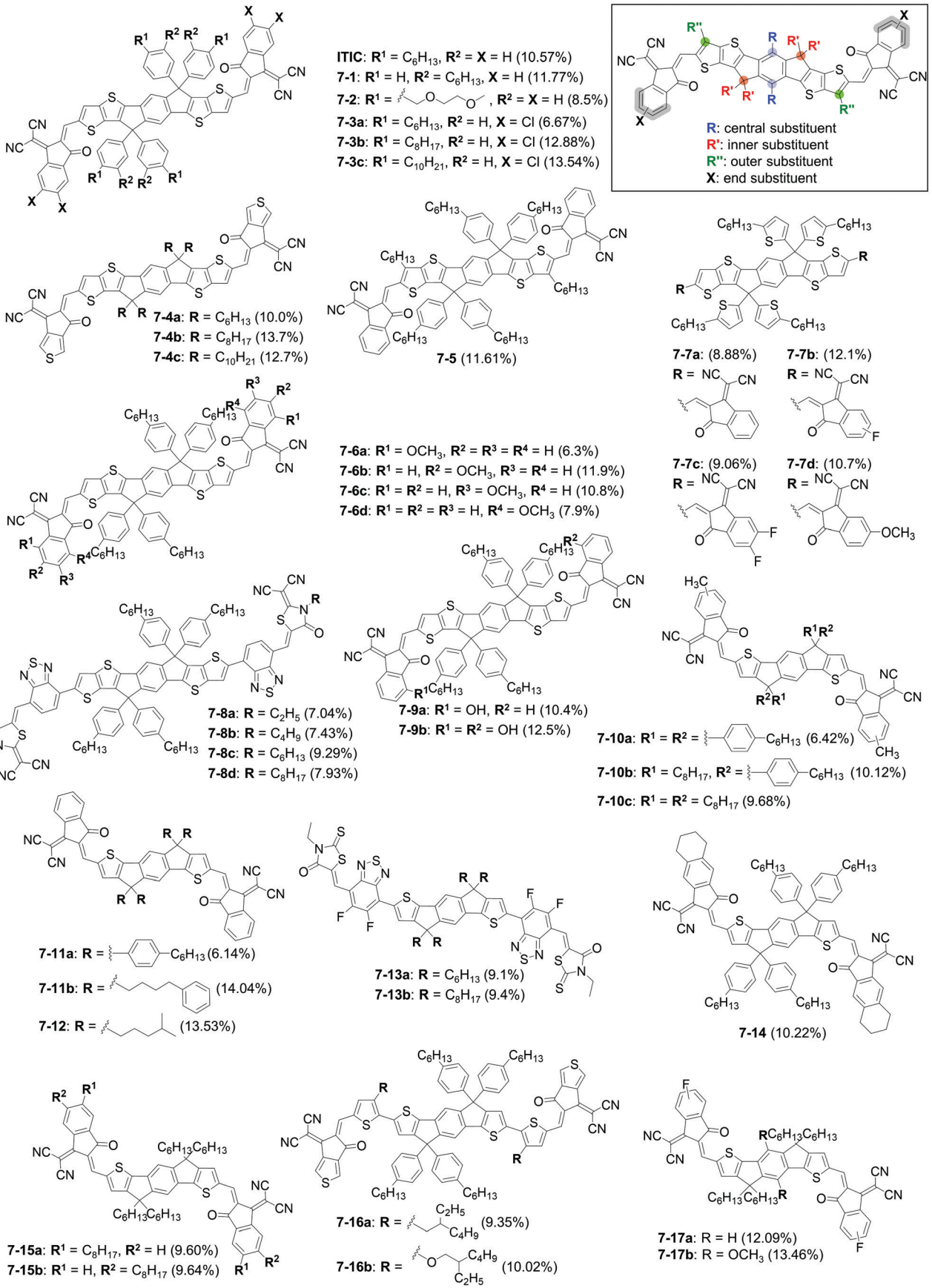

Fig. 13 Chemical structures of SMSCs **7-1-7-17**. The best PCEs obtained with each compound are shown in parentheses (see Table 7 for full OPV parameters). The inset shows relevant substitution positions of BDT-based SMSCs.

Table 7 Photovoltaic performance of SMSCs **7-1-7-17**[a]

Entry	Active layer	Solvent	Additional conditions	V_{OC}[b] (V)	J_{SC}[b] (mA cm^{-2})	FF[b] (%)	PCE[b] (%)	Ref.
7-1	J61 : **ITIC** (1 : 1)	CF	130 °C, 5 min	0.898	17.97	65.49	10.57	120
7-2	J61 : **7-1** (1 : 1)	CF	130 °C, 5 min	0.912	18.31	70.55	11.77	120
7-3	PBDB-T : **ITIC** (1 : 1)	CB	0.5 vol% DIO; 120 °C, 10 min	0.89	16.5	71	10.4	122
7-4	PBDB-T : **7-2** (1 : 1)	CB	0.5 vol% DIO; 120 °C, 10 min	0.85	14.8	67	8.5	122
7-5	PM6 : **7-3a** (1 : 1)	CB	100 °C, 10 min	0.78	18.85	45	6.67	124
7-6	PM6 : **7-3b** (1 : 1)	CB	100 °C, 10 min	0.83	20.44	76	12.88	124
7-7	PM6 : **7-3c** (1 : 1)	CB	100 °C, 10 min	0.87	20.32	77	13.54	124
7-8	PBT1-C : **7-4a** (1 : 1.3)	CF	0.5% DIO	0.85 ± 0.01	17.0 ± 0.3	66.7 ± 2.4	10.0 (9.6 ± 0.5)	126
7-9	PBT1-C : **7-4b** (1 : 1.3)	CF	0.5% DIO	0.88 ± 0.01	20.3 ± 0.2	74.6 ± 1.1	13.7 (13.4 ± 0.2)	126
7-10	PBT1-C : **7-4c** (1 : 1.3)	CF	0.5% DIO	0.98 ± 0.01	18.1 ± 0.3	71.3 ± 1.3	12.7 (12.5 ± 0.4)	126
7-11	PBDB-T : **7-5** (1 : 1)	CB	—	0.97	15.85	68	10.45	128
7-12	PBDB-T : **7-5** (1 : 1)	CB	125 °C, 10 min	0.97	16.41	73	11.61	128
7-13	PBDB-T : ITIC (1 : 1)	CB	0.5% DIO	0.91	16.27	69	10.21	128
7-14	PBDB-T : **7-6a** (1 : 1)	CB	0.5 vol% DIO; 150 °C, 30 min	1.01	12.31	51	6.3	129
7-15	PBDB-T : **7-6b** (1 : 1)	CB	0.5 vol% DIO; 150 °C, 30 min	0.93	17.53	73	11.9	129
7-16	PBDB-T : **7-6c** (1 : 1)	CB	0.5 vol% DIO; 150 °C, 30 min	0.97	16.38	68	10.8	129
7-17	PBDB-T : **7-6d** (1 : 1)	CB	0.5 vol% DIO; 150 °C, 30 min	0.96	14.69	56	7.9	129
7-18	FTAZ : **7-7a** (1 : 1.5)	CF	0.25 vol% DIO	0.915	15.84	61.26	8.88	130
7-19	FTAZ : **7-7b** (1 : 1.5)	CF	0.25 vol% DIO	0.849	19.33	73.73	12.1	130
7-20	FTAZ : **7-7c** (1 : 1.5)	CF	0.25 vol% DIO	0.751	17.19	70.07	9.06	130
7-21	FTAZ : **7-7d** (1 : 1.5)	CF	0.25 vol% DIO	0.962	16.34	68.33	10.7	130
7-22	PBDB-T : **7-8a** (1 : 1)	CB	0.3% DIO	0.89	13.47	59.03	7.04	132
7-23	PBDB-T : **7-8b** (1 : 1)	CB	0.3% DIO	0.90	14.94	55.09	7.43	132
7-24	PBDB-T : **7-8c** (1 : 1)	CB	0.3% DIO	0.89	14.94	58.21	8.26	132
7-25	PBDB-T : **7-8d** (1 : 1)	CB	0.3% DIO	0.90	14.88	59.35	7.93	132
7-26	PBDB-T : **7-8c** (1 : 1)	CB	0.3% DIO; THF vapour, 1 min; 120 °C, 10 min	0.88	16.30	64.18	9.29	132
7-27	PBDB-T : **ITIC** (1 : 1)	CB	0.5% DPE	0.87	15.45	57	7.8	133
7-28	PBDB-T : **7-9a** (1 : 1)	CB	0.5% DPE	0.89	16.71	70	10.4	133
7-29	PBDB-T : **7-9b** (1 : 1)	CB	0.5% DPE	0.87	18.04	70	11.0	133
7-30	PM6 : **7-9b** (1 : 1)	CB	0.5% DPE	0.96	17.78	73	12.5	133
7-31	PBDB-T : **7-10a** (1 : 0.5)	*o*-DCB	—	0.89	13.30	53.9	6.42	134
7-32	PBDB-T : **7-10b** (1 : 1)	*o*-DCB	—	0.88	16.18	71.1	10.12	134
7-33	PBDB-T : **7-10c** (1 : 1)	*o*-DCB	—	0.86	15.64	72.3	9.68	134
7-34	PBDB-T : **IDIC** (1 : 1)	CB	130 °C, 5 min	0.819	17.27	73.60	10.41	135
7-35	PBDB-T : **7-11a** (1 : 1)	CB	130 °C, 5 min	0.869	12.20	57.90	6.14	135
7-36	PBDB-T : **7-11b** (1 : 1)	CB	130 °C, 5 min	0.822	18.08	77.42	11.50	135
7-37	PM6 : **7-11b** (1 : 1)	CB	130 °C, 30 s	0.941	19.06	78.32	14.04	135
7-38	PM6 : **IDIC** (1 : 1)	CB	—	0.963	17.94	71.60	12.37	136
7-39	PM6 : **IDIC** (1 : 1)	CB	130 °C, 10 min	0.928	17.21	70.13	11.20	136
7-40	PM6 : **IDIC** (1 : 1)	CB	0.5 vol% DIO, 130 °C, 10 min	0.921	16.66	69.34	10.64	136
7-41	PM6 : **7-12** (1 : 1)	CB	—	0.963	18.55	73.26	13.10	136
7-42	PM6 : **7-12** (1 : 1)	CB	130 °C, 10 min	0.961	18.91	74.45	13.53	136
7-43	PM6 : **7-12** (1 : 1)	CB	0.5 vol% DIO, 130 °C, 10 min	0.926	18.87	75.58	13.21	136
7-44	PTB7-Th : **7-13a** (1 : 1.5)	CB	0.5% DIO, 120 °C, 5 min	0.940	16.9	57	9.1	137
7-45	PTB7-Th : **7-13b** (1 : 1.5)	CB	0.5% DIO, 120 °C, 5 min	0.940	17.0	59	9.4	137
7-46	PBDB-T : **7-14** (1.5 : 1)	CB	0.5% DIO, 120 °C, 5 min	0.93	14.43	76.41	10.22	138
7-47	PBDB-T : **IDIC** (1.5 : 1)	CB	0.5% DIO, 120 °C, 5 min	0.88	11.94	57.90	6.11	138
7-48	PBDB-T : **7-15a** (1 : 1)	*o*-DCB	—	0.92 ± 0.01	15.1 ± 0.47	68 ± 2	9.60 (9.40 ± 0.16)	139
7-49	PBDB-T : **7-15b** (1 : 1)	*o*-DCB	—	0.92 ± 0.01	14.8 ± 0.24	69 ± 2	9.64 (9.35 ± 0.24)	139
7-50	PBDB-T : **IDIC** (1 : 1)	*o*-DCB	—	0.85 ± 0.01	11.5 ± 0.35	71 ± 1	7.23 (6.96 ± 0.16)	139
7-51	PBDB-T : **7-16a** (1 : 1)	CF	160 °C, 2 min	0.917	16.56	61.61	9.35	140
7-52	PBDB-T : **7-16b** (1 : 1)	CF	160 °C, 2 min	0.943	16.25	65.41	10.02	140
7-53	PTQ10 : IDIC-2F	CF	120 °C, 5 min	0.892	18.94	71.7	12.09	141
7-54	PTQ10 : **7-17**	CF	110 °C, 5 min	0.906	19.87	74.8	13.46	141

[a] Structures of active-layer compounds are shown in Fig. 13 and 14. CF: chloroform, CB: chlorobenzene, *o*-DCB: *o*-dichlorobenzene, DIO: 1,8-diiodooctane, THF: tetrahydrofuran, DPE: diphenylether. [b] Data of the best-performing devices when available; otherwise, average of multiple devices.

as the alkyl chains were elongated from *n*-hexyl of **7-3a** (PCE = 6.67%) to *n*-octyl of **7-3b** (12.88%), and to *n*-decyl of **7-3c** (13.54%) (entries 7-5–7-7). The authors concluded that the short alkyl chains of **7-3a** induced the formation of tight molecular aggregations and excessive phase separation in BHJ films with PM6, leading to an increased non-radiative energy loss. The longer alkyl chains in **7-3b** and **7-3c**, in contrast, loosened intermolecular contacts and enabled finer phase separation, thereby suppressing the non-radiative energy loss.

Similarly, Ye *et al.* compared a series of A–D–A conjugates **7-4a–c** comprising a 6,6,12,12-tetraalkylated IT core and 2-(5-methylene-6-oxo-5,6-dihydro-4*H*-cyclopenta[*c*]thiophen-4-ylidene) malononitrile (TIC) end units.[126] Single-crystal X-ray structure analysis revealed that molecular stacking was largely affected by

the length of alkyl chains on the IT core, namely, molecules of *n*-hexyl derivative **7-4a** crystallized in a π–π stacking mode, *n*-octyl derivative **7-4b** in a mixed π–π/no π–π-stacking mode, and *n*-decyl derivative **7-4c** in a no π–π stacking mode. Meanwhile, BHJ OPVs with PBT1-C[127] as the p-type material showed maximum PCEs of 10.0% with **7-4a**, 13.7% with **7-4b**, and 12.7% with **7-4c** (entries 7-8–7-10). These results indicated that the end-group π–π staking could be non-critical in achieving sufficient charge-carrier transport and high photovoltaic efficiency; however, close side-atom contacts in non-π-staking modes could provide effective charge-carrier paths in the BHJ films. The authors also pointed out that energy loss was reduced with longer-alkyl derivatives.

Zhang *et al.* investigated the effect of outer substituents by comparing *n*-hexyl substituted derivative **7-5** with ITIC.[128] The steric hinderance of the outer *n*-hexyl groups was expected to lock the orientation of the end electron withdrawing units, leading to enhanced planarity of the overall π-conjugated system. In addition, these alkyl chains were found to weaken the π–π stacking, enhancing the compatibility of this compound with the donor polymer PBDB-T. These effects brought about a PCE of 10.45% which is slightly higher than that with the original ITIC (10.21%, entries 7-11 and 7-13). The efficiency was further improved to 11.61% (entry 7-12) after thermal annealing at 125 °C which induced a higher degree of phase separation and crystallization of the polymer to form fibrous morphology.

The effect of end-unit substituents in this class of n-type compounds has also been studied by several groups. For example, Li *et al.* evaluated four methoxy-substituted ITIC derivatives **7-6a–d** for their performance in BHJ OPVs with PBDB-T (entries 7-14–7-17).[129] Higher PCEs were obtained with **7-6b** (11.9%) and **7-6c** (10.8%) with methoxy groups at the 6- and 5-positions, respectively, of the two 2-(2-methylene-3-oxo-2,3-dihydro-1*H*-inden-1ylidene)malononitrile (IC) units. In contrast, the derivatives with 7- and 4-methoxy IC units (**7-6a** and **7-6d**) afforded considerably lower PCEs of 6.3% and 7.9%. The superiority of **7-6b** and **7-6c** was explained with higher planarity of their IC units due to lower steric hinderance, which led to a more efficient intermolecular π–π stacking and higher charge-carrier mobilities. The effect of these factors was observed as enhanced J_{SC} and FF.

In a related vein, Li *et al.* compared four 6,6,12,12-tetra(5-hexylthiophen-2-yl) IT derivatives differently substituted at the benzo moiety of the IC end-capping units: non-substituted **7-7a** (known as ITIC-Th), 5- or 6-fluoro derivative **7-7b**, 5,6-difluoro derivative **7-7c**, and 6-methoxy derivative **7-7d**.[130] These substituents altered not only the electronic structures of the main π-conjugated backbone, but also the intermolecular arrangement and the morphological behavior. Monosubstituted derivatives **7-7b** and **7-7c** showed a more ordered molecular packing, associated with higher crystallinity and longer coherence length than **7-7a** and **7-7d** in blended films with a p-type polymer FTAZ[131] as revealed by the 2D-GIWAXS data. Additionally, the monofluorinated derivative **7-7b** showed smaller-sized domains in the blended film with FTAZ, resulting in a higher PCE (12.1%) of the FTAZ:**7-7b** system than those of FTAZ:**7-7a** (8.88%), FTAZ:**7-7c** (9.06%), and FTAZ:**7-7d** (10.7%) (entries 7-18–7-21).

Qu *et al.* investigated the optimal length of end-alkyl chains on an A–D–A system comprising IT as the donor, rhodanine as the acceptor, and benzothiadiazole as the linker.[132] Among the four end-alkylated derivatives, the hexyl derivative **7-8c** afforded a higher PCE of 8.26% than the ethyl (**7-8a**, 7.04%), butyl (**7-8b**, 7.43%), and octyl (**7-8d**, 7.93%) derivatives in BHJ OPVs with PBDB-T as the p-type material (entries 7-22–7-25). The 2D-GIWAXS data of these BHJ films suggested that the size of crystallites increased in the order of PBDB-T:**7-8a** < PBDB-T:**7-8b** < PBDB-T:**7-8d** < PBDB-T:**7-8c**, roughly matching with the order of the J_{SC}s as well as PCEs. Note that derivative **7-8c** afforded an improved PCE of 9.29% after solvent-vapor annealing followed by thermal annealing (entry 7-26). In addition, derivative **7-8a** showed a higher crystallinity than the other derivatives in neat films, demonstrating that the morphology of blended films cannot be predicted based on the structure of neat films alone.

Hydrogen-bond-directed manipulation of molecular packing and film morphology was attempted with hydroxy-functionalized ITIC derivatives by Liu *et al.*[133] By comparing ITIC with end-hydroxyl derivatives **7-9a** and **7-9b**, the authors demonstrated that hydroxy substitution at the end-capping IC units brought about a higher packing order and crystallinity in BHJ films with PBDB-T, which was attributed to the formation of intermolecular hydrogen-bonding. Predictably, the dihydroxy derivative **7-9b** showed a higher crystallinity than the monohydroxy derivative **7-9a**. Consequently, the BHJ systems of PBDB-T:**7-9a** and PBDB-T:**7-9b** afforded PCEs of 10.4% and 11.0%, while PBDB-T:ITIC gave a somewhat lower PCE of 7.8% (entries 7-27–7-29). Furthermore, the diol **7-9b** gave an even higher PCE of 12.5% when combined with PM6 (entry 7-30).

Molecules with an indacenodithiophene core

IDIC has four hexyl chains directly attached onto the 4- and 9-carbons of the ID framework. As in the case of four 4-hexylphenyl groups on ITIC, these substituents are electrically insulating but still exert a significant impact on the photovoltaic process by preventing IDIC molecules from excessive π–π stacking and ensuring the formation of sufficient p–n junction areas in BHJ films.

In 2017, Feng *et al.* reported that nonsymmetric substitution of the ID core at the 4- and 9-carbons led to improved photovoltaic performance.[134] The authors evaluated three IDIC derivatives **7-10a–c**, and demonstrated that the nonsymmetric di(4-hexylpheny)–dioctyl derivative **7-10b** afforded a higher PCE (10.12%) than the tetra(4-hexylphenyl) derivative **7-10a** (6.42%) and the tetraoctyl derivative **7-10c** (9.68%) in BHJ OPVs with PBDB-T (entries 7-31–7-33). While the devices with symmetric derivatives suffered from either excessive phase separation (**7-10a**) or lower electron mobility (**7-10c**), the nonsymmetrically substituted **7-10b** yielded adequately attenuated crystallinity and improved charge-carrier mobilities in the BHJ film. Interestingly, photovoltaic efficiency of the PBDB-T:**7-10b** system was found to be less sensitive to active-layer thickness than other systems, giving a 9.17% PCE even in a >200 nm-thick film.

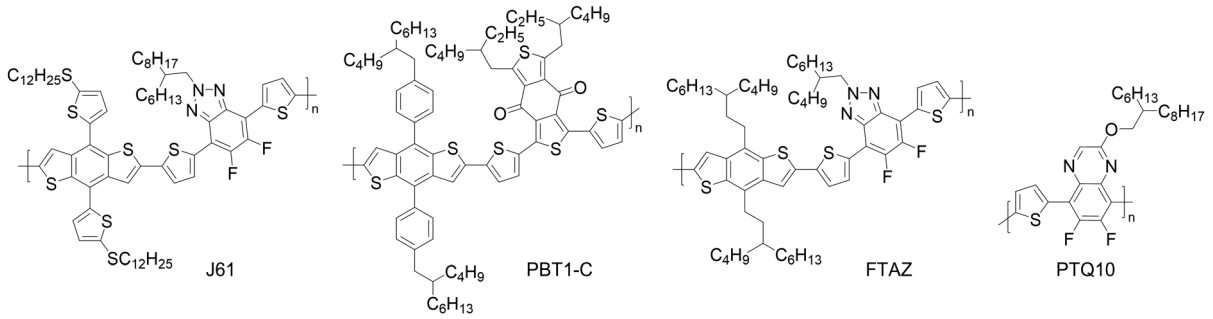

Fig. 14 Chemical structures of the compounds employed with **7-1-7-17** in OPV active layers. PBDB-T, PTB7-Th, and PM6 are shown in Fig. 2 or Fig. 4.

Li *et al.* proposed a different molecular design to avoid excessive aggregation while at the same time achieve efficient charge-carrier transport. The authors demonstrated the superiority of phenylbutyl over hexyl and 4-hexylpheny as 4,4,9,9-substituents on the ID core by comparing IDIC and its two derivatives **7-11a** and **7-11b**.[135] Evaluation of the three compounds resulted in PCEs of 10.41% (IDIC), 6.14% (**7-11a**), and 11.50% (**7-11b**) in BHJ OPVs with PBDB-T (entries 7-34–7-36). Here, the FF of the PBDB-T:**7-11b** device was as high as 77.42%, and impressively, it was further optimized to 78.32% when PM6 was used instead of PBDB-T (entry 7-37). Thus, introduction of a slightly bulky phenyl group at the tail, rather than the head, of core alkyl substituents would be an effective molecular design for obtaining optimal morphology in BHJ films.

In connection to the work by Li *et al.*, Chen *et al.* demonstrated that an even subtler difference in substituent structure could bring about appreciable differences in the morphology and performance of BHJ films.[136] They evaluated compound **7-12** which was differentiated from IDIC only by the alkyl substituents on the ID core (4-methylpentyl for **7-12**, hexyl for IDIC), and demonstrated that **7-12** afforded a higher PCE of 13.53% than IDIC (11.20%) in thermally annealed BHJ layers with PM6 (entries 7-39, 42). In a similar manner to the phenylbutyl groups of **7-11b**, the alkyl chains with a branched terminal in **7-12** modestly attenuated crystallization and self-aggregation without sacrificing π–π stacking and charge-carrier mobilities. The difference in morphological behavior between the PM6:**7-12** and PM6:IDIC systems could be noted when comparing their response to annealing treatments (entries 7-38–7-43).

Additionally, Chen *et al.* reported a related study with ID–benzothiadiazole–rhodanine conjugates **7-13a** and **7-13b**.[137] In this case, again, substitution with more extended alkyl chains (octyl) on the ID core adequately attenuated self-aggregation and phase separation when compared to more compact (hexyl) alkyl chains in BHJ films. Accordingly, higher photovoltaic performance resulted from **7-13b** (PCE = 9.4%) than **7-13a** (9.1%) in BHJ OPVs with PTB7-Th as the p-type material (entries 7-44 and 7-45).

Here, it would be worth pointing out that the ID core requires smaller substituents as compared to the IT core for obtaining BHJ layers with optimal morphology. Specifically, alkyl groups up to octyl are common for ID, while the considerably larger hexylphenyl is typical for IT. This difference should be a reflection of the size of these π-cores.

Regarding the end IC units, the positive effects of alkyl substitution have been reported in several papers. For example, Li *et al.* showed that cyclohexyl-fused derivative **7-14** performed better than IDIC, providing a PCE of 10.22% (6.11% with IDIC) in a BHJ OPV with PBDB-T (entries 7-46 and 7-47).[138] Also, Ryu *et al.* reported that derivatives **7-15a** and **7-15b** with end-octyl substituents afforded similarly high PCEs of 9.60% and 9.64%, respectively, while that with IDIC was only 7.23% at the best (entries 7-48–7-50).[139] In both examples, end-alkyl-substitution led to higher crystallinity of the corresponding BHJ films without excessive phase separation, which contributed to more balanced, higher charge-carrier mobilities and thus enhancement in J_{SC}. Note that the improvement in FF was also significant in the PBDB-T:**7-14** system, while the resultant increase of both J_{SC} and V_{OC} was achieved in the PBDB-T:**7-15** systems.

Luo *et al.* studied the effect of substituents at linker units in an ID–TIC-conjugate system by comparing 2-ethylhexyl substituted **7-16a** and 2-ethylhexyloxy substituted **7-16b**.[140] As can be expected from the alkoxy substituents' more electron-donating nature than that of alkyl ones, **7-16b** showed a higher LUMO level resulting in an enhanced V_{OC} in a BHJ device with PBDB-T (entries 7-51 and 7-52). In addition, the authors pointed out that more favorable phase separation and balanced charge-carrier mobilities were observed in **7-16b**, which contributed to the higher FF than that of the PBDB-T:**7-16a** BHJ system.

Li *et al.* reported in their article in 2019 that the introduction of methoxy groups as the core substituents led to higher photovoltaic efficiency (entries 7-53 and 7-54).[141] The best PCE obtained with the methoxy-substituted compound **7-17a** was 13.46% when used as the n-type material in BHJ OPVs in combination with the p-type polymer PTQ10. On the other hand, the PCE with the parent compound **7-17b** (commonly called IDIC-2F) remained 12.09% at the best. The methoxy derivative was designed in the context of simplifying the synthesis to realize easily accessible, cost-effective SMSCs for OPVs; at the same time, this work revealed the effectiveness of core substitution for achieving high-performance IDIC-based materials.

9. Substituents of di(thienothienopyrrolo)-benzothiadiazole-based π-conjugates

A benzothiadiazole-based fused-ring system 12,13-dihydrodi(thieno[2″,3″:4′,5′]thieno[2′,3′:4,5]pyrrolo[3,2-*e*:2′,3′-*g*])benzothiadiazole (TPBT, Fig. 15) is another outstanding core

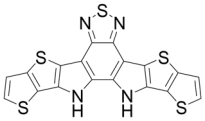

Fig. 15 Chemical structure of the TPBP framework.

unit for non-fullerene n-type molecules. The report of Y6 (Fig. 10b) by Yuan *et al.*[142] in 2019, which demonstrated an excellent PCE of 15.7% with the PM6:Y6 BHJ OPV, brought about the development of this class of molecules,[143] and optimization of peripheral substituents has been an important part of the research as in the case of other SMSCs. This section reviews relevant papers on this topic. The corresponding chemical structures and the photovoltaic data are summarized in Fig. 16 and Table 8, respectively.

The TPBT framework offers three types of positions to introduce substituents: pyrrolic nitrogens (inner), thieno β-carbons (outer), and end-benzo carbons (end) as depicted in the inset of Fig. 15. Soon after the first paper on Y6, Jiang *et al.* reported the photovoltaic performance of three derivatives **8-1a–c** which were differently substituted at the inner and outer positions.[144] Among the three derivatives, inner-3-ethylheptyl/outer-dodecyl **8-1b** performed better (PCE = 15.98%) than the original inner-2-ethylhexyl/outer-dodecyl Y6 (15.20%) in BHJ OPVs with PM6, while inner-dodecyl/outer-2-ethylhexyl **8-1a** and inner-4-ethyloctyl/outer-dodecyl **8-1c** afforded lower PCEs of 12.91% and 14.31%, respectively (entries 8-1–8-4). Derivative **8-1a** was found have lower solubility than the other three compounds, forming large domains in the BHJ film with PM6. Combined with the considerably lower PCE from **8-1a**, this result indicated that a certain degree of bulkiness of inner substituents would be necessary for the TPBT framework to form an adequate BHJ morphology. Meanwhile, the effect of branching positions in inner alkyl chains was found to be relatively minor, but still non-negligible. In relation to this work, Yu *et al.* compared 2-ethylhexyl and 3-ethylhexyl as the inner substituents of tetrachloro derivatives **8-2a** and **8-2b**, respectively. They found the latter worked slightly better in devices with PM6 to afford a PCE of 16.532%, while the former provided PCEs of up to 16.061% (entries 8-5 and 8-6).[145]

There have been several other reports regarding the optimization of the inner substituents of Y6-type systems. Han *et al.* introduced 4-phenylbutyl and 6-phenylhexyl instead of branched alkyl chains, and compared the performance of the resulting compounds **8-3a** and **8-3b** in BHJ OPVs bearing PM6

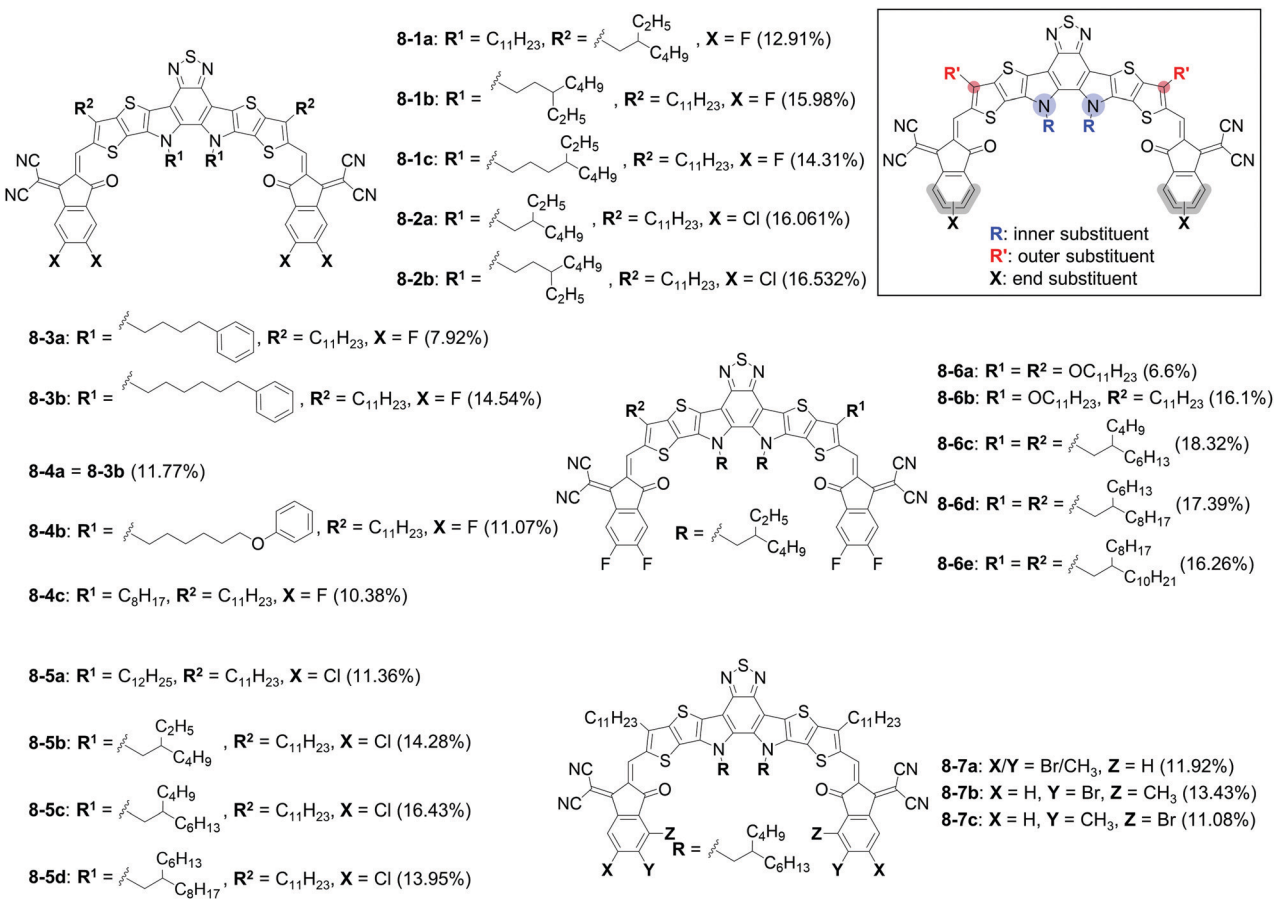

Fig. 16 Chemical structures of SMSCs **8-1**–**8-7**. The best PCEs obtained with each compound are shown in parentheses (see Table 8 for full OPV parameters). The inset shows relevant substitution positions of Y6 and its derivatives. Structures of the partner material in the photovoltaic active layer (PM6) are shown in Fig. 2.

Table 8 Photovoltaic parameters of SMSCs **8-1-8-7**[a]

Entry	Active layer	Solvent	Additional conditions	V_{OC}[b] (V)	J_{SC}[b] (mA cm^{-2})	FF[b] (%)	PCE[b] (%)	Ref.
8-1	PM6 : Y6 (1 : 1.2)	CF	0.05% CN; 90 °C, 5 min	0.847	24.02	74.7	15.20	144
8-2	PM6 : **8-1a** (1 : 1.2)	CF	0.05% CN; 90 °C, 5 min	0.852	21.47	70.6	12.91	144
8-3	PM6 : **8-1b** (1 : 1.2)	CF	0.05% CN, 90 °C, 5 min	0.837	25.81	73.9	15.98	144
8-4	PM6 : **8-1c** (1 : 1.2)	CF	0.05% CN, 90 °C, 5 min	0.819	25.01	69.9	14.31	144
8-5	PM6 : **8-2a** (1 : : 1.2)	CF	90 °C, 5 min	0.839	25.849	74.1	16.061	145
8-6	PM6 : **8-2b** (1 : 1.2)	CF	90 °C, 5 min	0.852	25.901	74.9	16.532	145
8-7	PM6 : **8-3a** (1 : 1.2)	CF	0.5 vol% CN	0.689	15.74	67.01	7.28	146
8-8	PM6 : **8-3b** (1 : 1.2)	CF	0.5 vol% CN	0.84	23.82	72.68	14.54	146
8-9	PM6 : **8-3a** (1 : 1.2)	CF	0.5 vol% CN; 100 °C	0.709	16.43	68.00	7.92	146
8-10	PM6 : **8-3b** (1 : 1.2)	CF	0.5 vol% CN; 100 °C	0.804	25.11	67.25	13.58	146
8-11	PM6 : **8-4a** (1 : 1.5)	CF	100 °C, 5 min	0.803	21.80	67.3	11.77	147
8-12	PM6 : **8-4b** (1 : 1.5)	CF	–	0.844	21.31	61.6	11.07	147
8-13	PM6 : **8-4c** (1 : 1.5)	CF	–	0.863	19.07	63.1	10.38	147
8-14	PM6 : **8-5a** (1 : 1.2)	CF	0.5 vol% DIO; 100 °C	0.84	19.82	68.27	11.36	148
8-15	PM6 : **8-5b** (1 : 1.2)	CF	0.5 vol% DIO; 100 °C	0.88	18.90	56.24	9.38	148
8-16	PM6 : **8-5c** (1 : 1.2)	CF	0.5 vol% DIO; 100 °C	0.85	24.80	72.20	15.13	148
8-17	PM6 : **8-5d** (1 : 1.2)	CF	0.5 vol% DIO; 100 °C	0.86	23.24	69.78	13.95	148
8-18	PM6 : **8-5b** (1 : 1.2)	CB	0.5 vol% DIO; 100 °C	0.83	25.13	68.94	14.28	148
8-19	PM6 : **8-5c** (1 : 1.2)	CB	0.5 vol% DIO; 100 °C	0.85	25.26	76.25	16.43	148
8-20	PM6 : Y6 (1 : 1.2)	CF	0.5 vol% CN; 100 °C, 5 min	0.82	25.3	75.5	15.7	149
8-21	PM6 : **8-6a** (1 : 1.2)	CF	0.5 vol% CN; 100 °C, 5 min	0.92	13.3	53.5	6.6	149
8-22	PM6 : **8-6b** (1 : 1.2)	CF	0.5 vol% CN; 100 °C, 5 min	0.89	23.2	78.5	16.1	149
8-23	PM6 : Y6 (1 : 1.2)	CF	0.25% DIO; 100 °C, 10 min	0.84	25.91	76.0	16.61	150
8-24	PM6 : **8-6c** (1 : 1.2)	CF	0.25% DIO; 100 °C, 10 min	0.87	25.72	81.5	18.32	150
8-25	PM6 : **8-6d** (1 : 1.2)	CF	0.25% DIO; 100 °C, 10 min	0.88	25.08	78.8	17.39	150
8-26	PM6 : **8-6e** (1 : 1.2)	CF	0.25% DIO; 100 °C, 10 min	0.89	24.57	74.6	16.26	150
8-27	PM6 : **8-7a** (1 : 1.2)	CF	0.5% CN; 100 °C, 10 min	0.94	20.31	62.53	11.92	151
8-28	PM6 : **8-7b** (1 : 1.2)	CF	0.5% CN; 100 °C, 10 min	0.92	21.38	68.25	13.43	151
8-29	PM6 : **8-7c** (1 : 1.2)	CF	0.5% CN; 100 °C, 10 min	0.95	18.79	61.79	11.08	151

[a] Structures of active-layer compounds are shown in Fig. 16. CF: chloroform, CB: chlorobenzene, DIO: 1,8-diiodooctane, CN: chloronaphthalene. [b] Data of the best-performing devices.

as the p-type material.[146] Indeed, the difference between the two compounds turned out to be significant, that is, the 4-phenylbutyl derivative **8-3a** gave a 7.28% PCE, while the 6-phenylhexyl derivative **8-3b** afforded a 14.54% PCE without annealing treatment (entries 8-7 and 8-8). With thermal annealing, PCEs were 7.92% for **8-3a** and 13.58% for **8-3b** (entries 8-9 and 8-10). The authors pointed out that the PM6:**8-3b** BHJ film showed stronger tendency for face-on orientation, tighter molecular stacking, and a larger crystallite coherence length than the PM6:**8-3a** blend. The superior performance of **8-3b** could be linked to the synergistic contribution of these morphological factors. In addition, Yi and co-workers demonstrated that 6-phenylhexyl was a better choice than 6-phenoxyhexyl and octyl as the inner substituent by comparing compounds **8-4a–8-4c** (**8-4a** = **8-3b**) in BHJ OPVs with PM6 (PCE = 11.77%, 11.07%, and 10.38%), although the difference was less significant as compared with the case of the **8-3** series (entries 8-11–8-13).[147]

Mo *et al.* comparatively evaluated **8-5a–d** in BHJ OPVs with PM6.[148] All these four compounds had chlorine atoms instead of fluorine atoms of Y6 at the end benzo units and were differentiated from each other by the structure of inner alkyl chains (dodecyl for **8-5a**, 2-ethylhexyl for **8-5b**, 2-butyloctyl for **8-5c**, and 2-hexyldecyl for **8-5d**). Interestingly, the authors successfully obtained a single-crystal X-ray structure of **8-5c** and revealed that the two inner alkyl chains extruded in the opposite directions from each other from the π-framework, indicating strong influence of the alkyl chains in determining π-stacking motif in the solid state. The OPV performance was indeed largely dependent on alkyl-chain lengths; specifically, PCEs were 11.36%, 9.38%. 15.13%, and 13.95% for **8-5a–d**, respectively, when the active layers were cast from chloroform solutions (entries 8-14–8-17). The unexpectedly low PCE with the 2-ethylhexyl derivative **8-5b** was due to its insufficient solubility in chloroform, which was improved to 14.28% when chlorobenzene was used to replace chloroform (entry 8-18). In addition, the 2-butyloctyl derivative **8-5c** afforded an impressive PCE of 16.43% when deposited from chlorobenzene (entry 8-19). The superiority of **8-5c** was partly attributed to the higher and more balanced charge-carrier mobilities in the corresponding BHJ film, which should be related to the shorter π–π stacking distance revealed by the 2D GIWAXS analysis. In general, the branched alkyl chains yielded more positive effects than the linear dodecyl chain regarding photovoltaic performance.

The impact of the outer alkyl groups was investigated by Chen *et al.*[149] They compared Y6 with symmetric dialkoxy derivative **8-6a** and non-symmetric alkyl/alkoxy derivative **8-6b** in BHJ OPVs with PM6 as the p-type polymer (entries 8-20–8-22). As could be expected from the more electron-donating nature of alkoxy groups as compared to that of alkyl groups, the LUMO level was increased upon replacing the dodecyl groups of Y6 with dodecyloxy to form **8-6a** (−3.89 → −3.76 eV). The increase in the LUMO level of the n-type material is in general favourable for obtaining a high V_{OC}, and this was the case in **8-6a** (0.82 → 0.92 V). However, the PCE with this didodecyloxy derivative was considerably lower than that with Y6 (6.6% *vs.* 15.7%). This

result was attributed to the poor solubility of **8-6a** in the cast solvent (chloroform) which induced excessive crystallinity and domain sizes. The non-symmetric alkyl/alkoxy derivative **8-6b**, on the other hand, showed both sufficient solubility and moderately improved V_{OC}, affording the best PCE (16.1%) among the three compounds.

In a similar vein, Li *et al.* comparatively evaluated Y6 and its three derivatives **8-6c–e** having 2-butyloctyl, 2-hexyldecyl, and 2-octyldodexyl, respectively, as the outer substituents.[150] The highest efficiency was obtained with **8-6c** (PCE = 18.32%) in a BHJ OPV using Y6 as the p-type material, while Y6, **8-6d**, and **8-6e** afforded PCEs of 16.61%, 17.39%, and 16.26% (entries 8-23–8-26). The better performance of the 2-butyloctyl derivative **8-6c** was attributed to its effective π–π contacts and an adequate degree of phase separation/crystallization in the BHJ active layer as indicated by XRD and microscopic analyses. The authors pointed out that the outer substituents are near the major π–π stack position of the Y6 derivative and thus an interesting structural factor to consider for tuning the molecular arrangement in the solid state.

Chen *et al.* studied the effect of end groups by evaluating compounds **8-7a–c** for performance in BHJ OPVs with PM6 (entries 8-27–8-29).[151] All the three compounds were substituted with a methyl group and a bromine atom at each end benzo moiety, with different substitution positions. Among the three isomers, **8-7b** afforded a higher PCE (13.43%) than **8-7a** (11.92%) and **8-7c** (11.08%), which was ascribed to the higher crystallinity of the PM6:**8-7b** film.

Overall, the currently available data point to the superiority of branched alkyls as both the inner and outer substituents, as well as the need for halogen end groups, for achieving the state-of-the-art Y6-derived acceptors. Nonsymmetric substitution may bring about additional improvement, which requires further systematic investigation.

10. Substituents of other π-conjugated systems

There have been several studies involving less common π-conjugated frameworks, but they still presented considerable substituent impact on the photovoltaic performance. These studies will serve as valuable references for further optimization of the currently available systems and can be even more so for developing new SMSCs based on novel π-conjugated backbones. This section reviews papers of this sort, roughly in the order of publication. The chemical structures and the photovoltaic data of the corresponding compounds are summarized in Fig. 17 and Table 9.

Compounds used as p-type

Ouchi *et al.* studied the effect of alkyl substituents on the supramolecular and photovoltaic behaviour of barbiturated oligo(butylthiophene)s **9-1a** and **9-1b**.[152] While similar tape-like hydrogen-bonded supramolecules were assembled from these isomeric compounds, their higher-order structures differed significantly; specifically, **9-1a** formed a helically twisted structure, and **9-2b** formed a lamellar packing (Fig. 18). These nano-architectures were generated even in blended films with $PC_{71}BM$, affording PCEs of 4.50% (**9-1a**) and 1.39% (**9-1b**) in the corresponding devices, respectively (entries 9-1 and 9-2). This example clearly demonstrates the importance of regulating higher order structures for obtaining optimal photovoltaic performance with supramolecular materials.

Suzuki and co-workers compared four alkylated derivatives of di(bithienyl)anthracene, **9-2a–d**.[153] Depending on the structure of end-alkyl groups, these compounds afforded considerably different V_{OC}s in BHJ OPVs: 0.966 V with **9-2a**, 0.419 V with **9-2b**, 0.499 V with **9-2c**, and 0.602 V with **9-2d**. Accordingly, the corresponding PCEs ranged widely from 1.46% to 4.02% (entries 9-3–9-6). The authors reasoned, based on single-crystal X-ray analysis and quantum chemical calculations, that the higher V_{OC} from **9-2a** was the result of its branched 2-ethylhexyl chains that effectively inhibited the formation of the non-slipped stacking of π-frameworks that would have otherwise led to an increase in the HOMO level and thus a decrease in V_{OC}. On the other hand, the linear alkyl chains in **9-2b–d** partially allowed the formation of the non-slipped stacking, and this tendency was stronger when alkyl chains were shorter. Note that compounds **9-2a–d** were deposited through a precursor approach similarly to the case of the **4-7** series in Section 5. The difference is that compounds **9-2a–d** were formed by a light-induced reaction, rather than thermally induce ones for **4-7**, from the corresponding α-diketone-type precursors **9-3a–d** (Scheme 2).[154] The relationship between the substituent structure, molecular packing, and photovoltaic properties was revealed in this study using the precursor approach which relieved the concerns regarding solubility.

Compounds used as n-type

In 2020, He *et al.* reported three near infrared-active n-type compounds comprising a di(thienopyrrolo)benzothiadiazole core, two IC end units, and two thienylene linkers (**9-4a–c**).[155] The three compounds differ in their alkyl chains on the β-positions of the thienylene linkers: inward decyl chains for **9-4a**, outward 2-ethylhexyl chains **9-4b**, and outward decyl chains **9-4c**. Evaluation in BHJ OPVs bearing PBDB-T as the p-type polymer showed that derivative **9-4c** (PCE = 13.75%) performed better than **9-4a** (6.98%) and **9-4b** (13.15%); thus, outward chains were better than inward, and linear chains were better than branched (entries 9-7–9-9). The authors pointed out that PBDB-T:**9-4c** showed the strongest intensity and the closest π–π stacking distance (3.55 Å) among the three BHJ systems, which brought about its superior photovoltaic performance.

An extensive screening of side alkyl substituents on the seven-ring-fused system was reported by Kan *et al.*[156] The authors introduced linear alkyl chains of different lengths to the outer side position of the fused-ring system to form compounds **9-5b–g** (**9-5a** was a non-substituted version), and evaluated them as n-type materials in BHJ OPVs with PM6 (entries 9-10–9-16). The octyl derivative **9-5e** was found to perform best among the seven compounds, providing a PCE

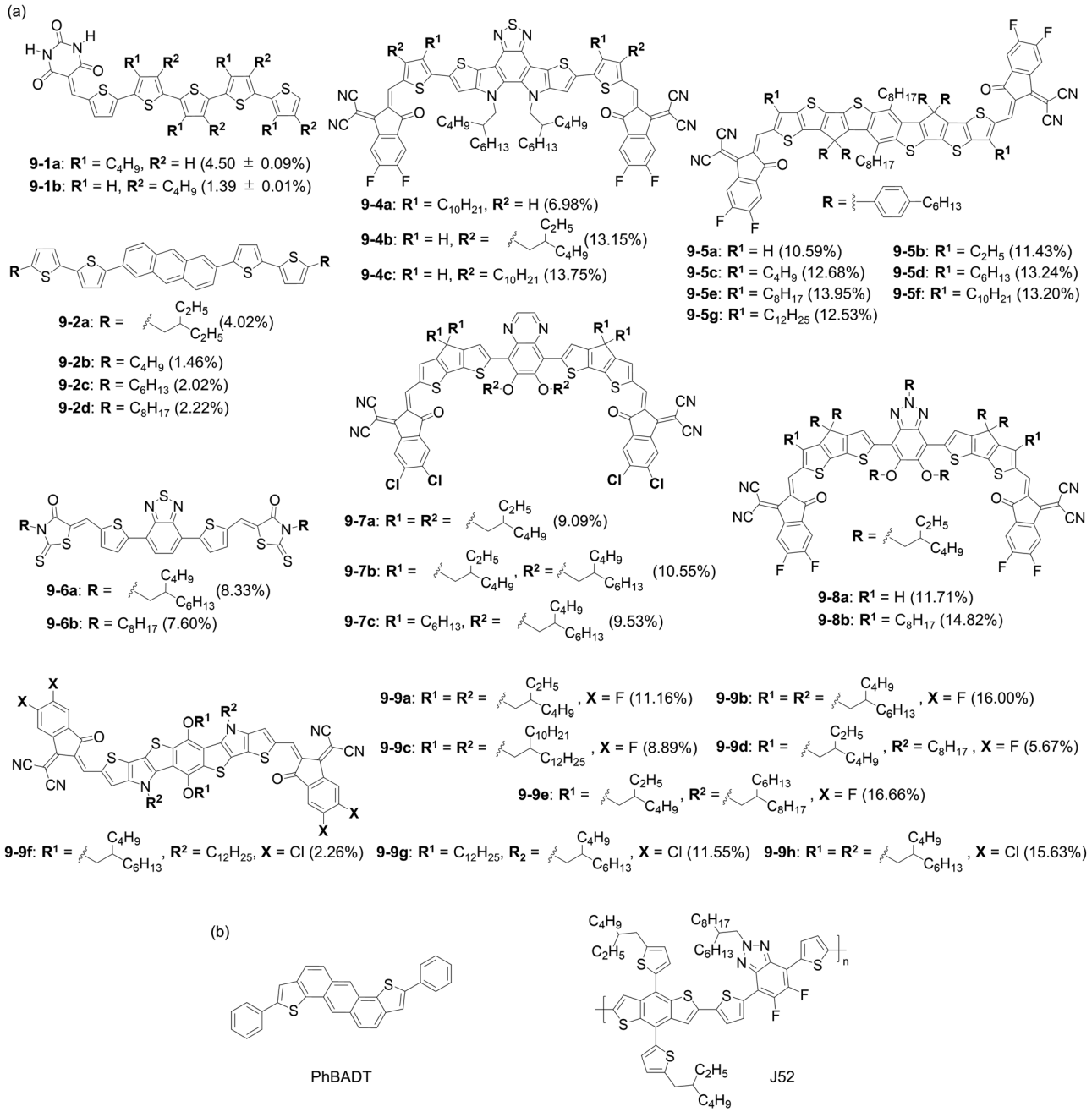

Fig. 17 Chemical structures of (a) SMSCs **9-1-9-9** and (b) the compounds employed with **9-1-9-9** in photovoltaic active layers. $PC_{71}BM$, PBDB-T, PM6, and PTB7-Th are shown in Fig. 2 or Fig. 4.

of 13.95%. Note that ternary system PM6:**9-5e**:F-Br gave an excellent PCE up to 15.34%.

Relatively simple, non-fused conjugates **9-6a** and **9-6b** were compared by Lee *et al.*[157] These compounds were flanked by different alkyl chains (2-butyloctyl for **9-6a** and octyl for **9-6b**) and their effects were examined in BHJ OPVs with PTB7-Th. The result was that **9-6b** (PCE = 6.21%) performed better than **9-6a** (5.97%) in the as-cast active layers, **9-6a** (8.33%) outperformed **9-6b** (7.60%) after solvent-vapour annealing (entries 9-17–9-20). It was found that the hole and electron mobilities were more balanced in the annealed PTB7-Th:**9-6a** blend as compared with PTB7-Th:**9-6b**.

A comparison between different alkyl side chains was also performed with a dialkoxyquinoxaline–cyclopentadithiophene conjugate system bearing chlorinated version of ICs (IC-4F) as end groups (**9-7a–c**).[158] The three compounds had different alkyl chains on the alkoxy units and the cyclopentadiene moieties. A general trend observed among them was that the introduction of longer branched alkyl chains induced a more favourable π–π stacking and phase separation in PBDB-T:**9-7** films. Accordingly, the 2-ethylhexyloxy/2-butyloctyl derivative **9-7b** afforded a higher PCE (10.55%) than the 2-ethylhexyloxy/2-ethylhexyl derivative **9-7a** (9.09%) and hexyl/

Table 9 Photovoltaic performance of SMSCs **9-1-9-8**[a]

Entry	Active layer	Solvent	Additional conditions	V_{OC}[b] (V)	J_{SC} (mA cm^{-2})	FF[b] (%)	PCE[b] (%)	Ref.
9-1	**9-1a** : $PC_{71}BM$ (1 : 1)	CF	CS_2 vapour, 80 s	0.74 ± 0.00	9.73 ± 0.20	62.2 ± 0.8	4.50 ± 0.09	152
9-2	**9-1b** : $PC_{71}BM$ (1 : 1)	CF	CS_2 vapour, 120 s	0.70 ± 0.02	3.95 ± 0.13	50.2 ± 0.4	1.39 ± 0.01	152
9-3	PhBADT/**9-2a** : $PC_{71}BM$ (2 : 1)/$PC_{71}BM$	CF	THF vapour, 60 s	0.966	6.71	62.0	4.02	153
9-4	PhBADT/**9-2b** : $PC_{71}BM$ (2 : 1)/$PC_{71}BM$	CF	THF vapour, 60 s	0.419	7.20	48.3	1.46	153
9-5	PhBADT/**9-2c** : $PC_{71}BM$(2 : 1)/$PC_{71}BM$	CF	THF vapour, 60 s	0.499	7.19	56.2	2.02	153
9-6	PhBADT/**9-2d** : $PC_{71}BM$ (2 : 1)/$PC_{71}BM$	CF	THF vapour, 60 s	0.602	6.83	54.1	2.22	153
9-7	PBDB-T : **9-4a** (1 : 1.2)	CF	0.5% CN; 150 °C, 10 min	0.784	16.81	53	6.98	155
9-8	PBDB-T : **9-4b** (1 : 1.2)	CF	0.5% CN; 150 °C, 10 min	0.781	24.40	69	13.15	155
9-9	PBDB-T : **9-4c** (1 : 1.2)	CF	0.5% CN; 150 °C, 10 min	0.757	25.84	70	13.75	155
9-10	PM6 : **9-5a** (1 : 1)	CB	0.5 vol% DIO; 140 °C, 10 min	0.806	19.49	67.39	10.59	156
9-11	PM6 : **9-5b** (1 : 1)	CB	0.5 vol% DIO; 140 °C, 10 min	0.836	20.30	67.38	11.43	156
9-12	PM6 : **9-5c** (1 : 1)	CB	0.5 vol% DIO; 140 °C, 10 min	0.883	21.03	68.31	12.68	156
9-13	PM6 : **9-5d** (1 : 1)	CB	0.5 vol% DIO; 140 °C, 10 min	0.887	21.70	68.79	13.24	156
9-14	PM6 : **9-5e** (1 : 1)	CB	0.5 vol% DIO; 140 °C, 10 min	0.901	22.36	69.23	13.95	156
9-15	PM6 : **9-5f** (1 : 1)	CB	0.5 vol% DIO; 140 °C, 10 min	0.896	22.61	65.16	13.20	156
9-16	PM6 : **9-5g** (1 : 1)	CB	0.5 vol% DIO; 140 °C, 10 min	0.909	22.32	61.77	12.53	156
9-17	PTBT-Th : **9-6a** (1 : 2)	CF	—	1.02	13.30	44	5.97	157
9-18	PTBT-Th : **9-6a** (1 : 2)	CF	THF vapour, 15 s	1.02	15.27	54	8.33	157
9-19	PTBT-Th : **9-6b** (1 : 2)	CF	—	0.92	14.99	45	6.21	157
9-20	PTBT-Th : **9-6b** (1 : 2)	CF	THF vapour, 15 s	0.95	15.82	51	7.60	157
9-21	PBDB-T : **9-7a** (1 : 1)	CF	10 min, 0.5% CN; 140 °C	0.807	18.65	60.3	9.09	158
9-22	PBDB-T : **9-7b** (1 : 1)	CF	10 min, 0.5% CN; 140 °C	0.816	19.39	66.9	10.55	158
9-23	PBDB-T : **9-7c** (1 : 1)	CF	10 min, 0.5% CN; 140 °C	0.780	19.16	63.8	9.53	158
9-24	J52 : **9-8a** (1 : 1.2)	CF	0.5% CN; 120 °C	0.769	24.69	61.69	11.71	159
9-25	J52 : **9-8b** (1 : 1.5)	CF	0.5% CN; 120 °C	0.814	26.02	69.96	14.82	159
9-26	PM6 : **9-9a** (1 : 1)	CF	0.5% CN; 90 °C, 5 min	0.88	19.76	63.84	11.16	160
9-27	PM6 : **9-9b** (1 : 1)	CF	0.5% CN; 90 °C, 5 min	0.90	24.63	72.09	16.00	160
9-28	PM6 : **9-9c** (1 : 1)	CF	0.5% CN; 90 °C, 5 min	0.87	18.28	55.74	8.89	160
9-29	PM6 : **9-9d** (1 : 1)	CF	0.5% CN; 90 °C, 5 min; PDIN buffer	0.96	11.34	51.96	5.67	161
9-30	PM6 : **9-9e** (1 : 1)	CF	0.5% CN; 90 °C, 5 min; PDIN buffer	0.92	22.39	70.10	14.50	161
9-31	PM6 : **9-9e** (1 : 1)	CF	0.5% CN; 90 °C, 5 min; PFNDI-Br buffer	0.91	24.03	76.22	16.66	161
9-32	PM6 : **9-9f** (1 : 1)	CF	0.5% CN; 100 °C, 5 min; Ag electrode	0.73	6.47	47.60	2.26	162
9-33	PM6 : **9-9g** (1 : 1)	CF	0.5% CN; 100 °C, 5 min; Ag electrode	0.88	21.67	60.27	11.55	162
9-34	PM6 : **9-9h** (1 : 1)	CF	0.5% CN; 100 °C, 5 min; Ag electrode	0.88	22.34	66.95	13.14	162
9-35	PM6 : **9-9h** (1 : 1)	CF	0.5% CN; 100 °C, 5 min; Al electrode	0.87	25.10	71.60	15.63	162

[a] Structures of active-layer compounds are shown in Fig. 17. CF: chloroform, CB: chlorobenzene, THF: tetrahydrofuran, CN: chloronaphthalene; DIO: 1,8-diiodooctane; PDIN: *N*,*N*′-di[3-(*N*″,*N*″-dimethylamino)propyl]perylene-3,4:9,10-tetracarboxylic diimide; PFNDI-Br: poly[(9,9-bis(3′-((*N*,*N*-dimethyl)-*N*-ethylammonium)propyl)-2,7-fluorene)-*alt*-5,5′-bis(2,2′-thiophene)-2,6-naphthalene-1,4,5,8-tetracaboxylic-*N*,*N*′-di(2-ethylhexyl) imide]dibromide. [b] Data of the best-performing devices when available; otherwise, average of multiple devices.

2-butyloxtyl derivative **9-7c** (9.53%) as shown in entries 9-21–9-23.

Zhan *et al.* compared two benzotriazole–cyclopentadithiophene–IC conjugates **9-8a** and **9-8b** as n-type materials in BHJ OPVs with p-type polymer J52.[159] The effect of the octyl chains on the outer side of cyclopentadithiophene was significant; compound **9-8b** afforded a PCE of 14.82%, while **9-8a** gave only 11.71% (entries 9-24 and 9-25). Addition of electron donating alkyl chains resulted in not only a higher LUMO energy level as reflected in a larger V_{OC}, but also higher crystallinity, improved conformational rigidity, and a smaller reorganization energy. In the BHJ film with J52, **9-8b** demonstrated balanced charge-carrier mobility, smaller energy loss, and more favorable morphology as compared to the non-substituted **9-8a**.

Recently, substituent impact was intensively studied on a series of A–D–A non-fullerene acceptors comprising the ladder type benzobis(dithienopyrrole) core as the central D unit (**9-9a–h**). When all the four alkyl substituents were branched (2-ethylhexyl, 2-butyloctyl, and 2-decyltetradexy for **9-9a**, **b**, and **c**), the derivative with medium-length chains (**9-9b**) performed the best to afford PCEs up to 16.00% in BHJ OPVs with PM6 (entries 9-26–28).[160] Either shorter alkyl (**9-9a**, PCE = 11.16%) or longer alkyl chains (**9-9c**, 8.89%) resulted in inferior performance. The authors pointed out that **9-9b** formed π–π stacking with a spacing of 3.45 Å, which was shorter than the corresponding values of **9-9a** (3.51 Å) and **9-9c** (4.08 Å). This shorter π–π stack distance was regarded as a cause for the higher charge-carrier mobilities, J_{SC}s, and thus PCEs with **9-9b**. In a different study, the same group compared derivatives **9-9d** and **9-9e**, which were differentiated by alkyl chains on the pyrrole nitrogens: linear *n*-octyl for **9-9d** and branched 2-hexyldecyl for **9-9e**.[161] Notably, the latter was found to preferably adopt a face-on orientation, while the former preferred an edge-on arrangement. Accordingly, **9-9e** afforded a considerably higher PCE (14.50%) than **9-9d** (5.67%) (entries 9-29, 30). Replacement of the cathode buffer material from PDIN to PFNDI-Br resulted in an even higher PCE of 16.66% with **9-9e**. A similar trend between molecular orientation and structure of alkyl substituents was observed with derivatives **9-9f–h**,[162] namely, when all the four alkyl groups are branched 2-butyloctyl, the π-framework adopted a face-on arrangement to show a higher PCE (13.14% with **9-9h**) as compared to those with linear dodecyl groups

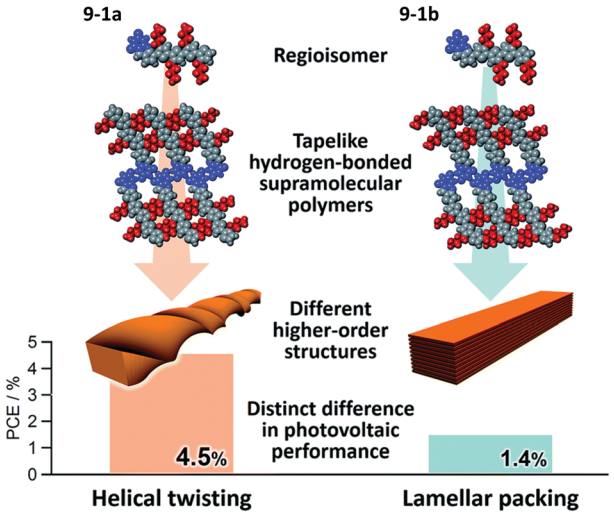

Fig. 18 Supramolecular structures and photovoltaic performance obtained with barbiturated oligo(butylthiophene)s **9-1a** and **9-1b**. Adopted from ref. 116 with permission. Copyright 2018, Royal Society of Chemistry.

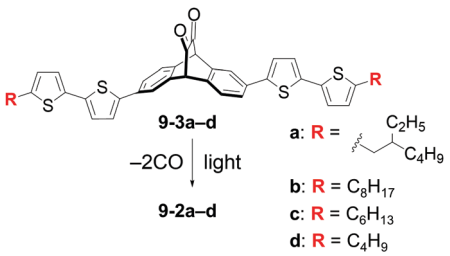

Scheme 2 Light-induced conversion of precursors **10-3a-d** to **10-2a-d**.

(2.26% with **9-9f**, 11.55% with **9-9g**) (entries 9-32–34). The PCE with **9-9h** was further improved to 15.63% by changing the cathode material from Ag to Al.

11. Summary and outlook

We have reviewed the impact of substituents on the photovoltaic performance of various types of SMSCs ranging from simple, single-π-core molecules to large, highly extended D–A conjugates. Although the substituents concerned herein played rather auxiliary roles in determining the electronic characteristics of isolated molecules, their impact was found to be significant, affecting all photovoltaic parameters J_{SC}, V_{OC}, FF, and thus PCE in many examples. This is because substituents generally dictate molecular packing and film morphology, which critically affect the efficacy of OPVs by altering orbital energy levels, exciton dynamics, or charge-carrier mobilities in BHJ active layers. Even a seemingly subtle change in the substituent structure or position induced a large difference in PCE as observed for, among many others, the **9-2** series.

Not surprisingly, the effects of substituents appeared very specific to each π-conjugated backbone. For example, 2-ethylhexyl performed better than hexyl as *N*-substituents of the DPP core between dithienyl-DPP derivatives **4-1a** (*N*-2-ethylhexyl, PCE = 3.0%) and **4-1b** (*N*-hexyl, 0.79%), while an opposite result was obtained with diphenyl-DPP derivatives **4-2a** (*N*-hexyl, 3.45%) and **4-2b** (*N*-2-ethylhexyl, 0.76%). The degree of substituent impact was also found case-by-case. In particular, the difference in the branch point of alkyl chains showed a relatively minor impact on the PCE in the case of core substituents of DTBDT–rhodanine conjugates **6-9a–c** (11.79–14.78%), while it significantly affected in the case of end substituents of BDT–rhodanine conjugates **6-14a–c** (0.90–12.40%). Another important aspect is that the modification of the substituent structure often substantially alters the morphological response of BHJ films to different types or conditions of the cast solvent, solvent additive, and annealing treatment. Furthermore, a partner material or materials in BHJ films regulate the outcome of substituent impact for a compound in question.

Such a complex, multifactorial nature of the substituent impact makes it difficult to extract general rules from previous examples. Indeed, accurate prediction of optimal substituent design for achieving ideal BHJ morphology remains quite a challenge even after decades of research. This is especially true for those molecules with highly extended π-conjugated frameworks that require many flexible solubilizing substituents. At the same time, with the substantial amount of knowledge and experience accumulated so far, we can now optimize substituent design through a systematic screening with a relatively narrow target distribution, rather than arduous examination of wide-range targets. In this context, this review is intended to provide an overview of the currently available knowledge and clues for an optimal substituent design of new SMSCs. For example, the state-of-the-art Y6-type SMSCs generally possess relatively bulky alkyls (typically the size of within 12 carbons) on the central ladder unit and small groups (typically halogen atoms) as the end substituents. This combination of substituents allows the resultant molecules to be sufficiently soluble and miscible, while maintaining effective intermolecular π–π contacts between end groups and certain degrees of packing order in OPV active layers. This substituent design is common also for other systems including IDIC and ITIC derivatives and can be a good starting point in optimization of substituents for novel SMSCs. One can then fine-tune the structure and position of substituents depending on the nature of the π-framework or partner compounds, and synthetic accessibility.

On the other hand, substituent engineering of simple model systems is still of considerable importance because it elucidates general rules hidden behind the complexity of experimental data. In addition, active control of solid-state molecular arrangement *via* the use of highly directional substituents (*e.g.*, hydrogen-bonding groups) should be useful in achieving an optimal BHJ morphology with high reliability. The precursor approach[89,153] and supramolecular approach[152] mentioned in Section 10 may be valuable in these contexts. Another important research direction would be to unravel the evolution of active-layer morphology during material deposition and annealing. Toward this end, *in situ* analysis of morphology should be of critical importance; indeed, *in situ* light absorption,

photoluminescence, and X-ray scattering analyses are becoming increasingly common in OPV research.[163–166] We also note that the use of computer-aided approaches should be widely extended to accelerate the understanding of the structure–morphology–performance relationship of OPV materials. There have been already several studies in this context,[167–173] and research efforts in this area will aid achieving PCEs nearing the theoretical limit.

Conflicts of interest

There are no conflicts to declare.

Acknowledgements

HY and MS thank Japan Society of the Promotion of Science (JSPS) for financial support (KAKENHI No. JP20H00379, JP20H05833 (HY), and 21K05213 (MS)).

References

1 O. Inganäs, *Adv. Mater.*, 2018, **30**, 1800388.
2 Y. Cui, Y. Xu, H. Yao, P. Bi, L. Hong, J. Zhang, Y. Zu, T. Zhang, J. Qin, J. Ren, Z. Chen, C. He, X. Hao, Z. Wei and J. Hou, *Adv. Mater.*, 2021, **33**, 2102420.
3 J. Wang and X. Zhan, *Acc. Chem. Res.*, 2021, **54**, 132–143.
4 H. Wang, J. Cao, J. Yu, Z. Zhang, R. Geng, L. Yang and W. Tang, *J. Mater. Chem. A*, 2019, **7**, 4313–4333.
5 Suman and S. P. Singh, *J. Mater. Chem. A*, 2019, **7**, 22701–22729.
6 F. Shen, J. Xu, X. Li and C. Zhan, *J. Mater. Chem. A*, 2018, **6**, 15433–15455.
7 G. Zhang, J. Zhao, P. C. Y. Chow, K. Jiang, J. Zhang, Z. Zhu, J. Zhang, F. Huang and H. Yan, *Chem. Rev.*, 2018, **118**, 3447–3507.
8 A. Karki, A. J. Gillett, R. H. Friend and T.-Q. Nguyen, *Adv. Energy Mater.*, 2021, **11**, 2003441.
9 Q. Li and Z. Li, *Acc. Chem. Res.*, 2020, **53**, 962–973.
10 F. Zhao, C. Wang and X. Zhan, *Adv. Energy Mater.*, 2018, **8**, 1703147.
11 M. E. Farahat, D. Patra, C.-H. Lee and C.-W. Chu, *ACS Appl. Mater. Interfaces*, 2015, **7**, 22542–22550.
12 H.-C. Liao, C.-C. Ho, C.-Y. Chang, M.-H. Jao, S. B. Darling and W.-F. Su, *Mater. Today*, 2013, **16**, 326–336.
13 Y. Huang, E. J. Kramer, A. J. Heeger and G. C. Bazan, *Chem. Rev.*, 2014, **114**, 7006–7043.
14 A. Wadsworth, Z. Hamid, J. Kosco, N. Gasparini and I. McCulloch, *Adv. Mater.*, 2020, **32**, 2001763.
15 L. Lu, T. Zheng, Q. Wu, A. M. Schneider, D. Zhao and L. Yu, *Chem. Rev.*, 2015, **115**, 12666–12731.
16 A. Mahmood and J.-L. Wang, *Sol. RRL*, 2020, **4** 2000337.
17 N. S. Güldal, T. Kassar, M. Berlinghof, T. Unruh and C. J. Brabec, *J. Mater. Res.*, 2017, **32**, 1855–1879.
18 P. Müller-Buschbaum, *Adv. Mater.*, 2014, **26**, 7692–7709.
19 Y. Yang, Z. Liu, G. Zhang, X. Zhang and D. Zhang, *Adv. Mater.*, 2019, **31**, 1903104.
20 J. Mei and Z. Bao, *Chem. Mater.*, 2014, **26**, 604–615.
21 S. Y. Son, S. Samson, S. Siddika, B. T. O'Connor and W. You, *Chem. Mater.*, 2021, **33**, 4745–4756.
22 X. Jiang, W. Xue, W. Lai, D. Xia, Q. Chen, W. Ma and W. Li, *J. Mater. Chem. C*, 2021, **9**, 16240–16246.
23 N. A. Tegegne, Z. Abdissa, W. Mammo, T. Uchiyama, Y. Okada-Shudo, F. Galeotti, W. Porzio, M. R. Andersson, D. Schlettwein, V. Vohra and H. Schwoerer, *J. Phys. Chem. C*, 2020, **124**, 9644–9655.
24 X. Bi, T. Zhang, C. An, P. Bi, K. Ma, S. Li, K. Xian, Q. Lv, S. Zhang, H. Yao, B. Xu, J. Zhang, S. Cao and J. Hou, *J. Mater. Chem. A*, 2020, **8**, 14706–14712.
25 L. Chen, W. Liu, Y. Yan, X. Su, S. Xiao, X. Lu, C. Uher and X. Tang, *J. Mater. Chem. C*, 2019, **7**, 2333–2344.
26 J. Tong, L. An, J. Li, J. Lv, P. Guo, L. Li, P. Zhang, C. Yang, Y. Xia and C. Wang, *J. Polym. Sci., Part A: Polym. Chem.*, 2018, **56**, 2059–2071.
27 S. Chen, L. Zhang, C. Ma, D. Meng, J. Zhang, G. Zhang, Z. Li, P. C. Y. Chow, W. Ma, Z. Wang, K. S. Wong, H. Ade and H. Yan, *Adv. Energy Mater.*, 2018, **8**, 1702427.
28 Q. Zhao, J. Qu and F. He, *Adv. Sci.*, 2020, **7**, 2000509.
29 H. Yao, J. Wang, Y. Xu, S. Zhang and J. Hou, *Acc. Chem. Res.*, 2020, **53**, 822–832.
30 G. P. Kini, S. J. Jeon and D. K. Moon, *Adv. Mater.*, 2020, **32**, 1906175.
31 Q. Fan, U. A. Méndez-Romero, X. Guo, E. Wang, M. Zhang and Y. Li, *Chem. – Asian J.*, 2019, **14**, 3085–3095.
32 Q. Zhang, M. A. Kelly, N. Bauer and W. You, *Acc. Chem. Res.*, 2017, **50**, 2401–2409.
33 F. Meyer, *Prog. Polym. Sci.*, 2015, **47**, 70–91.
34 C. W. Tang, *Appl. Phys. Lett.*, 1986, **48**, 183–185.
35 M. Hiramoto, H. Fujiwara and M. Yokoyama, *Appl. Phys. Lett.*, 1991, **58**, 1062–1064.
36 G. de la Torre, G. Bottari and T. Torres, *Adv. Energy Mater.*, 2017, **7**, 1601700.
37 Q.-D. Dao, T. Saito, S. Nakano, H. Fukui, T. Kamikado, A. Fujii, Y. Shimizu and M. Ozaki, *Appl. Phys. Express*, 2013, **6**, 122301.
38 H. Fukui, S. Nakano, T. Uno, Q.-D. Dao, T. Saito, A. Fujii, Y. Shimizu and M. Ozaki, *Org. Electron.*, 2014, **15**, 1189–1196.
39 S. Yamamoto and M. Kimura, *ACS Appl. Mater. Interfaces*, 2013, **5**, 4367–4373.
40 E. Zysman-Colman, S. S. Ghosh, G. Xie, S. Varghese, M. Chowdhury, N. Sharma, D. B. Cordes, A. M. Z. Slawin and I. D. W. Samuel, *ACS Appl. Mater. Interfaces*, 2016, **8**, 9247–9253.
41 X. Huang, M. Hu, X. Zhao, C. Li, Z. Yuan, X. Liu, C. Cai, Y. Zhang, Y. Hu and Y. Chen, *Org. Lett.*, 2019, **21**, 3382–3386.
42 J. Kesters, P. Verstappen, M. Kelchtermans, L. Lutsen, D. Vanderzande and W. Maes, *Adv. Energy Mater.*, 2015, **5**, 1500218.
43 L. Bucher, N. Desbois, P. D. Harvey, G. D. Sharma and C. P. Gros, *Sol. RRL*, 2017, **1**, 1700127.

44 K. Gao, Y. Kan, X. Chen, F. Liu, B. Kan, L. Nian, X. Wan, Y. Chen, X. Peng, T. P. Russell, Y. Cao and A. K.-Y. Jen, *Adv. Mater.*, 2020, **32**, 1906129.
45 Y. Matsuo, J. Hatano and T. Nakagawa, *J. Phys. Org. Chem.*, 2014, **27**, 87–93.
46 H. Wang, L. Xiao, L. Yan, S. Chen, X. Zhu, X. Peng, X. Wang, W.-K. Wong and W.-Y. Wong, *Chem. Sci.*, 2016, **7**, 4301–4307.
47 X. Zhou, W. Tang, P. Bi, L. Yan, X. Wang, W.-K. Wong, X. Hao, B. S. Ong and X. Zhu, *J. Mater. Chem. A*, 2018, **6**, 14675–14680.
48 K. Ogumi, T. Nakagawa, H. Okada, R. Sakai, H. Wang and Y. Matsuo, *J. Mater. Chem. A*, 2017, **5**, 23067–23077.
49 K. Ogumi, T. Nakagawa, H. Okada and Y. Matsuo, *Org. Electron.*, 2019, **71**, 50–57.
50 W. T. Hadmojo, D. Yim, S. Sinaga, W. Lee, D. Y. Ryu, W.-D. Jang, I. H. Jung and S.-Y. Jang, *ACS Sustainable Chem. Eng.*, 2018, **6**, 5306–5313.
51 Y. Guo, Y. Liu, Q. Zhu, C. Li, Y. Jin, Y. Puttisong, W. Chen, F. Liu, F. Zhang, W. Ma and W. Li, *ACS Appl. Mater. Interfaces*, 2018, **10**, 32454–32461.
52 X. Pan, J. Wu, L. Xiao, B. Yap, R. Xia and X. Peng, *ChemSusChem*, 2021, **14**, 1–9.
53 M.-C. Tsai, C.-M. Hung, Z.-Q. Chen, Y.-C. Chiu, H.-C. Chen and C.-Y. Lin, *ACS Appl. Mater. Interfaces*, 2019, **11**, 45991–45998.
54 F. Fernández-Lázaro, N. Zink-Lorre and Á. Sastre-Santos, *J. Mater. Chem. A*, 2016, **4**, 9336–9346.
55 M. J. Sung, M. Huang, S. H. Moon, T. H. Lee, S. Y. Park, J. Y. Kim, S.-K. Kwon, H. Choi and Y.-H. Kim, *Sol. Energy*, 2017, **150**, 90–95.
56 J. Feng, W. Jiang and Z. Wang, *Chem. – Asian J.*, 2018, **13**, 20–30.
57 K. Fujimoto, M. Takahashi, S. Izawa and M. Hiramoto, *Materials*, 2020, **13**, 2148.
58 M. Li, H. Yin and G.-Y. Sun, *Appl. Mater. Today*, 2020, **21**, 100799.
59 V. Sharma, J. D. B. Koenig and G. C. Welch, *J. Mater. Chem. A*, 2021, **9**, 6775–6789.
60 H. Sun, X. Song, J. Xie, P. Sun, P. Gu, C. Liu, F. Chen, Q. Zhang, Z.-K. Chen and W. Huang, *ACS Appl. Mater. Interfaces*, 2017, **9**, 29924–29931.
61 W. Chen, X. Yang, G. Long, X. Wan, Y. Chen and Q. Zhang, *J. Mater. Chem. C*, 2015, **3**, 4698–4705.
62 M. Guide, S. Pla, A. Sharenko, P. Zalar, F. Fernández-Lázaro, Á. Sastre-Santos and T.-Q. Nguyen, *Phys. Chem. Chem. Phys.*, 2013, **15**, 18894–18899.
63 J.-P. Sun, A. D. Hendsbee, A. J. Dobson, G. C. Welch and I. G. Hill, *Org. Electron.*, 2016, **35**, 151–157.
64 J. J. Dittmer, E. A. Marseglia and R. H. Friend, *Adv. Mater.*, 2000, **12**, 1270–1274.
65 Z. Lu, X. Zhang, C. Zhan, B. Jiang, X. Zhang, L. Chen and J. Yao, *Phys. Chem. Chem. Phys.*, 2013, **15**, 11375–11385.
66 W. Jiang, L. Ye, X. Li, C. Xiao, F. Tan, W. Zhao, J. Hou and Z. Wang, *Chem. Commun.*, 2014, **50**, 1024–1026.
67 S. V. Dayneko, A. D. Hendsbee and G. C. Welch, *Small Methods*, 2018, **2**, 1800081.
68 M. Vespa, J. R. Cann, S. V. Dayneko, O. A. Melville, A. D. Hendsbee, Y. Zou, B. H. Lessard and G. C. Welch, *Eur. J. Org. Chem.*, 2018, 4592–4599.
69 H.-C. Chen, B.-H. Jiang, C.-P. Hsu, Y.-Y. Tsai, R.-J. Jeng, C.-P. Chen and K.-T. Wong, *Chem. – Eur. J.*, 2018, **24**, 17590–17597.
70 J. Wang, L.-K. Ma, J. Huang, M. Chen, Z. Liu, G. Jiang and H. Yan, *Mater. Chem. Front.*, 2018, **2**, 2104–2108.
71 S. Li, W. Liu, C.-Z. Li, F. Liu, Y. Zhang, M. Shi, H. Chen and T. P. Russell, *J. Mater. Chem. A*, 2016, **4**, 10659–10665.
72 D. Meng, H. Fu, C. Xiao, X. Meng, T. Winands, W. Ma, W. Wei, B. Fan, L. Huo, N. L. Doltsinis, Y. Li, Y. Sun and Z. Wang, *J. Am. Chem. Soc.*, 2016, **138**, 10184–10190.
73 G. Zhang, J. Feng, X. Xu, W. Ma, Y. Li and Q. Peng, *Adv. Funct. Mater.*, 2019, **29**, 1906587.
74 H. Fu, D. Meng, X. Meng, X. Sun, L. Huo, Y. Fan, Y. Li, W. Ma, Y. Sun and Z. Wang, *J. Mater. Chem. A*, 2017, **5**, 3475–3482.
75 W. Li, K. H. Hendriks, M. M. Wienk and R. A. J. Janssen, *Acc. Chem. Res.*, 2016, **49**, 78–85.
76 C. Zhao, Y. Guo, Y. Zhang, N. Yan, S. You and W. Li, *J. Mater. Chem. A*, 2019, **7**, 10174–10199.
77 Q. Liu, S. E. Bottle and P. Sonar, *Adv. Mater.*, 2020, **32**, 1903882.
78 W. W. Bao, R. Li, Z. C. Dai, J. Tang, X. Shi, J. T. Geng, Z. F. Deng and J. Hua, *Front. Chem.*, 2020, **8**, 679.
79 X. Zou, S. Cui, J. Li, X. Wei and M. Zheng, *Front. Chem.*, 2021, **9**, 199.
80 M. Privado, H. Dahiya, P. de la Cruz, M. L. Keshtov, F. Langa and G. D. Sharma, *J. Mater. Chem. C*, 2021, **9**, 16272–16281.
81 J. H. Seo, *Synth. Met.*, 2012, **162**, 748–752.
82 A. B. Tamayo, X.-D. Dang, B. Walker, J. Seo, T. Kent and T.-Q. Nguyen, *Appl. Phys. Lett.*, 2009, **94**, 103301.
83 R. B. Zerdan, N. T. Shewmon, Y. Zhu, J. P. Mudrick, K. J. Chesney, J. Xue and R. K. Castellano, *Adv. Funct. Mater.*, 2014, **24**, 5993–6004.
84 J. D. A. Lin, J. Liu, C. Kim, A. B. Tamayo, C. M. Proctor and T.-Q. Nguyen, *RSC Adv.*, 2014, **4**, 14101–14108.
85 W. Shin, T. Yasuda, G. Watanabe, Y. S. Yang and C. Adachi, *Chem. Mater.*, 2013, **25**, 2549–2556.
86 V. S. Gevaerts, E. M. Herzig, M. Kirkus, K. H. Hendriks, M. M. Wienk, J. Perlich, P. Müller-Buschbaum and R. A. J. Janssen, *Chem. Mater.*, 2014, **26**, 916–926.
87 M. Más-Montoya and R. A. J. Janssen, *Adv. Funct. Mater.*, 2017, **27**, 1605779.
88 M. Jung, D. Seo, K. Kwak, A. Kim, W. Cha, H. Kim, Y. Yoon, M. J. Ko, D.-K. Lee, J. Y. Kim, H. J. Son and B. Kim, *Dyes Pigm.*, 2015, **115**, 23–34.
89 K. Takahashi, D. Kumagai, N. Yamada, D. Kuzuhara, Y. Yamaguchi, N. Aratani, T. Koganezawa, S. Koshika, N. Yoshimoto, S. Masuo, M. Suzuki, K. Nakayama and H. Yamada, *J. Mater. Chem. A*, 2017, **5**, 14003–14011.
90 H. Yamada, D. Kuzuhara, M. Suzuki, H. Hayashi and N. Aratani, *Bull. Chem. Soc. Jpn.*, 2020, **93**, 1234–1267.
91 T. S. van der Poll, J. A. Love, T.-Q. Nguyen and G. C. Bazan, *Adv. Mater.*, 2012, **24**, 3646–3649.

92 D. Ye, X. Li, L. Yan, W. Zhang, Z. Hu, Y. Liang, J. Fang, W.-Y. Wong and X. Wang, *J. Mater. Chem. A*, 2013, **1**, 7622–7629.
93 M. Reyes-Reyes, K. Kim and D. L. Carroll, *Appl. Phys. Lett.*, 2005, **87**, 083506.
94 W.-Y. Wong, X.-Z. Wang, Z. He, A. B. Djurišić, C.-T. Yip, K.-Y. Cheung, H. Wang, C. S. K. Mak and W.-K. Chan, *Nat. Mater.*, 2007, **6**, 521–527.
95 Y. Liu, X. Wan, B. Yin, J. Zhou, G. Long, S. Yin and Y. Chen, *J. Mater. Chem.*, 2010, **20**, 2464–2468.
96 J. Min, Y. N. Luponosov, N. Gasparini, M. Richter, A. V. Bakirov, M. A. Shcherbina, S. N. Chvalun, L. Grodd, S. Grigorian, T. Ameri, S. A. Ponomarenko and C. J. Brabec, *Adv. Energy Mater.*, 2015, **5**, 1500386.
97 M. Jung, Y. Yoon, J. H. Park, W. Cha, A. Kim, J. Kang, S. Gautam, D. Seo, J. H. Cho, H. Kim, J. Y. Choi, K. H. Chae, K. Kwak, H. J. Son, M. J. Ko, H. Kim, D.-K. Lee, J. Y. Kim, D. H. Choi and B. Kim, *ACS Nano*, 2014, **8**, 5988–6003.
98 D. Han, T. Kumari, S. Jung, Y. An and C. Yang, *Sol. RRL*, 2018, **2**, 1800009.
99 L. Ye, S. Zhang, L. Huo, M. Zhang and J. Hou, *Acc. Chem. Res.*, 2014, **47**, 1595–1603.
100 H. Yao, L. Ye, H. Zhang, S. Li, S. Zhang and J. Hou, *Chem. Rev.*, 2016, **116**, 7397–7457.
101 B. Zheng, L. Huo and Y. Li, *NPG Asia Mater.*, 2020, **12**, 1–22.
102 Y. Liang, Z. Xu, J. Xia, S.-T. Tsai, Y. Wu, G. Li, C. Ray and L. Yu, *Adv. Mater.*, 2010, **22**, E135–E138.
103 Q. Wang, J. J. van Franeker, B. J. Bruijnaers, M. M. Wienk and R. A. J. Janssen, *J. Mater. Chem. A*, 2016, **4**, 10532–10541.
104 X. Zhang, J. Yao and C. Zhan, *Adv. Mater. Interfaces*, 2016, **3**, 1600323.
105 Y. Kan, C. Liu, L. Zhang, K. Gao, F. Liu, J. Chen and Y. Cao, *J. Mater. Chem. A*, 2016, **4**, 14720–14728.
106 M. R. Busireddy, V. N. R. Mantena, N. R. Chereddy, B. Shanigaram, B. Kotamarthi, S. Biswas, G. D. Sharma and J. R. Vaidya, *Org. Electron.*, 2016, **37**, 312–325.
107 H. Bin, Y. Yang, Z.-G. Zhang, L. Ye, M. Ghasemi, S. Chen, Y. Zhang, C. Zhang, C. Sun, L. Xue, C. Yang, H. Ade and Y. Li, *J. Am. Chem. Soc.*, 2017, **139**, 5085–5094.
108 X. Yin, Q. An, J. Yu, F. Guo, Y. Geng, L. Bian, Z. Xu, B. Zhou, L. Xie, F. Zhang and W. Tang, *Sci. Rep.*, 2016, **6**, 25355.
109 J. Min, C. Cui, T. Heumueller, S. Fladischer, X. Cheng, E. Spiecker, Y. Li and C. J. Brabec, *Adv. Energy Mater.*, 2016, **6**, 1600515.
110 V. Piradi, G. Zhang, T. Li, M. Zhang, Q. Peng, X. Zhan and X. Zhu, *ACS Appl. Mater. Interfaces*, 2020, **12**, 41506–41514.
111 R. Zhou, Z. Jiang, Y. Shi, Q. Wu, C. Yang, J. Zhang, K. Lu and Z. Wei, *Adv. Funct. Mater.*, 2020, **30**, 2005426.
112 D. Patra, T.-Y. Huang, C.-C. Chiang, R. O. V. Maturana, C.-W. Pao, K.-C. Ho, K.-H. Wei and C.-W. Chu, *ACS Appl. Mater. Interfaces*, 2013, **5**, 9494–9500.
113 A. Tang, C. Zhan and J. Yao, *Adv. Energy Mater.*, 2015, **5**, 1500059.
114 Q. V. Hoang, C. E. Song, I.-N. Kang, S.-J. Moon, S. K. Lee, J.-C. Lee and W. S. Shin, *RSC Adv.*, 2016, **6**, 28658–28665.
115 L. Yang, S. Zhang, C. He, J. Zhang, Y. Yang, J. Zhu, Y. Cui, W. Zhao, H. Zhang, Y. Zhang, Z. Wei and J. Hou, *Chem. Mater.*, 2018, **30**, 2129–2134.
116 Q. Wu, D. Deng, R. Zhou, J. Zhang, W. Zou, L. Liu, S. Wu, K. Lu and Z. Wei, *ACS Appl. Mater. Interfaces*, 2020, **12**, 25100–25107.
117 J. Zhang, X. W. Zhu, C. He, H. J. Bin, L. W. Xue, W. G. Wang, Y. K. Yang, N. Y. Yuan, J. N. Ding, Z. X. Wei, Z.-G. Zhang and Y. F. Li, *J. Mater. Chem. A*, 2016, **4**, 11747–11753.
118 Y. Lin, J. Wang, Z.-G. Zhang, H. Bai, Y. Li, D. Zhu and X. Zhan, *Adv. Mater.*, 2015, **27**, 1170–1174.
119 Y. Lin, Q. He, F. Zhao, L. Huo, J. Mai, X. Lu, C.-J. Su, T. Li, J. Wang, J. Zhu, Y. Sun, C. Wang and X. Zhan, *J. Am. Chem. Soc.*, 2016, **138**, 2973–2976.
120 Y. Yang, Z.-G. Zhang, H. Bin, S. Chen, L. Gao, L. Xue, C. Yang and Y. Li, *J. Am. Chem. Soc.*, 2016, **138**, 15011–15018.
121 H. Bin, Z.-G. Zhang, L. Gao, S. Chen, L. Zhong, L. Xue, C. Yang and Y. Li, *J. Am. Chem. Soc.*, 2016, **138**, 4657–4664.
122 X. Liu, B. Xie, C. Duan, Z. Wang, B. Fan, K. Zhang, B. Lin, F. J. M. Colberts, W. Ma, R. A. J. Janssen, F. Huang and Y. Cao, *J. Mater. Chem. A*, 2018, **6**, 395–403.
123 D. Qian, L. Ye, M. Zhang, Y. Liang, L. Li, Y. Huang, X. Guo, S. Zhang, Z. Tan and J. Hou, *Macromolecules*, 2012, **45**, 9611–9617.
124 X. Liu, Z. Zheng, Y. Xu, J. Wang, Y. Wang, S. Zhang and J. Hou, *J. Mater. Chem. C*, 2020, **8**, 12568–12577.
125 M. Zhang, X. Guo, W. Ma, H. Ade and J. Hou, *Adv. Mater.*, 2015, **27**, 4655–4660.
126 L. Ye, K. Weng, J. Xu, X. Du, S. Chandrabose, K. Chen, J. Zhou, G. Han, S. Tan, Z. Xie, Y. Yi, N. Li, F. Liu, J. M. Hodgkiss, C. J. Brabec and Y. Sun, *Nat. Commun.*, 2020, **11**, 6005.
127 T. Liu, L. Huo, S. Chandrabose, K. Chen, G. Han, F. Qi, X. Meng, D. Xie, W. Ma, Y. Yi, J. M. Hodgkiss, F. Liu, J. Wang, C. Yang and Y. Sun, *Adv. Mater.*, 2018, **30**, 1707353.
128 Z. Zhang, J. Yu, X. Yin, Z. Hu, Y. Jiang, J. Sun, J. Zhou, F. Zhang, T. P. Russell, F. Liu and W. Tang, *Adv. Funct. Mater.*, 2018, **28**, 1705095.
129 S. Li, L. Ye, W. Zhao, S. Zhang, H. Ade and J. Hou, *Adv. Energy Mater.*, 2017, **7**, 1700183.
130 Z. Li, S. Dai, J. Xin, L. Zhang, Y. Wu, J. Rech, F. Zhao, T. Li, K. Liu, Q. Liu, W. Ma, W. You, C. Wang and X. Zhan, *Mater. Chem. Front.*, 2018, **2**, 537–543.
131 S. C. Price, A. C. Stuart, L. Yang, H. Zhou and W. You, *J. Am. Chem. Soc.*, 2011, **133**, 4625–4631.
132 J. Qu, Z. Mu, H. Lai, H. Chen, T. Liu, S. Zhang, W. Chen and F. He, *ACS Appl. Energy Mater.*, 2018, **1**, 4724–4730.
133 X. Liu, X. Wang, Y. Xiao, Q. Yang, X. Guo and C. Li, *Adv. Energy Mater.*, 2020, **10**, 1903650.
134 S. Feng, C. Zhang, Y. Liu, Z. Bi, Z. Zhang, X. Xu, W. Ma and Z. Bo, *Adv. Mater.*, 2017, **29**, 1703527.
135 Y. Li, N. Zheng, L. Yu, S. Wen, C. Gao, M. Sun and R. Yang, *Adv. Mater.*, 2019, **31**, 1807832.

136 C. Han, H. Jiang, P. Wang, L. Yu, J. Wang, J. Han, W. Shen, N. Zheng, S. Wen, Y. Li and X. Bao, *Mater. Chem. Front.*, 2021, **5**, 3050–3060.
137 M. Chen, Y. Nian, Z. Hu and L. Zhang, *J. Mater. Sci.: Mater. Electron.*, 2021, **32**, 219–231.
138 R. Li, G. Liu, R. Xie, Z. Wang, X. Yang, K. An, W. Zhong, X.-F. Jiang, L. Ying, F. Huang and Y. Cao, *J. Mater. Chem. C*, 2018, **6**, 7046–7053.
139 H. S. Ryu, H. G. Lee, S.-C. Shin, J. Park, S. H. Kim, E. J. Kim, T. J. Shin, J. W. Shim, B. J. Kim and H. Y. Woo, *J. Mater. Chem. A*, 2020, **8**, 23894–23905.
140 Z. Luo, Y. Zhao, Z.-G. Zhang, G. Li, K. Wu, D. Xie, W. Gao, Y. Li and C. Yang, *ACS Appl. Mater. Interfaces*, 2017, **9**, 34146–34152.
141 X. Li, F. Pan, C. Sun, M. Zhang, Z. Wang, J. Du, J. Wang, M. Xiao, L. Xue, Z.-G. Zhang, C. Zhang, F. Liu and Y. Li, *Nat. Commun.*, 2019, **10**, 519.
142 J. Yuan, Y. Zhang, L. Zhou, G. Zhang, H.-L. Yip, T.-K. Lau, X. Lu, C. Zhu, H. Peng, P. A. Johnson, M. Leclerc, Y. Cao, J. Ulanski, Y. Li and Y. Zou, *Joule*, 2019, **3**, 1140–1151.
143 X. Li, H. Lu and W. Zhu, *ChemPlusChem*, 2021, **86**, 700–708.
144 K. Jiang, Q. Wei, J. Y. L. Lai, Z. Peng, H. K. Kim, J. Yuan, L. Ye, H. Ade, Y. Zou and H. Yan, *Joule*, 2019, **3**, 3020–3033.
145 H. Yu, R. Ma, Y. Xiao, J. Zhang, T. Liu, Z. Luo, Y. Chen, F. Bai, X. Lu, H. Yan and H. Lin, *Mater. Chem. Front.*, 2020, **4**, 2428–2434.
146 Y. Han, W. Song, J. Zhang, L. Xie, J. Xiao, Y. Li, L. Cao, S. Song, E. Zhou and Z. Ge, *J. Mater. Chem. A*, 2020, **8**, 22155–22162.
147 L. Yi, S. Dai, R. Sun, W. Wang, Y. Wu, X. Jiao, C. Zhang and J. Min, *Org. Electron.*, 2020, **87**, 105963.
148 D. Mo, H. Chen, J. Zhou, N. Tang, L. Han, Y. Zhu, P. Chao, H. Lai, Z. Xie and F. He, *J. Mater. Chem. A*, 2020, **8**, 8903–8912.
149 Y. Chen, F. Bai, Z. Peng, L. Zhu, J. Zhang, X. Zou, Y. Qin, H. K. Kim, J. Yuan, L.-K. Ma, J. Zhang, H. Yu, P. C. Y. Chow, F. Huang, Y. Zou, H. Ade, F. Liu and H. Yan, *Adv. Energy Mater.*, 2021, **11**, 2003141.
150 C. Li, J. Zhou, J. Song, J. Xu, H. Zhang, X. Zhang, J. Guo, L. Zhu, D. Wei, G. Han, J. Min, Y. Zhang, Z. Xie, Y. Yi, H. Yan, F. Gao, F. Liu and Y. Sun, *Nat. Energy*, 2021, **6**, 605–613.
151 L. Chen, C. Cao, H. Lai, Y. Zhu, M. Pu, N. Zheng and F. He, *ACS Appl. Mater. Interfaces*, 2021, **13**, 29737–29745.
152 H. Ouchi, T. Kizaki, M. Yamato, X. Lin, N. Hoshi, F. Silly, T. Kajitani, T. Fukushima, K. Nakayama and S. Yagai, *Chem. Sci.*, 2018, **9**, 3638–3643.
153 M. Suzuki, K. Terai, C. Quinton, H. Hayashi, N. Aratani and H. Yamada, *Chem. Sci.*, 2020, **11**, 1825–1831.
154 M. Suzuki, T. Aotake, Y. Yamaguchi, N. Noguchi, H. Nakano, K. Nakayama and H. Yamada, *J. Photochem. Photobiol., C*, 2014, **18**, 50–70.
155 C. He, Y. Li, Y. Liu, Y. Li, G. Zhou, S. Li, H. Zhu, X. Lu, F. Zhang, C.-Z. Li and H. Chen, *J. Mater. Chem. A*, 2020, **8**, 18154–18161.
156 X. Zhang, Y. Ding, H. Feng, H. Gao, X. Ke, H. Zhang, C. Li, X. Wan and Y. Chen, *Sci. China Chem.*, 2020, **63**, 1799–1806.
157 T. Lee, C. E. Song, S. K. Lee, W. S. Shin and E. Lim, *ACS Omega*, 2021, **6**, 4562–4573.
158 S. Ye, S. Chen, S. Li, Y. Pan, X. Xia, W. Fu, L. Zuo, X. Lu, M. Shi and H. Chen, *ChemSusChem*, 2021, **14**, 1–9.
159 X. Zhang, C. Li, L. Qin, H. Chen, J. Yu, Y. Wei, X. Liu, J. Zhang, Z. Wei, F. Gao, Q. Peng and H. Huang, *Angew. Chem., Int. Ed.*, 2021, **60**, 17720–17725.
160 Y. Ma, D. Cai, S. Wan, P. Yin, P. Wang, W. Lin and Q. Zheng, *Natl. Sci. Rev*, 2020, **7**, 1886–1895.
161 Y. Ma, M. Zhang, S. Wan, P. Yin, P. Wang, D. Cai, F. Liu and Q. Zheng, *Joule*, 2021, **5**, 197–209.
162 P. Wang, Y. Ma, P. Yin, D. Cai, S. Wan and Q. Zheng, *Chem. Eng. J.*, 2021, **418**, 129497.
163 Y. Yu, R. Sun, T. Wang, X. Yuan, Y. Wu, Q. Wu, M. Shi, W. Yang, X. Jiao and J. Min, *Adv. Funct. Mater.*, 2021, **31**, 2008767.
164 J. Yuan, D. Liu, H. Zhao, B. Lin, X. Zhou, H. B. Naveed, C. Zhao, K. Zhou, Z. Tang, F. Chen and W. Ma, *Adv. Energy Mater.*, 2021, **11**, 2100098.
165 Z. Wang, K. Gao, Y. Kan, M. Zhang, C. Qiu, L. Zhu, Z. Zhao, X. Peng, W. Feng, Z. Qian, X. Gu, A. K.-Y. Jen, B. Z. Tang, Y. Cao, Y. Zhang and F. Liu, *Nat. Commun.*, 2021, **12**, 332.
166 Y. Liu, A. Yangui, R. Zhang, A. Kiligaridis, E. Moons, F. Gao, O. Inganäs, I. G. Scheblykin and F. Zhang, *Small Methods*, 2021, **5**, 2100585.
167 S. Nagasawa, E. Al-Naamani and A. Saeki, *J. Phys. Chem. Lett.*, 2018, **9**, 2639–2646.
168 H. Sahu, W. Rao, A. Troisi and H. Ma, *Adv. Energy Mater.*, 2018, **8**, 1801032.
169 D. Padula, J. D. Simpson and A. Troisi, *Mater. Horiz.*, 2019, **6**, 343–349.
170 A. Saeki and K. Kranthiraja, *Jpn. J. Appl. Phys.*, 2020, **59**, SD0801.
171 W. Sun, Y. Zheng, K. Yang, Q. Zhang, A. A. Shah, Z. Wu, Y. Sun, L. Feng, D. Chen, Z. Xiao, S. Lu, Y. Li and K. Sun, *Sci. Adv.*, 2019, **5**, eaay4275.
172 Y. Huang, J. Zhang, E. S. Jiang, Y. Oya, A. Saeki, G. Kikugawa, T. Okabe and F. S. Ohuchi, *J. Phys. Chem. C*, 2020, **124**, 12871–12882.
173 K. Kranthiraja and A. Saeki, *Adv. Funct. Mater.*, 2021, **31**, 2011168.